The Effect of Tunnelling in Quantum Field Theory

DANIEL LUKE MILNE

The Effect of Tunnelling in Quantum Field Theory

Daniel Luke Milne

A Thesis presented for the degree of
Doctor of Philosophy

Institute for Particle Physics Phenomenology
Department of Physics
Durham University
United Kingdom

May 2023

The Effect of Tunnelling in Quantum Field Theory

Daniel Luke Milne

Submitted for the degree of Doctor of Philosophy

May 2023

Abstract: The phenomenon of quantum tunnelling is a familiar one, allowing a particle to 'escape' from a potential well where it does not have enough energy classically to penetrate the potential barrier. Quantum tunnelling is well studied and familiar to most physicists from processes such as alpha decay. In this thesis we will examine the phenomenon of tunnelling in Quantum Field Theory which will yield a rich phenomenology. In the strong and electroweak sectors it gives rise to the instanton, a field configuration which tunnels between degenerate minima of the field strength. In the strong sector we will compute the cross section for these processes at hadron colliders before examining potential search strategies. In the electroweak sector we will show that such processes are always exponentially suppressed and hence unobservable at any present or future colliders. Finally we will look at the phenomenon of tunnelling in the early universe in the context of first-order phase transitions; here tunnelling can lead to the production of gravitational waves which could be observable at future gravitational wave detectors, and models giving rise to such signals can also be used to solve other shortcomings of the Standard Model such as the hierarchy problem and the absence of dark matter.

Contents

List of Figures

List of Tables

Declaration

The work in this thesis is based on research carried out in the Department of Physics at Durham University. No part of this thesis has been submitted elsewhere for any degree or qualification.

This thesis is based on joint research:

1. Chapter 2 is based on [2]: V. V. Khoze, D. L. Milne and M. Spannowsky, *Searching for QCD Instantons at Hadron Colliders*, *Phys. Rev. D* **103** (2021) 014017, [2010.02287].

2. Chapter 3 is based on [3]: V. V. Khoze and D. L. Milne, *Suppression of Electroweak Instanton Processes in High-energy Collisions*, *Int. J. Mod. Phys. A* **36** (2021) 2150032, [2011.07167].

3. Chapter 4 is based on [4] with V. V. Khoze (submitted for publication).

Other research projects published during my studies but not included in this thesis are:

1. [5]: V. A. Khoze, V. V. Khoze, D. L. Milne and M. G. Ryskin, *Hunting for QCD instantons at the LHC in events with large rapidity gaps*, *Phys. Rev. D* **104** (2021) 054013, [2104.01861].

2. [6]: V. A. Khoze, V. V. Khoze, D. L. Milne and M. G. Ryskin, *Central instanton production*, *Phys. Rev. D* **105** (2022) 036008, [2111.02159].

3. [7]: M. Tasevsky, V. Khoze, D. Milne and M. Ryskin, *Searches for QCD instantons with forward proton tagging*, *Eur. Phys. J. C* **83** (2023) 35, [2208.14089].

4. [8]: V. V. Khoze and D. L. Milne, *Optical effects of domain walls*, *Phys. Lett. B* **829** (2022) 137044, [2107.02640].

Acknowledgements

Firstly I would like to thank my supervisor, Valya Khoze, for his help and guidance during my PhD and without which I would not have been able to complete this thesis. I would also like to thank all of the PhD students at the IPPP for their help with various problems over the course of my PhD as well as for being a good group of friends.

Chapter 1

Introduction

1.1 A Review of the Standard Model

The Standard Model of particle physics (SM) is a Quantum Field Theory based on the transformations of different fields under the action of various Lie groups, namely $SU(3)_c \times SU(2)_L \times U(1)_Y$. Lie groups can be related to their respective Lie algebras by the exponential map i.e.

$$\forall x \in G, \exists\, y \in \mathfrak{g} \text{ s.t. } x = e^y \tag{1.1.1}$$

where G is the Lie group and $\mathfrak{g}$ the Lie algebra. Conversely

$$y \in \mathfrak{g} \implies e^y \in G. \tag{1.1.2}$$

It can be shown that the Lie algebra forms a vector space and hence we can choose a basis, conventionally denoted T^a where $a = 1, ..., \dim \mathfrak{g}$ is an index and $\dim \mathfrak{g}$ is the dimension of the Lie algebra.

Given a group we may also consider different representations of the group. A representation is a map from the group to square matrices which preserves the group structure, that is, $D : G \to M_{n\times n}$, where $M_{n\times n}$ is the set of $n \times n$ matrices, is a

representation if and only if

$$D(a)D(b) = D(a * b) \tag{1.1.3}$$

where the objects on the left hand side are composed through ordinary matrix multiplication and $*$ is the operation of the group under consideration. We will be primarily interested in the group $SU(n)$, the group of $n \times n$ matrices which are unitary and have determinant one, i.e.

$$SU(n) = \{U \in M_{n\times n} : UU^\dagger = U^\dagger U = \mathbb{1}_{n\times n} \text{ and } \det U = 1\} \tag{1.1.4}$$

where $\mathbb{1}_{n\times n}$ is the $n \times n$ identity matrix. We will also deal with the group $U(1)$,

$$U(1) = \{e^{i\theta} \ : \ 0 \leq \theta < 2\pi\}. \tag{1.1.5}$$

We will be mostly interested in the fundamental and adjoint representations. For $SU(n)$ and $U(1)$ the fundamental representation is defined by $D(U) = U$. The adjoint representation is slightly more complicated to define. When considering a representation, rather than directly considering the matrix we may instead consider the matrix as an action on a vector space. We call this space the representation space. The adjoint representation is then the representation where the dimension of the representation space and the dimension of the Lie algebra are the same.

To move on to the applications to particle physics, gauge transformations represent redundancy in the system, i.e. we have chosen an object with too many degrees of freedom to represent reality. Gauge transformations allow us to transform our fields in certain ways but since these represent unphysical degrees of freedom it must be the case that physical observables are invariant under gauge transformations. As objects in QFT are calculated through the path integral, to ensure this invariance we demand that the Lagrangian (and hence the action and subsequently the path integral) is invariant under gauge transformations.

If we now try to construct a Lagrangian for a complex scalar field which transforms in the fundamental representation of $SU(n)$ ($\phi \to U\phi$, $U \in SU(n)$), then we initially

try to write

$$\mathcal{L} = \left(\partial_\mu \phi\right)^\dagger \left(\partial^\mu \phi\right) - m^2 \phi^\dagger \phi \tag{1.1.6}$$

in order to recover the Klein-Gordon equation. However since U is a gauge transformation, it depends on the space-time variable x (although we suppress this dependence for brevity) and the derivatives mean that this Lagrangian is not gauge invariant. In order to recover gauge invariance we must introduce an additional field, A_μ, known as a gauge boson, which must carry a Lorentz index if it is to cancel the additional terms generated by the derivative. We then demand that under a gauge transformation

$$A_\mu \to U\left(A_\mu + \frac{i}{g}\partial_\mu\right)U^\dagger \tag{1.1.7}$$

where g is the coupling constant associated with the group G. Note that we follow the conventions of [9] and so $A_\mu = A_\mu^a T^a$ and so we see that we obtain as many gauge bosons/fields as there are dimensions of the Lie group. We then write the Lagrangian

$$\mathcal{L} = \left(D_\mu \phi\right)^\dagger \left(D^\mu \phi\right) - m^2 \phi^\dagger \phi \tag{1.1.8}$$

where we have defined the covariant derivative, $D_\mu = \partial_\mu - igA_\mu^a T^a$, then we recover gauge invariance; Eq. (1.1.8) is invariant under gauge transformations. In general we expand this definition of the covariant derivative so that T^a is replaced by the generators of the group in the representation under which the field transforms (here ϕ transforms in the fundamental representation). Also note that for a non-abelian theory g must be the same for all fields while for an abelian theory different fields can possess different charges under the group. However in order to make the A-field dynamical and propagate, we must also add the term

$$-\frac{1}{2}\mathrm{Tr}\left(F_{\mu\nu}F^{\mu\nu}\right) \tag{1.1.9}$$

where the trace runs over the indices of the Lie algebra and we have defined the gauge field strength tensor

$$F_{\mu\nu} = \partial_\mu A_\nu - \partial_\nu A_\mu - ig[A_\mu, A_\nu]. \tag{1.1.10}$$

When dealing with commutators in a Lie algebra, one can use the relation

$$[T^a, T^b] = if^{abc}T^c \tag{1.1.11}$$

where f^{abc} are known as the structure constants of the Lie algebra. One can show that the non-interacting terms quadratic in the A-field generate the correct equations of motion for vector boson fields, e.g. the photon in QED or the gluon in QCD. One can show that the field strength tensor transforms as $F_{\mu\nu} \to UF_{\mu\nu}U^\dagger$ (although if G is an abelian group this simplifies and in fact $F_{\mu\nu}$ is invariant under gauge transformations) and hence (1.1.9) is invariant. Using the normalisation of the generators of a Lie group, conventionally chosen so that in the fundamental representation $Tr(T^aT^b) = \frac{\delta^{ab}}{2}$, one may rewrite Eq. (1.1.9) as

$$-\frac{1}{2}\mathrm{Tr}\left(F_{\mu\nu}F^{\mu\nu}\right) = -\frac{1}{2}F^a_{\mu\nu}F^{b,\mu\nu}\mathrm{Tr}\left(T^aT^b\right) = -\frac{1}{4}F^a_{\mu\nu}F^{a,\mu\nu} \tag{1.1.12}$$

although in the case of a $U(1)$ theory, $a = 1$ and we drop the index.

Since we will later require it, we will develop the theory of path integrals here. We use the notation that $D\phi$ represents an integral over all functions ϕ and define the partition function as

$$Z = \int \mathcal{D}\phi_1 \ldots \mathcal{D}\phi_n \, e^{iS[\phi_1,\ldots,\phi_n]}. \tag{1.1.13}$$

The partition function is the central object in Quantum Field Theory as given the partition function, one is then able to calculate all propagators in the theory.

However a problem arises when we wish to add fermions to our theory. In order to properly encode the spin-statistics theorem the functions representing fields must anticommute. We do this by introducing Grassmann-valued variables. Grassman numbers are anticommuting e.g. $\eta\theta = -\theta\eta$. This has the consequence that the square of a Grassmann number vanishes and all functions of Grassmann numbers can be at most linear, i.e. for an arbitrary function f, $f(\theta) = A + B\theta$ for some constants A and B. In order to retain shift invariance of the integral, we define integration over

Grassmann-valued variables as follows:

$$\int \mathrm{d}\theta \; (A + B\theta) = B. \tag{1.1.14}$$

We also have the problem that there is an ambiguity in performing integrals over multiple Grassmann-valued variables due to the ordering. We take the convention that the innermost integral is performed first. Now we take the variables associated with fermionic fields to be Grassmann-valued and we have the path integral for a free Dirac fermion:

$$Z = \int \mathcal{D}\psi \mathcal{D}\bar{\psi}\, e^{\bar{\psi}\left(i\not{\partial} - m\right)\psi}. \tag{1.1.15}$$

Having dealt with fermions we return to examining gauge invariance. The problem of gauge transformations, i.e. that of redundant degrees of freedom in the theory, is not merely a physical issue but also a mathematical one as it causes the divergence of the path integral. Consider

$$Z = \int \mathcal{D}A\, e^{iS} \tag{1.1.16}$$

where S is given by the integral of Eq. (1.1.9). One can show that this integral diverges due to the integral over physically equivalent field configurations [9]. To resolve this issue we insert the factor

$$1 = \int \mathcal{D}\alpha\, \delta\left(G\left(A^{\alpha}\right)\right) \det\left(\frac{\delta G\left(A^{\alpha}\right)}{\delta \alpha}\right) \tag{1.1.17}$$

where α is the parameter of an infinitesimal gauge transformation, A^{α} is the gauge field under such a transformation and G is an arbitrary function. We then choose $G\left(A\right) = \partial^{\mu} A^{a}_{\mu} - \omega^{a}\left(x\right)$ for an arbitrary function ω and average over ω with a gaussian weight to obtain

$$Z = \int \mathcal{D}A\, \mathcal{D}\alpha\, \mathcal{D}\omega\, e^{-i\int \mathrm{d}^4x\, \frac{\omega^2}{2\xi}} \delta\left(G\left(A^{\alpha}\right)\right) \det\left(\frac{\delta G\left(A^{\alpha}\right)}{\delta \alpha}\right) e^{-S}. \tag{1.1.18}$$

Note that we have chosen $G\left(A\right)$ to depend on $\partial^{\mu} A^{a}_{\mu}$ to align with the usual Lorentz gauge but of course one may choose another gauge, e.g. the Coulomb gauge where

$G(A)$ would depend on $\nabla.\mathbf{A}$[1]. After some simplification we obtain

$$Z = N\det\left(\frac{1}{g}\partial^\mu D_\mu\right)\int \mathcal{D}A\, e^{-S} e^{-i\int \mathrm{d}^4x\, \frac{1}{2\xi}\left(\partial_\mu A^\mu\right)^2} \tag{1.1.19}$$

where N is a constant and the covariant derivative here is given by $D_\mu\alpha^a = \partial_\mu\alpha^a + gf^{abc}A^b_\mu\alpha^c$, i.e. it is the covariant derivative as if it were acting on an object in the adjoint representation. Note that ξ is a free parameter and by inspection we see that these manipulations are equivalent to adding to the Lagrangian a term

$$\mathcal{L}_{GF} = -\frac{1}{2\xi}\left(\partial_\mu A^\mu\right)^2. \tag{1.1.20}$$

Faddeev and Popov showed that the functional determinant can be written as

$$\det\left(\frac{1}{g}\partial^\mu D_\mu\right) = \int \mathcal{D}c\mathcal{D}\bar{c}\, e^{i\int \mathrm{d}^4x\, \bar{c}\left(-\partial^\mu D_\mu\right)c} \tag{1.1.21}$$

where c is an anticommuting scalar field (i.e. it is Grassmann-valued) which transforms in the adjoint representation of the respective Lie group. These fields are known as ghosts and again this procedure can be seen as equivalent to adding to the Lagrangian a term

$$\mathcal{L}_{\text{ghost}} = \bar{c}\left(-\partial^\mu D_\mu\right)c. \tag{1.1.22}$$

One should note that due to the construction of these ghosts they are not physical particles and cannot appear as external legs in a Feynman diagram (and otherwise would violate the spin-statistics theorem) but may still run in loops and thus contribute to the amplitude. A physical interpretation of the ghosts is that they cancel the contribution from the unphysical degrees of freedom of gauge bosons. Note that in an abelian theory (e.g. $U(1)$) $f^{abc} = 0$ and so (in this case) $D_\mu = \partial_\mu$ and the ghosts decouple from all other fields in the theory, i.e. ghosts may be ignored in an abelian theory.

Now that we have dealt with the underlying structure, we can construct the Standard

[1] In fact, instantons are usually treated in the gauge where $D_\mu\left(\delta A_\mu\right) = 0$ where D_μ is the covariant derivative in the background of the instanton configuration which will be derived at the end of this chapter and δA_μ are fluctuations about the instanton solution. Also note that this constraint is stated in Euclidean space as is standard in the study of instantons.

Model. The SM is based on the gauge group $SU(3)_c \times SU(2)_L \times U(1)_Y$, where the subscripts indicate colour, left and hypercharge respectively, denoting which fields transform under those particular gauge transformations. However the gauge structure of the SM is slightly complicated by spontaneous symmetry breaking so we shall tackle this issue first. The Higgs field is a complex scalar field charged under $SU(2)_L$ and $U(1)_Y$ with hypercharge $Y = \frac{1}{2}$. Hence writing the Higgs Lagrangian we have

$$\mathcal{L} = \left(D_\mu H\right)^\dagger \left(D^\mu H\right) - V\left(H\right) \tag{1.1.23}$$

where H is the Higgs field and $V\left(H\right)$ is the Higgs potential and is given by

$$V\left(H\right) = -\mu^2 H^\dagger H + \lambda \left(H^\dagger H\right)^2 \tag{1.1.24}$$

where μ and λ are free parameters. Note that this is the most general Lagrangian allowed by gauge invariance. We see that if $\mu^2 < 0$ then the potential is at a minimum at $H^\dagger H = 0$ but if $\mu^2 > 0$ then the potential has a minimum away from the origin at

$$H^\dagger H = \frac{\mu^2}{2\lambda}. \tag{1.1.25}$$

In this case we say the Higgs field develops a vacuum expectation value (vev) i.e. in vacuum the field takes on a non-zero value. Experimentally we know that this is the case realised in nature, $\mu^2_{\mathrm{SM}} > 0$. In this case, by means of a gauge transformation, it is always possible to write the Higgs field as

$$H = \frac{1}{\sqrt{2}} \begin{pmatrix} 0 \\ v + h \end{pmatrix} \tag{1.1.26}$$

where $v = \sqrt{\frac{\mu^2}{\lambda}}$ is the vev of the Higgs field and h is a fluctuating field which is zero in vacuum. Now we consider the Higgs kinetic term $\left(D_\mu H\right)^\dagger \left(D^\mu H\right)$ where $D_\mu = \partial_\mu - i g_w W^a_\mu \frac{\sigma^a}{2} - i\frac{g'}{2} B_\mu$, g_w is the coupling constant associated with $SU(2)_L$, g' the coupling constant associated with $U(1)_Y$, $W^{1,2,3}$ the three gauge bosons of $SU(2)$ and B_μ the gauge boson of $U(1)_Y$. Also $\sigma^{1,2,3}$ are the usual Pauli matrices ($\frac{\sigma^a}{2}$ are the generators of $SU(2)$ appropriately normalised). If we now consider this

term in vacuum i.e. $h = 0$ then we obtain

$$\left(D_\mu H\right)^\dagger (D^\mu H)|_{h=0} = \frac{v^2}{8}\left(g_w^2 W_\mu^1 W_{1,\mu} + g_w^2 W_\mu^2 W_{2,\mu} + \left(-g_w W_\mu^3 + g' B_\mu\right)\left(-g_w W^{3,\mu} + g' 2B^\mu\right)\right). \tag{1.1.27}$$

We see clearly that W_μ^3 and B_μ are not the states which propagate as there are terms quadratic in the fields which mix W_μ^3 and B_μ whereas we must reproduce the Klein-Gordon equation which contains no mixed terms. If we now define the fields

$$W_\mu^\pm = \frac{1}{2}\left(W_\mu^1 \mp i W_\mu^2\right) \tag{1.1.28}$$

$$Z_\mu = \frac{1}{\sqrt{g_w^2 + g'^2}}\left(g_w W_\mu^3 - g' B_\mu\right) \tag{1.1.29}$$

$$A_\mu = \frac{1}{\sqrt{g_w^2 + g'^2}}\left(g_w W_\mu^3 + g' B_\mu\right) \tag{1.1.30}$$

then Eq. (1.1.27) becomes

$$\left(D_\mu H\right)^\dagger (D^\mu H)|_{h=0} = m_W^2 W^{+,\mu} W_\mu^- + \frac{1}{2} m_Z^2 Z^\mu Z_\mu \tag{1.1.31}$$

where $m_W = \frac{g_w v}{2}$ and $m_Z = \frac{v\sqrt{g_w^2+g'^2}}{2}$. Note that these states are no longer the pure states associated with the Lie groups $SU(2)$ or $U(1)$ but we have also now given a mass to our gauge bosons which was previously forbidden by gauge invariance. Note that the field A_μ is the QED photon and remains massless. Further algebra also reveals that the field h develops a mass $m_h^2 = 2\lambda v^2$. h is the physical Higgs boson which we can observe.

Similarly let us try to generate a mass for fermions. Direct mass terms for Dirac fermions are forbidden in the Standard Model; consider a Dirac mass term written in the chiral basis

$$m\bar{\psi}\psi = m\left(\bar{\psi}_R^\alpha \psi_{L,\alpha} + \bar{\psi}_{L,\dot{\alpha}} \psi_R^{\dot{\alpha}}\right) \tag{1.1.32}$$

where $\alpha, \dot{\alpha}$ are Dirac indices and $\psi_{L,R}$ are the left- and right-handed Weyl spinors. We see that a Dirac mass term such as this mixes the left- and right-handed spinors

and so cannot be invariant under $SU(2)_L$. Note that the Dirac kinetic term

$$\mathcal{L}_{\text{Dirac}}^{\text{kinetic}} = i\bar{\psi}\not{D}\psi = i\bar{\psi}_L\not{D}\psi_L + i\bar{\psi}_R\not{D}\psi_R \tag{1.1.33}$$

where $\not{D} = \gamma_\mu D^\mu$, does not mix left- and right-handed spinors and is therefore allowed. To generate a mass for our fermions we must write Yukawa terms:

$$\mathcal{L}_Y = -y_d\bar{Q}_L H d_R - y_u\bar{Q}_L\tilde{H}u_R + \text{h.c.} \tag{1.1.34}$$

where $\tilde{H} = i\sigma^2 H^*, Q = (u,d)^T$, h.c. represents that we should add the hermitian conjugate of the previous terms to the Lagrangian and u and d are the up and down quarks respectively. y_u and y_d are the up and down yukawa couplings. Note that here we have only written the Yukawa terms for the first generation of quarks but the other two generations are exactly analogous. The leptons are slightly different since neutrinos are massless in the Standard Model and so we do not write the second term, hence

$$\mathcal{L}_Y^{\text{lepton}} = -y_e\bar{L}_L H e_R + \text{h.c.} \tag{1.1.35}$$

where $L = (\nu, e)^T$, ν and e are the neutrino and electron fields and y_e is the electron yukawa coupling. It can clearly be seen from here that once the Higgs doublet takes the form of Eq. (1.1.26) then Eqs. (1.1.34), (1.1.35) take the form of a Dirac mass term with fermion mass $m_f = \frac{1}{\sqrt{2}}y_f v$ (as well as generating a coupling term between h and fermions). Finally we include Table 1.1, showing the transformation of all particles in the Standard Model under the three groups $SU(3)_c$, $SU(2)_L$, $U(1)_Y$. It can be seen that with the assignments given by this table that the Standard Model Lagrangian:

$$\mathcal{L}_{SM} = \mathcal{L}_{\text{kinetic}} + \mathcal{L}_Y + \mathcal{L}_{\text{Higgs}} + \mathcal{L}_{GF} + \mathcal{L}_{\text{ghost}} \tag{1.1.36}$$

is invariant under gauge transformations.

Matter fields	$SU(3)_c$	$SU(2)_L$	$U(1)_Y$
Q_L^i	3	2	$\frac{1}{6}$
$\bar{u}_R^i$	$\bar{3}$	1	$-\frac{2}{3}$
$\bar{d}_R^i$	$\bar{3}$	1	$\frac{1}{3}$
L_L^i	1	2	$-\frac{1}{2}$
$\bar{e}_R^i$	1	1	1
H	1	2	$\frac{1}{2}$

Table 1.1: Table showing the gauge transformations of all SM matter fields where i is a generation index. For the non-abelian groups, the number gives the dimension of the representation the field transforms in (1 is the trivial representation or equivalently the field does not transform) and for the abelian group, $U(1)_Y$, the number gives the charge of each field under this group.

1.2 The Instanton in Quantum Mechanics

The instanton arises in theories with multiple degenerate vacua. To derive important aspects of the instanton theory we shall begin with the simplest such theory, the double-well potential in one-dimensional quantum mechanics following [10]. Let us consider a 1D system with $V(q) = \frac{1}{2}\left(q^2-1\right)^2$, noting that this clearly has two degenerate minima at $q = \pm 1$. Then the classical Lagrangian is given by

$$\mathcal{L} = \frac{1}{2}\dot{q}^2 - \frac{1}{2}\left(q^2-1\right)^2 \tag{1.2.1}$$

and the action by

$$S = \int L \, \mathrm{d}t = \frac{1}{2}\int_{-t_0/2}^{t_0/2} \mathrm{d}t \, \left(\dot{q}^2 - \left(q^2-1\right)^2\right). \tag{1.2.2}$$

Instantons are always treated in Euclidean space so we now perform a Wick rotation, $t \to -i\tau$ to obtain the Euclidean action:

$$S = iS_E = \frac{i}{2}\int_{-\tau_0/2}^{\tau_0/2} \mathrm{d}\tau \, \left(\left(\frac{dq}{d\tau}\right)^2 + \left(q^2-1\right)^2\right). \tag{1.2.3}$$

So our path integral becomes

$$Z = N\int Dq \, e^{-S_E}. \tag{1.2.4}$$

We see that only events with a finite Euclidean action can contribute to the path integral, as the Euclidean action is real and positive definite. If we let $\tau_0 \to \infty$ we see that for the Euclidean action to be finite we must have that as $\tau_0 \to \pm\infty$, $\frac{dq}{d\tau} \to 0$. We must also have $V(q) \to 0 \implies q \to \pm 1$, i.e. the solution must come to reside in one of the minima as time goes to positive and negative infinity. Let us arbitarily pick that at $\tau = -\infty$ we have $q = -1$ and at $\tau = \infty$ we have $q = 1$ as boundary conditions (we choose that this is the instanton and the solution which begins at $q = 1$ and goes to $q = -1$ is the anti-instanton) and consider the equation of motion:

$$\frac{\partial L}{\partial q} - \frac{d}{d\tau}\left(\frac{\partial L}{\partial \dot{q}}\right) = \ddot{q} - 2q\left(q^2 - 1\right) = 0. \tag{1.2.5}$$

We can check that this equation is satisfied by

$$q^I(\tau) = \tanh(\tau - \tau_0) \tag{1.2.6}$$

where τ_0 is a constant of integration known as the centre of the instanton. We can now expand the action around this solution:

$$S = S_0 + \left.\frac{\delta S}{\delta q}\right|_{S=S_0} \delta q + \left.\frac{\delta^2 S}{\delta q^2}\right|_{S=S_0} (\delta q)^2 \tag{1.2.7}$$

where S_0 is the value of the action for the instanton solution which can be calculated to be $S_0 = \frac{4}{3}$ through straightforward application of Eq. (1.2.3). Since Eq. (1.2.6) satisfies the equations of motion the first order correction vanishes and we are left with:

$$S = S_0 + \frac{1}{2}\int \mathrm{d}\tau\, \delta q \left(-\frac{d^2}{d\tau^2} + V''\left(q^I\right)\right) \delta q. \tag{1.2.8}$$

Now we consider the operator $-\frac{d^2}{d\tau^2} + V''(q)$; this is a hermitian operator and so we can find a complete set of orthonormal eigenfunctions:

$$\left(-\frac{d^2}{d\tau^2} + V''\left(q^I\right)\right) v_i(\tau) = \lambda_i v_i(\tau) \tag{1.2.9}$$

$$\int \mathrm{d}\tau\ v_i(\tau)\, v_j(\tau) = \delta_{ij} \tag{1.2.10}$$

where λ_i is the eigenvalue of the i-th eigenfunction v_i and we impose the boundary conditions that $v_i\left(\pm\frac{\tau_0}{2}\right)=0$. As the eigenfunctions form a complete set, an arbitrary function f can be written as $f(\tau)=F(\tau)+\sum_{i=0}^{\infty}a_i v_i(\tau)$ for coefficients a_i and $F(\tau)$ is any function matching f on the boundary. We can use this to rewrite δq in terms of eigenfunctions and substitute this into Eq. (1.2.8). This gives

$$S=S_0+\frac{1}{2}\sum_{i,j=1}^{\infty}\int \mathrm{d}\tau\ a_i v_i(\tau)\,a_j\lambda_j v_j(\tau)=S_0+\frac{1}{2}\sum_{i=1}^{\infty}\lambda_i a_i^2 \tag{1.2.11}$$

by Eq. (1.2.10). Also note that since δq vanishes at the boundary we have chosen $F(\tau)\equiv 0$. It is a standard result that the measure in the path integral can be written as an integral over coefficients of an expansion and so our path integral now looks like:

$$Z=N\int Dq\ e^{-S_E}=N'e^{-S_0}\prod_{i=1}^{\infty}\left(\int \mathrm{d}a_i\right)\ e^{-\frac{1}{2}\sum_{j=1}^{\infty}\lambda_j a_j^2} \tag{1.2.12}$$

absorbing any constant factors in the measure into our normalisation constant. We proceed with the calculation:

$$Z=N'e^{-S_0}\prod_{i=1}^{\infty}\left(\int \mathrm{d}a_i\right)\ e^{-\frac{1}{2}\sum_{j=1}^{\infty}\lambda_j a_j^2} \tag{1.2.13}$$

$$=N'e^{-S_0}\prod_{i=1}^{\infty}\left(\int \mathrm{d}a_i\, e^{-\frac{1}{2}\lambda_i a_i^2}\right) \tag{1.2.14}$$

$$=N'e^{-S_0}\prod_{i=1}^{\infty}\sqrt{\frac{2\pi}{\lambda_i}} \tag{1.2.15}$$

$$=\frac{N''e^{-S_0}}{\sqrt{\det\left(\frac{d^2}{d\tau^2}+V''(q)\right)}} \tag{1.2.16}$$

where we have defined the determinant of an operator to be the product of its eigenvalues. It can be seen that this expression is problematic if the operator has a zero eigenvalue; in fact this turns out to be the case. There is a zero eigenvalue which corresponds to the direction in function space associated with changing τ_0 as it can clearly be seen that the value of the action does not depend on τ_0, note that the corresponding eigenfunction is known as a zero mode. Here we shall work more generally so that our results may easily be transferred to the case of

instantons in a gauge theory. Since we have that $S[q^I(\tau,\tau_0)] = S[q^I(\tau,\tau_0+\delta\tau_0)]$ and $q^I(\tau,\tau_0+\delta\tau_0) = q^I(\tau,\tau_0) + \frac{\partial q^I}{\partial\tau_0}\delta\tau_0$, we can see that the requisite zero mode is proportional to $\frac{\partial q^I}{\partial\tau_0}$. In fact the correct normalisation (in this case) is given by $v_0 = \frac{1}{\sqrt{S_0}}\frac{\partial q^I}{\partial\tau_0}$.

We also see that in order for the action not to change, this zero mode must be annihilated by the second functional derivative of the action, i.e. we can set δq equal to our zero mode in Eq. (1.2.7) and all terms but the zeroth order must vanish. Hence our zero mode does indeed have a vanishing eigenvalue for the operator in Eq. (1.2.13) (which is just the second functional derivative of the action) as stated above. Clearly for this direction in the function space, our Gaussian approximation is no longer valid and we must perform the integral more carefully.

Since we are expanding around the instanton solution we are integrating over solutions of the form $q(\tau) = q^I(\tau) + \sum_{i=0}^{\infty} a_i v_i(\tau)$. We see that $\frac{\partial q}{\partial a_0} = v_0(\tau)$ and $\frac{\partial q}{\partial\tau_0} = \frac{\partial q^I}{\partial\tau_0} = \sqrt{S_0}\, v_0(\tau)$ and so we see that $da_0 = \sqrt{S_0}\, d\tau_0$. So finally

$$Z = \frac{N'' e^{-S_0}\sqrt{S_0}\, d\tau_0}{\sqrt{\det{}'\left(\frac{d^2}{d\tau^2} + V''(q)\right)}} \tag{1.2.17}$$

where $\det'$ denotes the product over non-zero eigenvalues. We point out that these methods are completely general and will transfer directly to the study of gauge theories, namely that we must integrate over parameters which produce no change in the action and include a factor coming from the Jacobian. It is possible to explicitly calculate the determinant and the normalisation constant here but this will be of no use in our study of gauge theories and so we refer the interested reader to [10].

1.3 The Instanton in Gauge Theories

We now turn to the case of the instanton in gauge theories. We will start by considering the case of a pure Yang-Mills theory (no fermions) in $SU(2)$ again following [10]. However as instantons are always treated in Euclidean space we shall

first show how to formulate a Yang-Mills theory in Euclidean space. Briefly we have:

$$x_4^E = ix_0^M,\ x_i^E = x_i^M \tag{1.3.1}$$

$$A_4^E = -iA_0^M,\ A_i^E = -A_i^M \tag{1.3.2}$$

$$\gamma_4^E = \gamma_0^M,\ \gamma_i^E = -i\gamma_i^M \tag{1.3.3}$$

$$\psi^E = \psi^M,\ \bar{\psi}^E = i\bar{\psi}^M \tag{1.3.4}$$

where the 'M' and 'E' labels denote objects in Minkowski and Euclidean space respectively.

In a Yang-Mills theory the vacua are defined by $Tr(F_{\mu\nu}F_{\mu\nu}) = 0$ since this is the lowest order gauge invariant observable we can construct. This is clearly also satisfied if $F_{\mu\nu} = 0$. Note that, since instantons are always treated by means of the path integral, we will always be implicitly working in Euclidean space and so do not need to differentiate between covariant and contravariant indices, although we still employ the convention that repeated indices are summed over. The field strength tensor is vanishing if the gauge field has the form of a pure gauge i.e.

$$A_\mu = iU\partial_\mu U^\dagger,\ U \in SU(2) \implies F_{\mu\nu} = 0. \tag{1.3.5}$$

So demanding that we have a vacuum at infinity i.e. $F_{\mu\nu} = 0$ as $x \to \infty$ is equivalent to defining a map $f : S^3 \to SU(2)$ as spatial infinity in a four-dimensional space is topologically equivalent to the 3-sphere. Homotopy theory tells us that such maps are classified by $\Pi_3(SU_2) \cong \mathbb{Z}$. Hence we have one vacuum for every integer and all vacua are degenerate. We can classify this by

$$n = \frac{g^2}{32\pi^2}\int \mathrm{d}^4x\ Tr\left(\tilde{F}_{\mu\nu}F_{\mu\nu}\right) \tag{1.3.6}$$

where $\tilde{F}^{\mu\nu}$ is the dual field strength tensor, $\tilde{F}^{\mu\nu} = \frac{1}{2}\varepsilon^{\rho\sigma\mu\nu}F_{\rho\sigma}$. n is an integer known as the winding number or Pontryagin index and is the integer which classifies our separate vacua. As before the instanton is the solution which moves from one vacuum to another; the instanton increases the winding number by one whilst the

anti-instanton decreases it by one.

To look for the instanton and anti-instanton solutions we shall use the Bogomolny bound. First we note that:

$$\int \mathrm{d}^4x\, Tr\left(\left(F_{\mu\nu} \pm \tilde{F}_{\mu\nu}\right)^2\right) \geq 0 \implies \tag{1.3.7}$$

$$\int \mathrm{d}^4x\, Tr\left(F_{\mu\nu}F_{\mu\nu} + \frac{1}{4}F_{\rho\sigma}F_{\rho'\sigma'}\varepsilon_{\mu\nu\rho\sigma}\varepsilon_{\mu\nu\rho'\sigma'} \pm 2F_{\mu\nu}\tilde{F}_{\mu\nu}\right) \geq 0 \tag{1.3.8}$$

However we recognise the first term as four times the action and after using Eq. (1.3.6) along with the fact that

$$\varepsilon_{\mu\nu\rho\sigma}\varepsilon_{\mu\nu\rho'\sigma'} = 2\left(\delta_{\rho\rho'}\delta_{\sigma\sigma'} - \delta_{\rho\sigma'}\delta_{\sigma\rho'}\right) \tag{1.3.9}$$

we obtain

$$S \geq \frac{8\pi^2 \mid Q \mid}{g^2}. \tag{1.3.10}$$

From Eq. (1.3.7) we see that this bound is saturated when the field strength tensor is self-dual or anti self-dual, i.e. $F_{\mu\nu} = \pm\tilde{F}_{\mu\nu}$ and one can also see that a self-dual or anti-self-dual field strength tensor automatically satisfies the equations of motion:

$$D_\mu\tilde{F}_{\mu\nu} = \frac{1}{2}\varepsilon_{\mu\nu\rho\sigma}D_\mu F_{\rho\sigma} = \frac{1}{6}\varepsilon_{\mu\nu\rho\sigma}\left(D_\mu F_{\rho\sigma} + D_\rho F_{\sigma\mu} + D_\sigma F_{\mu\rho}\right) = 0 \tag{1.3.11}$$

where the second equality is just a relabelling of dummy indices and the final equality follows from the Bianchi identity. Hence to find the instanton, the solution which minimises the action and satisfies the classical equations of motion, we need only to find a potential $A_\mu(x)$, which gives rise to a self-dual field strength tensor.

Firstly since instantons are localised in spacetime we must have that as $x_\mu \to \infty$, $A_\mu \to \frac{i}{g}U\partial_\mu U^\dagger$ in order for the field strength to vanish. By means of a gauge transformation we can always choose the form of U at infinity to be

$$U = \frac{i\sigma^+_\mu x_\mu}{\sqrt{x^2}} \tag{1.3.12}$$

where $\sigma^\pm = (\sigma, \mp i\mathbb{1}_2)$. It can be verified that this matrix has the required properties

(i.e. it is an element of $SU(2)$). This then gives

$$A_\mu \to \frac{1}{g}\eta_{a\mu\nu}\sigma^a\frac{x_\nu}{x^2} \tag{1.3.13}$$

where the self-dual t'Hooft eta symbols are defined as[1]:

$$\eta_{a\mu\nu} = \begin{cases} \varepsilon_{a\mu\nu} & 1 \leq \mu,\nu \leq 3 \\ -\delta_{a\nu} & \mu = 4 \\ \delta_{a\mu} & \nu = 4 \\ 0 & \mu,\nu = 4. \end{cases} \tag{1.3.14}$$

The anti-self-dual eta symbols, $\bar{\eta}_{a\mu\nu}$ are defined the same way with a change in sign of the Kronecker deltas. We make an ansatz that the instanton retains the same angular structure and so

$$A_\mu\left(x_\nu\right) = \frac{1}{g}f\left(x^2\right)\eta_{a\mu\nu}\sigma^a\frac{x_\nu}{x^2} \tag{1.3.15}$$

where f is a function to be found. Our above boundary condition becomes $f\left(x^2\right) \to 1$ as $x^2 \to \infty$ and we also require $f\left(x^2\right) \to cx^2$ for some constant c as $x \to 0$ to avoid a singularity. With this ansatz we obtain

$$F_{\mu\nu} = \frac{2\sigma^a}{g}\left[\left(x^2f' - f + f^2\right)\left(\eta_{a\nu\rho}\frac{x_\mu x_\rho}{x^4} - \eta_{a\mu\rho}\frac{x_\nu x_\rho}{x^4}\right) - \frac{1}{x^2}\eta_{a\mu\nu}\left(f - f^2\right)\right]. \tag{1.3.16}$$

Constructing the dual field strength tensor then gives

$$\tilde{F}_{\mu\nu} = \frac{2\sigma^a}{g}\left[-\left(x^2f' - f + f^2\right)\left(\eta_{a\nu\rho}\frac{x_\mu x_\rho}{x^4} - \eta_{a\mu\rho}\frac{x_\nu x_\rho}{x^4}\right) - \eta_{a\mu\nu}f'\right] \tag{1.3.17}$$

Hence we see that the field strength tensor given by our ansatz is self-dual if f satisfies the following differential equation:

$$f\left(y\right) - f^2\left(y\right) = yf'\left(y\right). \tag{1.3.18}$$

[1]We have also used the identities $\sigma^-_\mu\sigma^+_\nu = \mathbb{1}_2\delta_{\mu\nu} + i\bar{\eta}_{a\mu\nu}\sigma^a$, $\sigma^+_\mu\sigma^-_\nu = \mathbb{1}_2\delta_{\mu\nu} + i\eta_{a\mu\nu}\sigma^a$.

By inspection one can see that the solution is given by

$$f(y) = \frac{y}{y + \rho^2} \tag{1.3.19}$$

where ρ is a constant of integration known as the scale of the instanton.

Now substituting this into our ansatz we obtain the full instanton solution:

$$A_\mu(x) = \frac{\sigma^a}{g}\eta_{a\mu\nu}\frac{x_\nu}{x^2 + \rho^2}. \tag{1.3.20}$$

This is more commonly written in component notation as

$$A^a_\mu(x) = \frac{2}{g}\eta_{a\mu\nu}\frac{(x - x_0)_\nu}{(x - x_0)^2 + \rho^2} \tag{1.3.21}$$

where here we have taken an instanton with centre x_0 rather than one centred at the origin. The anti-instanton can be obtained by the substitution $\eta_{a\mu\nu} \to \bar{\eta}_{a\mu\nu}$. This is the instanton in the so-called 'regular gauge', where the gauge potential has no singularities. However, when we later wish to perform integration (to LSZ reduce the gauge field), the instanton in this form does not fall off fast enough as $x^2 \to \infty$ for the integral to converge. We can solve this issue by performing a gauge transformation (Eq. (1.1.7)) with

$$U = \frac{i\sigma^+_\mu (x - x_0)_\mu}{\sqrt{(x - x_0)^2}}. \tag{1.3.22}$$

This then allows us to construct the instanton in the so-called 'singular gauge':

$$A^a_\mu(x) = \frac{2}{g}\bar{\eta}_{a\mu\nu}(x - x_0)_\nu \frac{\rho^2}{(x - x_0)^2\left((x - x_0)^2 + \rho^2\right)}. \tag{1.3.23}$$

Here we have only considered the case of instantons in $SU(2)$ but the more general case of an instanton in $SU(n)$ is easily constructed by embedding the $SU(2)$ solution in the upper-left corner of an $n \times n$ matrix. This can then be turned into a more general form by the use of gauge transformations.

In the next chapter we shall need to compute Green's functions involving the instanton; this follows a similar procedure to the computation of the partition function in

quantum mechanics shown in the preceding subsection. We need to integrate over the zero modes of the instanton, as in quantum mechanics the centre of the instanton (τ in quantum mechanics or $x_{0,\mu}$ in gauge theories) does not affect the action, leading to four zero modes in gauge theories. In the case of Yang-Mills theory, we also obtain new zero modes; one coming from the scale of the instanton and three coming from orientation in the $SU(2)$ space as it can clearly be seen from Eq. (1.3.10) that the action does not depend on ρ or the choice of gauge. Hence overall there are eight zero modes for the $SU(2)$ instanton.

In addition to integration over zero modes, we also obtain determinants of operators coming from the gaussian integration over fluctuations around the instanton solution. These determinants must be appropriately regulated since they are divergent. They must also be appropriately normalised. The technical and computational details of this process are not necessary for this thesis, we simply quote the appropriate results and refer the interested reader to [11].

1.3.1 Fermions

Now we may examine how the presence of fermions charged under the gauge group changes the theory.

Firstly we note that the presence of fermions, clearly does not affect the vacuum of the gauge fields and the instanton solution remains the same. However if we once again consider the path integral, noting that the fermionic part of the Lagrangian is given by the standard Dirac Lagrangian and recalling that ψ and $\bar{\psi}$ are in fact Grassmann-valued variables we obtain:

$$Z = \int \mathcal{D}\psi \mathcal{D}\bar{\psi}\, e^{\bar{\psi}\left(-i\not{D}-im\right)\psi} = \det\left(-i\not{D} - im\right). \tag{1.3.24}$$

It is a well known fact in the literature that this operator can have a zero eigenvalue only if the particle in question is massless. We will now see if there are any zero

modes of $i\not{D}$, i.e. whether we can find ψ such that

$$i\not{D}\psi = 0. \tag{1.3.25}$$

If we use the Weyl representation then this reduces to

$$\sigma_\mu^+ D_\mu \psi_L = 0,\ \sigma_\mu^- D_\mu \psi_R = 0. \tag{1.3.26}$$

We now act on the first equation with $\sigma_\mu^- D_\mu$ and the second with $\sigma_\mu^+ D_\mu$ to obtain

$$(D^2 + \frac{g}{2} F_{\mu\nu}\bar{\eta}^{a\mu\nu}\sigma^a)\psi_L = 0 \tag{1.3.27}$$

$$(D^2 + \frac{g}{2} F_{\mu\nu}\eta^{a\mu\nu}\sigma^a)\psi_R = 0 \tag{1.3.28}$$

In the instanton background, the field strength is dual so $F_{\mu\nu}\bar{\eta}^{a\mu\nu}$ vanishes, leaving us with $D^2\psi_L = 0$ and as $-D^2$ is a positive definite operator there are no non-trivial solutions. A similar argument applies to the right-handed spinor in the case of an anti-instanton. So we know that any zero modes (if they exist) must be right-handed for the instanton and left-handed for the anti-instanton. We can substitute into Eq. (1.3.27) the explicit form of the field strength using Eq. (1.3.21) to get[1]

$$D^2\psi_R = 12\frac{\rho^2}{\left((x-x_0)^2+\rho^2\right)^2}\psi_R. \tag{1.3.29}$$

It can be shown that the solution to this equation (in the regular gauge) is given by[2]

$$\psi_R^{\alpha u} = \frac{1}{\sqrt{2}\pi}\frac{\rho\epsilon^{\alpha u}}{\left(x^2+\rho^2\right)^{\frac{3}{2}}} \tag{1.3.30}$$

where α is the spin index and u is the $SU(2)$ index.

Hence we see that we obtain one right-handed fermion zero mode and one left-handed anti-fermionic zero mode for each light fermion in the theory. This is closely related to the chiral anomaly in QCD, which will be discussed in the next chapter.

[1] After using the relation $\eta_{a\mu\nu}\eta_{b\mu\nu} = 4\delta_{ab}$

[2] Also requiring the normalisation that $\int d^4x\, \psi^\dagger\psi = 1$

Chapter 2

The Instanton in QCD

Instantons are arguably the best motivated non-perturbative effects in the Standard Model, and yet they have not been observed so far. Our motivation in this chapter is to re-examine QCD instanton contributions to high-energy scattering processes at hadron colliders building up on the recent work [12] in establishing a robust QCD instanton computational formalism focused on applications to proton colliders and discussing experimental signatures.

The status of the SM as the theory of the currently accessible fundamental interactions in particle physics is well-established. To a large extent, the evidence for the SM as the most precise theoretical framework for describing strong and electroweak interactions comes from comparing perturbative calculations with the data from particle experiments. The reliance on the weakly coupled perturbation theory is justified at high energies thanks to the asymptotic freedom in Yang-Mills theories. There is, however, another consequence of the non-Abelian nature of the theory that necessitates an inclusion of non-perturbative effects. The non-Abelian nature of QCD and of the weak interactions is known to give rise to a rich vacuum structure in the Standard Model. This vacuum structure is well-understood in the semi-classical picture [13, 14] and amounts to augmenting the perturbative vacuum with an infinite set of topologically non-trivial vacuum sectors in a Yang-Mills theory.

Instanton field configurations [15] are classical solutions of Yang-Mills equations of

motion in Euclidean space which interpolate between the different semi-classical vacuum sectors in the theory. At weak coupling instantons provide dominant contributions to the path integral and correspond to quantum tunnelling between different vacuum sectors of the SM. These effects are beyond the reach of ordinary perturbation theory and in particular in the electroweak theory they lead to the violation of baryon plus lepton number (B+L), while in QCD instanton processes violate chirality [11, 16],

$$g + g \;\rightarrow\; n_g \times g \;+\; \sum_{f=1}^{N_f} (q_{Rf} + \bar{q}_{Lf})\,, \tag{2.0.1}$$

where N_f is the number of light (i.e. nearly massless relative to the energy scale probed by the instanton) quark flavours. The QCD instanton-generated process, Eq. (2.0.1), with two gluons in the initial state going to an arbitrary number, n_g, of gluons in the final state along with $2N_f$ quarks will be the focus of our discussion in Section 2.2.

The purpose of this chapter is to provide the most up-to-date computationally robust calculation of QCD instanton contributions to high-energy scattering processes relevant for hadron colliders. At the level of the partonic instanton cross-section, there are two main ingredients in the approach we follow. We shall use the optical theorem approach that will effectively allow us to sum over all final states with arbitrary numbers of gluons. This is achieved by evaluating the imaginary part of the forward elastic scattering amplitude computed in the background of the instanton–anti-instanton configuration. This formalism was originally developed in [17] based on the instanton–anti-instanton field configuration constructed in [18].

The second ingredient of our approach relies on the inclusion of certain higher-order effects in the instanton perturbation theory. Specifically we will take into account resummed radiative exchanges between the hard partons in the initial state [19, 20], as they provide the dominant contribution to breaking the classical scale invariance of QCD in quantum theory. Inclusion of these quantum effects (often referred to in the instanton literature as the hard-hard quantum corrections) is required in order

to resolve the well-known non-perturbative infra-red (IR) problem that arises from the contribution of QCD instantons with large scale-sizes as was first shown in [12]. We will see that the contribution of QCD instantons with large size is automatically cut-off by the inclusion of these quantum effects.

To a large extent the theory formalism we employ for computing QCD instanton rates is the same as in the earlier work [12], but we are able to carry out a more complete evaluation of instanton integrals without relying on the saddle-point approximation. Specifically, in Sec. 2.2.3 we will numerically compute integrals over all instanton–anti-instanton collective coordinates that correspond to positive modes of the instanton–anti-instanton action. Only the final integration over the single negative mode that gives rise to the imaginary part of the amplitude, as required by the optical theorem, will be carried out in the saddle-point approximation. There are also a number of other more minor technical improvements, in particular in relation to the computation of the mean number of gluons in the final state in Sec. 2.3.1. Our results summarised in Tables 2.1 and 2.2 present cross-sections for instanton-generated processes at partonic and hadronic levels for the LHC and the Tevatron as well as for 30 TeV and 100 TeV future hadron colliders.

In section 2.2.4 we explain how to generalise the calculation of the instanton process to the case where a jet is emitted from one of the initial state partons. We find that cross-sections calculated for processes where the instanton recoils against a jet with large momentum are too small to be observable at any present or envisioned high-energy collider. In order to obtain sensitivity to instantons one must disentangle their spherical radiation profile, made of fairly soft jets, from the perturbative backgrounds.

The event topology of instanton events consisting of a spherically symmetric energy distribution and a large number of final-state objects is visibly distinguishable from the usual few-jet events generated in perturbative-QCD processes at the LHC, as discussed in Sec. 2.3, but QCD instanton processes occur predominantly at small partonic centre-of-mass energies. The combination of both these characteristics

suggests that QCD-instanton events are *soft bombs* [12], using the terminology of [21], where the phenomenology of such events was first investigated in the context of beyond the Standard Model physics. In our case the soft bombs are fully Standard Model-made. At high-energy colliders, such events struggle to pass trigger and event reconstruction cuts. In Secs. 2.3.3 and 2.3.4 we assess whether the comparably large hadronic instanton cross-sections might give rise to visible signatures at hadron colliders, in particular the LHC or the Tevatron. Examination of data collected with a minimum bias trigger shows that it should be possible to either discover instantons or severely constrain their cross-section.

In this chapter we will first develop some of the underlying theory of the QCD instanton before examining in detail the cross section and phenomenology.

2.1 Theory

As mentioned in the previous chapter, the fermionic zero modes of the instanton are closely related to the chiral anomaly in QCD and so we shall derive the relevant formulae here. It is well known that the Lagrangian of a massless fermion is classically invariant under the symmetry $\psi \to \exp\left(i\alpha\gamma^5\right)\psi$ and so by Noether's theorem one would expect to find a conserved current $j^\mu = \bar{\psi}\gamma^\mu\gamma^5\psi$, however if one actually calculates the divergence of the Noether current it is non-vanishing. This is the so-called chiral anomaly or Adler-Bell-Jackiw (ABJ) anomaly. We briefly return to Minkowski space for the derivation of this result; although the same derivation is possible in Euclidean space we perform it in Minkowski space for convenience to avoid changing the definition of the Noether current. Here we follow [22,23] although this approach to the anomaly was first formulated in [24,25].

Consider the action of a massless fermion in the Weyl representation:

$$S = \int \mathrm{d}^4x \, \left(i\psi_L\sigma_\mu^+ D^\mu\psi_L + i\psi_R\sigma_\mu^- D^\mu\psi_R\right). \tag{2.1.1}$$

We can now consider the path integral and as usual we expand in terms of a basis

given by the eigenfunctions of $i\not{D}$ and integrate over the coefficients (c.f. Eq. (1.2.13), Eq. (1.3.24)). Note that the measure is defined to be

$$\mathcal{D}\bar{\psi}\mathcal{D}\psi = \prod_n db_n da_n \tag{2.1.2}$$

where a_n are the coefficients of the expansion of ψ in terms of eigenfunctions of the Dirac operator, i.e. $i\not{D}\phi_n = \lambda_n\phi_n$ and $\psi = \sum_n a_n\phi_n$. Similarly b_n are the coefficients of the expansion of $\bar{\psi}$. If we now consider an infinitesimal transformation then we have

$$\delta\psi = i\epsilon\gamma^5\psi \implies \sum_n \delta a_n\phi_n = i\epsilon\sum_m a_m\gamma^5\phi_m \tag{2.1.3}$$

where ϕ_n are our basis elements. Using the orthogonality of our basis elements:

$$\int \mathrm{d}^4x\,\bar{\phi}_n\phi_m = \delta_{mn} \tag{2.1.4}$$

we then have

$$\delta a_n = i\sum_m \int \mathrm{d}^4x\,\epsilon\bar{\phi}_n\gamma^5\phi_m a_m = \epsilon\sum_m X_{nm}a_m \tag{2.1.5}$$

where we have defined $X_{nm} = i\int d^4x\,\bar{\phi}_n\gamma^5\phi_m$. This then allows us to compute the Jacobian for our transformation but due to the properties of Grassmann variables, it comes with the inverse determinant:

$$J = \det{}^{-1}\left(\delta_{nm} + \epsilon X_{nm}\right). \tag{2.1.6}$$

Since we are looking at an infinitesimal transformation we work to leading order:

$$J \approx \det\left(1-\epsilon X\right) \approx \det e^{-\epsilon X} = e^{-\epsilon Tr X}. \tag{2.1.7}$$

To calculate this trace we must introduce a regulator and aim to use information about eigenvalues of the Dirac operator:

$$Tr\,X = i\int \mathrm{d}^4x\,\langle x|\mathrm{tr}\;\gamma^5|x\rangle = \lim_{\Lambda\to\infty} i\int \mathrm{d}^4x\,\langle x|\mathrm{tr}\left(\gamma^5 e^{\left(i\not{D}\right)^2/\Lambda^2}\right)|x\rangle \tag{2.1.8}$$

where tr traces only over spinor indices. We then perform a change of basis.

$$\langle x|\gamma^5 e^{\left(i\not{D}\right)^2/\Lambda^2}|x\rangle = \int \frac{\mathrm{d}^4k}{(2\pi)^4}\langle x|k\rangle\langle k|\mathrm{tr}\left(\gamma^5 e^{\left(i\not{D}\right)^2/\Lambda^2}\right)|x\rangle =$$

$$\int \frac{\mathrm{d}^4k}{(2\pi)^4} e^{-ik.x} \mathrm{tr}\left(\gamma^5 e^{\left(i\not{D}\right)^2/\Lambda^2}\right) e^{ik.x} \tag{2.1.9}$$

If we now use the fact that $\not{D}^2 = D^2 - \frac{ig}{2}\gamma^\mu\gamma^\nu F_{\mu\nu}$ and ignore higher order terms coming from the BCH formula (which will vanish in the limit $\Lambda \to \infty$) then we get:

$$\exp\left(-ik.x\right)\exp\left(\frac{\left(i\not{D}\right)^2}{\Lambda^2}\right)\exp\left(ik.x\right) = \exp\left(\frac{-\left(ik_\mu - iA_\mu\right)^2}{\Lambda^2}\right)\exp\left(\frac{ig}{2}\gamma^\mu\gamma^\nu F_{\mu\nu}\right) \tag{2.1.10}$$

Since we are computing the trace over spinor indices only the second term is directly relevant to the trace. We then Taylor expand this, the first two terms vanish upon multiplying by γ^5 and taking the trace to leave[1]:

$$Tr\, X = -i\frac{g^2}{8\Lambda^4}\int \frac{\mathrm{d}^4k}{(2\pi)^4} e^{k^2/\Lambda^2} Tr\left(\gamma^5\gamma^\mu\gamma^\nu\gamma^\rho\gamma^\sigma\right) Tr\left(F_{\mu\nu}F_{\rho\sigma}\right) \tag{2.1.11}$$

$$= -\frac{g^2}{2\Lambda^4}\epsilon^{\mu\nu\rho\sigma} Tr\left(F_{\mu\nu}F_{\rho\sigma}\right)\int \frac{\mathrm{d}^4k}{(2\pi)^4} e^{k^2/\Lambda^2} \tag{2.1.12}$$

having also performed a trivial shift in the k-integration to eliminate the gauge field. Finally after Wick rotation of the integral we have

$$\int \frac{\mathrm{d}^4k}{(2\pi)^4} e^{k^2/\Lambda^2} = i\int \frac{\mathrm{d}^4k_E}{(2\pi)^4} e^{-k_E^2/\Lambda^2} = \frac{i\Lambda^4}{16\pi^2}. \tag{2.1.13}$$

Hence

$$Tr\, X = -\frac{ig^2}{32\pi^2}\epsilon^{\mu\nu\rho\sigma} Tr\left(F_{\mu\nu}F_{\rho\sigma}\right). \tag{2.1.14}$$

We now return to computing the divergence of the Noether current. Under an infinitesimal transformation, with parameter ϵ, we have

$$\delta S = \int \mathrm{d}^4x\, \epsilon\partial_\mu j^\mu \tag{2.1.15}$$

with $j^\mu = \bar{\psi}\gamma^\mu\gamma^5\psi$. Hence

$$Z \to \int \mathcal{D}\bar{\psi}'\mathcal{D}\psi'\, e^{iS\left[\psi',\bar{\psi}'\right]}$$

$$= \int \mathcal{D}\bar{\psi}'\mathcal{D}\psi'\, e^{iS\left[\psi,\bar{\psi}\right]+i\int \mathrm{d}^4x\,\epsilon\partial_\mu j^\mu}$$

[1] We follow the conventions of [9] where $\gamma^5 = i\gamma^0\gamma^1\gamma^2\gamma^3$ and so tr $\gamma^5 = 0$, $\mathrm{tr}\left(\gamma^5\gamma^\mu\gamma^\nu\right) = 0$, $\mathrm{tr}\left(\gamma^5\gamma^\mu\gamma^\nu\gamma^\rho\gamma^\sigma\right) = -4i\epsilon^{\mu\nu\rho\sigma}$.

$$= \int \mathcal{D}\bar{\psi}\mathcal{D}\psi \, e^{i\int \mathrm{d}^4x \epsilon \frac{g^2}{16\pi^2}\epsilon^{\mu\nu\rho\sigma}F_{\mu\nu}F_{\rho\sigma}} e^{iS[\psi,\bar{\psi}]+i\int \mathrm{d}^4x\, \epsilon\partial_\mu j^\mu}. \tag{2.1.16}$$

Note that we obtain two factors of the Jacobian due to the separate integrals over ψ and $\bar{\psi}$. Since we must have $Z[\psi] = Z[\psi']$ as the function is just a dummy variable we obtain:

$$\partial_\mu j^\mu = -\frac{1}{8\pi^2}F_{\mu\nu}\tilde{F}^{\mu\nu} \tag{2.1.17}$$

after using the definiton of the dual field strength. If instead there are N_f flavours of massless fermions

$$\partial_\mu j^\mu = -\frac{N_f}{8\pi^2}F_{\mu\nu}\tilde{F}^{\mu\nu}. \tag{2.1.18}$$

Thus we see that

$$\Delta Q^A = \int \mathrm{d}^4x\, \partial_0 j^0 = -\int \mathrm{d}^4x\, \frac{N_f}{8\pi^2}F_{\mu\nu}\tilde{F}^{\mu\nu} = -2N_f\Delta n \tag{2.1.19}$$

where n is the winding number. Note above we have neglected a total divergence $(-\partial_i j^i)$ which vanishes upon integration. Thus we see that the fermionic zero modes of the instanton violate the axial symmetry by precisely the right amount. To expand on this we have the two identities:

$$\int \mathcal{D}\bar{\psi}\mathcal{D}\psi \, e^{\bar{\psi}A\psi} = \det A \tag{2.1.20}$$

$$\int \mathcal{D}\bar{\psi}\mathcal{D}\psi \, \bar{\psi}_n\psi_n e^{\bar{\psi}A\psi} = \det{}_n A \tag{2.1.21}$$

where ψ_n is the eigenfunction of A with eigenvalue λ_n and $\det_n A$ denotes the product of the eigenvalues of A, not including λ_n. Hence we see that in order to get a non-zero result, all of the fermionic zero modes must sit in front of the path integral and therefore couple to the instanton and be produced, satisfying the chiral anomaly as required.

We anticipate the need for the optical theorem and derive it here. To derive the optical theorem, we first write the scattering matrix as $S = \mathbb{1} + iT$. Unitarity of the S-matrix then gives

$$SS^\dagger = 1 \implies -i\left(T - T^\dagger\right) = T^\dagger T. \tag{2.1.22}$$

We now sandwich both sides of this identity between states $|k_1 k_2\rangle$ and $|p_1 p_2\rangle$[1]:

$$-(2\pi)^4 \delta^{(4)}(k_1+k_2-p_1-p_2)\, i\left(\mathcal{M}(k_1k_2\to p_1p_2)-\mathcal{M}^*(p_1p_2\to k_1k_2)\right)$$
$$=\langle p_1p_2|T^\dagger T|k_1k_2\rangle. \tag{2.1.23}$$

To compute the right hand side we insert a complete set of states:

$$\begin{aligned}\langle p_1p_2|T^\dagger T|k_1k_2\rangle =& \sum_n \left(\prod_{i=1}^n \int \frac{\mathrm{d}^3q_i}{(2\pi)^3}\frac{1}{2E_i}\right)\langle p_1p_2|T^\dagger|\{q_i\}\rangle\langle\{q_i\}|T|k_1k_2\rangle \\ =& \sum_n \left(\prod_{i=1}^n \int \frac{\mathrm{d}^3q_i}{(2\pi)^3}\frac{1}{2E_i}\right)\mathcal{M}^*(p_1p_2\to\{q_i\})\,\mathcal{M}(k_1k_2\to\{q_i\}) \\ & (2\pi)^4\delta^{(4)}\left(k_1+k_2-\sum_i q_i\right)\delta^{(4)}\left(p_1+p_2-\sum_i q_i\right).\end{aligned} \tag{2.1.24}$$

We now set $p_1,\, p_2 = k_1,\, k_2$, i.e. the initial and final states are now the same and divide by E_{CM}, p_{CM}. Following standard treatments, e.g. [9], this then gives:

$$\begin{aligned}&-\frac{(2\pi)^4}{E_{CM}p_{CM}}\delta^{(4)}(0)\, i\left(\mathcal{M}(k_1k_2\to k_1k_2)-\mathcal{M}^*(k_1k_2\to k_1k_2)\right) \\ &=\sum_n\left(\prod_{i=1}^n\int\frac{\mathrm{d}^3q_i}{(2\pi)^3}\frac{1}{2E_i}\right)\frac{1}{E_{CM}p_{CM}}|\mathcal{M}(k_1k_2\to\{q_i\})|^2\delta^{(4)}\left(k_1+k_2-\sum_i q_i\right) \\ &=\sum_n\left(\prod_{i=1}^n\int\frac{\mathrm{d}^3q_i}{(2\pi)^3}\frac{1}{2E_i}\right)\sigma(k_1k_2\to\{q_i\})\end{aligned} \tag{2.1.25}$$

This is usually written as (taking the initial state to be massless):

$$\sigma_{tot}(k_1k_2\to\text{anything})=\frac{1}{s}\mathrm{Im}\mathcal{M}(\mathrm{k_1k_2}\to\mathrm{k_1k_2}). \tag{2.1.26}$$

2.2 The Instanton Cross Section

We now return to examination of the instanton. The scattering amplitude for the $2\to n_g+2N_f$ instanton-generated process, Eq. (2.0.1), is computed by expanding the path integral around the instanton field configuration.

The amplitude takes the form of an integral over the instanton collective coordinates,

[1] Recall $\langle p_1\dots p_m|T|k_1\dots k_n\rangle=(2\pi)^4\delta^{(4)}\left(\sum_{i=1}^n k_i-\sum_{j=1}^m p_j\right)\mathcal{M}(k_1\dots k_n\to p_1\dots p_n)$

$$\mathcal{A}_{2\to n_g+2N_f} = \int \mathrm{d}^4x_0 \int_0^\infty \mathrm{d}\rho\, D(\rho) e^{-S_I} \prod_{i=1}^{n_g+2} A^{\mathrm{inst}}_{\mathrm{LSZ}}(p_i;\rho) \prod_{j=1}^{2N_f} \psi^{(0)}_{\mathrm{LSZ}}(p_j;\rho). \tag{2.2.1}$$

The integral, Eq. (2.2.1), is over the instanton position x_0^μ and the scale-size collective coordinate ρ, and it involves the instanton density function $D(\rho)$, the semiclassical suppression factor e^{-S_I} by the instanton action.

Eq. (2.2.1) also contains the product of vector boson and fermion field configurations, one for each external leg of the amplitude, computed on the instanton solutions, and LSZ-reduced.

The instanton density $D(\rho)$ in Eq. (2.2.1) arises from computing quadratic fluctuation determinants in the instanton background in the path integral. This is a one-loop effect in the perturbation theory around the instanton and the result is given by [11],

$$D(\rho,\mu_r) = \kappa \frac{1}{\rho^5} \left(\frac{2\pi}{\alpha_s(\mu_r)}\right)^{2N_c} (\rho\mu_r)^{b_0}, \tag{2.2.2}$$

where κ is the normalisation constant of the instanton density in the $\overline{\mathrm{MS}}$ scheme [26–28],

$$\kappa = \frac{2e^{5/6-1.511374N_c}}{\pi^2(N_c-1)!(N_c-2)!} e^{0.291746N_f} \simeq 0.0025 e^{0.291746N_f}, \tag{2.2.3}$$

and $b_0 = (11/3)N_c - (2/3)N_f$.

Expressions for the LSZ-reduced instanton field insertions on the right hand side of the integral in Eq. (2.2.1) are obtained from the momentum-space representation of the instanton solution, Eq. (1.3.23),

$$A^{a\,\mathrm{inst}}_{LSZ}(p,\lambda) = \lim_{p^2\to 0} p^2 \epsilon^\mu(\lambda) A^{a\,\mathrm{inst}}_\mu(p) = \epsilon^\mu(\lambda) \bar{\eta}^a_{\mu\nu} p_\nu \frac{4i\pi^2\rho^2}{g} e^{ip\cdot x_0}, \tag{2.2.4}$$

where $\epsilon^\mu(\lambda)$ is the polarisation vector for a gluon with a helicity λ. A similar expression also holds for the LSZ-amputated fermion zero modes, in this case, $\psi^{(0)}_{\mathrm{LSZ}} \propto \rho$ rather than $A^{\mathrm{inst}}_{LSZ} \propto \rho^2$ for the gauge field.

Combining all the ingredients above, it is now easy to see that the ρ-integral in the leading-order instanton amplitude, Eq. (2.2.1) is power-like divergent – a well-known fact that signals the breakdown of the leading-order instanton calculation in QCD at

large distances ($\rho \gtrsim 1/\Lambda$) where the coupling becomes strong and the semi-classical approximation is invalid. Instantons are solutions to classical equations and unless quantum effects due to field fluctuations around instantons are appropriately taken into account, there is no scale in the microscopic QCD Lagrangian to cut-off large values of the instanton size – ρ is a classically flat direction. To break classical scale-invariance we need to include quantum corrections that describe interactions of the external states. This amounts to inserting propagators in the instanton background between pairs of external fields in the pre-exponential factor in Eq. (2.2.1) and re-summing the resulting perturbation theory. The dominant effect comes from interactions between the two initial hard gluons [19] (these are the states that carry the largest kinematic invariant $p_1 \cdot p_2 = \hat{s}/2$). In [20] Mueller showed that these quantum corrections formally exponentiate and the resulting expression for the resummed quantum corrections around the instanton generates the factor,

$$e^{-(\alpha_s(\mu_r)/16\pi)\rho^2 E^2 \log E^2/\mu_r^2}, \tag{2.2.5}$$

where E is the partonic CoM energy, $E^2 \equiv \hat{s}$. This exponential factor provides an automatic cut-off of large instanton sizes and the instanton integral over ρ can now be safely evaluated.

To proceed, we need to select a value for the renormalisation scale μ_r. Recall that the integrand in Eq. (2.2.1) contains the factor,

$$(\rho\mu_r)^{b_0}\, e^{-\frac{2\pi}{\alpha_s(\mu_r)}} \;=\; e^{-\frac{2\pi}{\alpha_s(1/\rho)}}\,, \tag{2.2.6}$$

where $(\rho\mu_r)^{b_0}$ comes from the instanton density and the factor $e^{-\frac{2\pi}{\alpha_s(\mu_r)}}$ accounts for the contribution of the instanton action $S_I = \frac{2\pi}{\alpha_s(\mu_r)}$. The r.h.s. of Eq. (2.2.6) is RG-invariant at one-loop, it does not depend on the choice of μ_r, instead the scale of the running coupling constant is set at the inverse instanton size. To take advantage of this and to remove large powers of ρ from the integrand, from now on and until

the end of this section, we will set the RG scale value at the instanton size,

$$\mu_r \;=\; 1/\rho\,. \tag{2.2.7}$$

The amplitude integrand including Mueller's exponentiated quantum effect is given by,

$$\begin{aligned}\mathcal{A}_{2\to n_g+2N_f} = \kappa \int \mathrm{d}^4x_0 \int_0^\infty \frac{\mathrm{d}\rho}{\rho^5}\left(\frac{2\pi}{\alpha_s}\right)^6 e^{-\frac{2\pi}{\alpha_s(1/\rho)}-\frac{\alpha_s(1/\rho)}{16\pi}\rho^2E^2\log E^2\rho^2} \\ \times \prod_{i=1}^{n_g+2} A^{\mathrm{inst}}_{\mathrm{LSZ}}(p_i;\rho)\prod_{j=1}^{2N_f}\psi^{(0)}_{\mathrm{LSZ}}(p_j;\rho).\end{aligned} \tag{2.2.8}$$

Keeping careful track of the powers of ρ, the resulting integral in Eq. (2.2.8) is proportional to the following expression[1]:

$$\mathcal{A}_{2\to n_g+2N_f} \sim \int_0^\infty \mathrm{d}\rho\,(\rho^2)^{n_g+2+N_f-5/2} e^{-\frac{\alpha_s(1/\rho)}{16\pi}E^2\rho^2\log(E^2\rho^2)-\frac{2\pi}{\alpha_s(1/\rho)}}. \tag{2.2.9}$$

The integral is no longer divergent in the IR limit of large ρ and can be evaluated and the resulting expression for the amplitude can be used to compute the instanton cross-section. In the following section we will obtain the instanton cross-section in a more efficient manner using the optical theorem approach.

Before we conclude this section, we would like to comment on the structure of the leading-order instanton expression, Eq. (2.2.8). Note that the integrand on the right hand side of Eq. (2.2.8) contains a simple product of bosonic and fermionic components of instanton field configurations, one for each external line of the amplitude. Such fully factorised structure of the field insertions implies that at the leading order in instanton perturbation theory there are no correlations between the momenta of the external legs in the instanton amplitude. Emission of individual particles in the final state are mutually independent, apart from the overall momentum conservation. The expression in Eq. (2.2.8) looks like a multi-particle point-like vertex integrated over the instanton position and size. Thanks to its point-like structure, the instanton

[1]The integral over the instanton position $\int d^4x_0$ gives a momentum-conserving delta function which we drop, along with the overall constant and ρ-independent factors

vertex in the centre of mass frame describes the scattering process into a spherically symmetric multi-particle final state. The number of gluons, n_g, is unconstrained and can be as large as is energetically viable [29, 30] (in practice, the dominant contribution will come from $\langle n_g \rangle \sim 4\pi/\alpha_s \gg 1$), and a fixed number of quarks (a $q_L \bar{q}_R$ pair for each light quark flavour).

2.2.1 The Optical theorem approach

To compute a total parton-level instanton cross-section $\hat{\sigma}_{\rm tot}^{\rm inst}$ for the process $gg \to X$, we use the optical theorem to relate the cross-section to the imaginary part of the forward elastic scattering amplitude computed in the background of the instanton–anti-instanton ($I\bar{I}$) configuration,

$$\hat{\sigma}_{\rm tot}^{\rm inst} = \frac{1}{E^2} {\rm Im} \mathcal{A}_4^{\rm I\bar{I}}({\rm p}_1, {\rm p}_2, -{\rm p}_1, -{\rm p}_2), \tag{2.2.10}$$

where $E = \sqrt{\hat{s}} = \sqrt{(p_1 + p_2)^2}$ is the partonic CoM energy.

If we wish to compute the instanton cross section using the optical theorem we must compute the amplitude $\langle gg \to I | \bar{I} \to gg \rangle$. As usual this matrix element may be calculated using the path integral:

$$\begin{aligned} &\langle 0 | T\{A_{1,\mu}(w)\, A_{2,\nu}(x)\, A_{3,\rho}(y)\, A_{4,\sigma}(z)\} | 0 \rangle = \\ &\int \mathcal{D}A\, A_{1,\mu}(w)\, A_{2,\nu}(x)\, A_{3,\rho}(y)\, A_{4,\sigma}(z)\; e^{-S}. \end{aligned} \tag{2.2.11}$$

As alway it is more convenient to work in momentum space and so we use the LSZ theorem:

$$\begin{aligned} &\langle 0 | T\{A_{1,\mu}(p_1)\, A_{2,\nu}(p_2)\, A_{3,\rho}(p_3)\, A_{4,\sigma}(p_4)\} | 0 \rangle = \\ &\int \mathcal{D}A\, A_{1,\mu}^{LSZ}(p_1)\, A_{2,\nu}^{LSZ}(p_2)\, A_{3,\rho}^{LSZ}(p_3)\, A_{4,\sigma}^{LSZ}(p_4)\; e^{-S} \end{aligned} \tag{2.2.12}$$

where A_μ^{LSZ} is the field treated with the usual LSZ procedure. As shown in the previous section the integrals over fields become determinants over operators (raised to the power $-1/2$ for bosonic fields) with integrals over zero modes. All Jacobians

(associated with going from integrals over fields to integrals over zero modes) as well as determinants were calculated in [11]. With these results we can proceed; the collective-coordinate integral for the forward scattering amplitude reads,

$$\mathcal{A}_4^{I\bar{I}}(p_1,p_2,-p_1,-p_2) = \int_0^\infty \mathrm{d}\rho \int_0^\infty \mathrm{d}\bar{\rho} \int \mathrm{d}^4R \int \mathrm{d}\Omega\, D(\rho)D(\bar{\rho}) e^{-S_{I\bar{I}} - \frac{\alpha_s}{16\pi}(\rho^2+\bar{\rho}^2)E^2 \log \frac{E^2}{\mu_r^2}} A_{LSZ}^{\mathrm{inst}}(p_1) A_{LSZ}^{\mathrm{inst}}(p_2) A_{LSZ}^{\overline{\mathrm{inst}}}(-p_1) A_{LSZ}^{\overline{\mathrm{inst}}}(-p_2) \mathcal{K}_{\mathrm{ferm}}. \tag{2.2.13}$$

The only term appearing in Eq. (2.2.13) which is yet to be defined is $\mathcal{K}_{\mathrm{ferm}}$. This factor arises from the overlap of the fermion zero modes in the instanton and anti-instanton background. A precise formula will be defined later in this section.

For the reader's convenience in Appendix A we cover in more detail the main steps of the formalism to represent the forward elastic scattering amplitude as the integral over collective coordinates of the instanton–anti-instanton field configuration following the valley method approach developed in [17, 18, 31–34].

For our purposes it is sufficient to simply note that the instanton–anti-instanton gauge field is a trajectory in the topological charge zero sector of the field configuration space parameterised by instanton and anti-instanton collective coordinates. This trajectory interpolates between the sum of an infinitely separated instanton and anti-instanton and the perturbative vacuum,

$$R \to \infty : \quad A_\mu^{I\bar{I}}(x) \to A_\mu^I(x - x_0) + A_\mu^{\bar{I}}(x - x_0 - R)\,, \tag{2.2.14}$$

$$R \to 0 : \quad A_\mu^{I\bar{I}}(x) \to 0\,. \tag{2.2.15}$$

The configuration $A_\mu^{I\bar{I}}(x)$ for arbitrary values of the collective coordinates is determined by solving the gradient flow equation known as the valley equation.

In Eq. (2.2.13) we integrate over all collective coordinates: ρ and $\bar{\rho}$ are the instanton and anti-instanton sizes, $R_\mu = (R_0, \vec{R})$ is the separation between the I and $\bar{I}$ positions in Euclidean space and Ω is the 3×3 matrix of relative $I\bar{I}$ orientations in the $SU(3)$ colour space. $D(\rho)$ and $D(\bar{\rho})$ represent the instanton and the anti-instanton densities, Eq. (2.2.2), and the field insertions $A_{LSZ}^{\mathrm{inst}}(p)$ and $A_{LSZ}^{\overline{\mathrm{inst}}}(p')$ are the LSZ-

reduced instanton and anti-instanton fields, Eq. (2.2.4). For each pair of gluon legs with the same incoming/outgoing momentum we have,

$$\frac{1}{3}\sum_{a=1}^{3}\frac{1}{2}\sum_{\lambda=1,2}A^{a\,\mathrm{inst}}_{LSZ}(p,\lambda)A^{a\,\overline{\mathrm{inst}}}_{LSZ}(-p;\lambda)=\frac{1}{6}\left(\frac{2\pi^2}{g}\rho\bar{\rho}\sqrt{\hat{s}}\right)^2 e^{iR\cdot p}, \tag{2.2.16}$$

and now for the combination of all four external gluon insertions in Eq. (2.2.13) we have,

$$A^{\mathrm{inst}}_{LSZ}(p_1)A^{\mathrm{inst}}_{LSZ}(p_2)A^{\overline{\mathrm{inst}}}_{LSZ}(-p_1)A^{\overline{\mathrm{inst}}}_{LSZ}(-p_2)=\frac{1}{36}\left(\frac{2\pi^2}{g}\rho\bar{\rho}\sqrt{\hat{s}}\right)^4 e^{iR\cdot(p_1+p_2)}. \tag{2.2.17}$$

The contribution $e^{iR\cdot(p_1+p_2)}$ arises from the exponential factors $e^{ip_i\cdot x_0}$ and $e^{-ip_i\cdot\bar{x}_0}$ from the two instanton and two anti-instanton legs, which upon Wick rotation to Minkowski space becomes $e^{R_0\sqrt{\hat{s}}}$.

We now turn to the exponent in Eq. (2.2.13). The action of the instanton–anti-instanton configuration was computed in [17, 32, 33], it is a function of a single variable z, known as the conformal ratio of the (anti-)instanton collective coordinates,

$$z=\frac{R^2+\rho^2+\bar{\rho}^2+\sqrt{(R^2+\rho^2+\bar{\rho}^2)^2-4\rho^2\bar{\rho}^2}}{2\rho\bar{\rho}} \tag{2.2.18}$$

and takes the form $S_{I\bar{I}}(z)=\frac{4\pi}{\alpha_s}\mathcal{S}(z)$ where,

$$\mathcal{S}(z)=3\frac{6z^2-14}{(z-\frac{1}{z})^2}-17-3\log(z)\left(\frac{(z-\frac{5}{z})(z+\frac{1}{z})^2}{(z-\frac{1}{z})^3}-1\right). \tag{2.2.19}$$

For more detail on the derivation of the instanton–anti-instanton valley trajectory and a plot of the action as a function of the inter-instanton separation we refer the reader to Appendix A and [17, 18, 32, 33].

The second term in the exponent in Eq. (2.2.13) is recognised as Mueller's quantum effect of the hard-hard gluon exchanges in the initial state, Eq. (2.2.5), and a similar factor for the anti-instanton gluon exchanges in the final state. It comes from calculating the gluon propagator in the instanton background and inserting this propagator into all loop-level diagrams involving the two initial state gluons. If one then takes the high-energy limit and on-shell gluons then these corrections formally

exponentiate giving the term in Eq. (2.2.13). See Sec. 3.3.1 for more details.

The final factor appearing in Eq. (2.2.13) that needs to be defined is $\mathcal{K}_{\rm ferm}(z)$. This simply comes from calculating the overlap between the instanton and anti-instanton fermion zero modes [35],

$$\omega = \int \mathrm{d}^4x\, \psi_0^{\bar{I}}(x)\, i\not{D}\psi_0^{I}(x)\,. \tag{2.2.20}$$

[35] also found an integral expression for this which was then calculated analytically in [36] and this expression is then raised to the power $2N_f$, the number of fermions. It arises from the $2N_f$ fermions in the final state of the process, Eq. (2.0.1). As the instanton–anti-instanton action function $\mathcal{S}(z)$, the fermion factor $\mathcal{K}_{\rm ferm}(z)$ is a function of a single variable – the conformal ratio z defined in Eq. (2.2.18). We have,

$$\mathcal{K}_{\rm ferm} = (\omega_{\rm ferm})^{2N_f}, \tag{2.2.21}$$

where $\omega_{\rm ferm}(z)$ was computed in [36],

$$\omega_{\rm ferm}(z) = \frac{3\pi}{8}\frac{1}{z^{3/2}}\,{}_2F_1\left(\frac{3}{2},\frac{3}{2};4;1-\frac{1}{z^2}\right). \tag{2.2.22}$$

Putting everything together we can now write down the instanton cross-section, Eq. (2.2.10), as a finite-dimensional integral in the form,

$$\begin{aligned}\hat{\sigma}_{\rm tot}^{\rm inst} \simeq & \frac{1}{E^2}\mathrm{Im}\frac{\kappa^2\pi^4}{36\cdot 4}\int\frac{\mathrm{d}\rho}{\rho^5}\int\frac{\mathrm{d}\bar{\rho}}{\bar{\rho}^5}\int\mathrm{d}^4\mathrm{R}\int\mathrm{d}\Omega\left(\frac{2\pi}{\alpha_{\rm s}(\mu_{\rm r})}\right)^{14}(\rho^2\mathrm{E})^2(\bar{\rho}^2\mathrm{E})^2\mathcal{K}_{\rm ferm}(\mathrm{z})\\ & (\rho\mu_r)^{b_0}(\bar{\rho}\mu_r)^{b_0}\exp\left(R_0E-\frac{4\pi}{\alpha_s(\mu_r)}\mathcal{S}(z)-\frac{\alpha_s(\mu_r)}{16\pi}(\rho^2+\bar{\rho}^2)E^2\log\frac{E^2}{\mu_r^2}\right).\end{aligned} \tag{2.2.23}$$

To further simplify the integrand we would like to select a natural value for the renormalisation scale that removes the $(\rho\mu_r)^{b_0}(\bar{\rho}\mu_r)^{b_0}$ factor in the pre-exponent. Hence we choose the value of μ_r to be set by the geometric average of the instanton sizes,

$$\mu_r = 1/\sqrt{\rho\bar{\rho}}, \tag{2.2.24}$$

and as a result, all the running coupling constants appearing on the right hand side

of Eq. (2.2.23) are given by the following 1-loop expression,

$$\frac{4\pi}{\alpha_s(1/\sqrt{\rho\bar{\rho}})} = \frac{4\pi}{\alpha_s(E)} - b_0 \log\left(\rho\bar{\rho}E^2\right). \tag{2.2.25}$$

2.2.2 More on instanton–anti-instanton interaction

It can be useful to separate the instanton–anti-instanton interaction potential $U_{\rm int}$ from the total action $S_{I\bar{I}}$,

$$U_{\rm int}(z) = S_I + S_{\bar{I}} - S_{I\bar{I}}(z) = \frac{4\pi}{\alpha_s(\mu_r)}\left(1 - \mathcal{S}(z)\right), \tag{2.2.26}$$

where

$$S_I = \frac{2\pi}{\alpha_s(\mu_r)} = S_{\bar{I}}, \tag{2.2.27}$$

denote the individual actions of the single instanton and the single anti-instanton. It then follows from our earlier discussion that in the limit of large separations, the interaction potential vanishes, and in the opposite limit where the individual instantons mutually annihilate, the interaction cancels the effect of the individual instanton actions,

$$\lim_{z\to\infty} U_{\rm int} = \frac{6}{z^2} + \mathcal{O}\left(\frac{1}{z^4}\log z\right) \to 0, \tag{2.2.28}$$

$$\lim_{z\to 1} U_{\rm int} = 2S_I\left(1 - \frac{6}{5}(z-1)^2 + \mathcal{O}\left((z-1)^3\right)\right) \to 2S_I. \tag{2.2.29}$$

The exponent of the instanton–anti-instanton action appearing in the optical theorem expression for the instanton total cross-section, Eq. (2.2.23), can be interpreted as a series expansion in powers of the instanton interaction potential,

$$\exp\left(-\frac{4\pi}{\alpha_s(\mu_r)}\mathcal{S}(z)\right) = \sum_{n=0}^{\infty}\frac{1}{n!}\left(U_{\rm int}\right)^n \exp\left(-S_I - S_{\bar{I}}\right), \tag{2.2.30}$$

where n is the number of cut propagators in the imaginary part of the forward elastic scattering amplitude, i.e. the number of final state gluons in the instanton process. The expression Eq. (2.2.30) will be useful in the following section for obtaining the mean number of final state gluons from our optical-theorem-based approach.

We should further note that the expression Eq. (2.2.19) given above corresponds to the action of the instanton–anti-instanton configuration for the choice of the relative orientation matrix Ω that corresponds to maximal attraction between the instanton and the anti-instanton. In general one should integrate over all relative orientations on the right hand side of Eq. (2.2.23). The result of this integration (see Appendix B) is,

$$\begin{aligned}\int \mathrm{d}\Omega e^{-\frac{4\pi}{\alpha_s(\mu_r)}\mathcal{S}(z,\Omega)} &= \frac{1}{9\sqrt{\pi}}\left(\frac{3}{U_{\rm int}}\right)^{7/2} e^{-\frac{4\pi}{\alpha_s(\mu_r)}\mathcal{S}(z)} \\ &= \frac{1}{9\sqrt{\pi}}\left(\frac{3\alpha_s(\mu_r)}{4\pi(1-\mathcal{S}(z))}\right)^{7/2} e^{-\frac{4\pi}{\alpha_s(\mu_r)}\mathcal{S}(z)}. \end{aligned} \tag{2.2.31}$$

2.2.3 The master integral

We now introduce dimensionless integration variables,

$$r_0 = R_0 E, \qquad r = |\vec{R}|E, \tag{2.2.32}$$

$$y = \rho\bar{\rho}E^2, \qquad x = \rho/\bar{\rho}, \tag{2.2.33}$$

and use them to write down the instanton parton-level cross-section $\hat{\sigma}^{\rm inst}_{\rm tot}$ integral in Eq. (2.2.23) in the form,

$$\hat{\sigma}^{\rm inst}_{\rm tot}(E) = \frac{1}{E^2}\mathrm{Im}\int_{-\infty}^{+\infty} \mathrm{dr_0\, e^{r_0}\, G(r_0, E)}, \tag{2.2.34}$$

where

$$\begin{aligned} G(r_0,E) = \frac{\kappa^2\pi^4}{2^{17}}\sqrt{\frac{\pi}{3}}\int_0^\infty r^2\mathrm{d}r\int_0^\infty\frac{\mathrm{d}x}{x}\int_0^\infty\frac{\mathrm{d}y}{y}\left(\frac{4\pi}{\alpha_s}\right)^{21/2}\left(\frac{1}{1-\mathcal{S}(z)}\right)^{7/2} \\ \mathcal{K}_{\rm ferm}(z)\exp\left(-\frac{4\pi}{\alpha_s}\mathcal{S}(z) - \frac{\alpha_s}{4\pi}\frac{x+1/x}{4}y\log y\right). \end{aligned} \tag{2.2.35}$$

Here κ, $\mathcal{S}(z)$ and $\mathcal{K}_{\rm ferm}(z)$ are given by Eq. (2.2.3), Eq. (2.2.19) and Eq. (2.2.21)-(2.2.22), and the conformal ratio variable z is expressed in terms of our dimensionless variables via

$$z = \frac{1}{2}(\xi + (\xi^2-4)^{1/2}) \tag{2.2.36}$$

where

$$\xi = \frac{r_0^2 + r^2}{y} + x + \frac{1}{x}, \tag{2.2.37}$$

in agreement with the the expression Eq. (2.2.18).

The final ingredient we need is the expression Eq. (2.2.25) for running couplings in terms of the y variable,

$$\begin{aligned}\frac{4\pi}{\alpha_s}(y;E) =& \frac{4\pi}{\alpha_s(E)} - b_0 \log y \\ =& \frac{4\pi}{0.416} + 2b_0 \log \frac{E}{1\text{GeV}} - b_0 \log y,\end{aligned} \tag{2.2.38}$$

as follows from Eq. (2.2.25) and Eq. (2.2.33). We will thus set $\frac{4\pi}{\alpha_s} = \frac{4\pi}{\alpha_s}(y;E)$ in the integrand, Eq. (2.2.35) (including the function in the exponent and the non-exponential terms in the integrand in Eq. (2.2.35)).

To compute the instanton cross-section, Eq. (2.2.34), we first numerically evaluate the integral Eq. (2.2.35) and obtain values for $G(r_0, E)$ for a wide range of both arguments, r_0 and E. After that we perform the final integration over r_0 in Eq. (2.2.34) by expanding the integrand in

$$\hat{\sigma}_{\text{tot}}^{\text{inst}}(E) = \frac{1}{E^2}\text{Im}\int_{-\infty}^{+\infty} \text{dr}_0\, \text{e}^{\text{r}_0 + \log \text{G}(\text{r}_0,\text{E})}, \tag{2.2.39}$$

around the stationary point of r_0 for the function $r_0 + \log G(r_0, E)$ in the exponent

$$r_0(E) : \partial_{r_0} \log G(r_0, E) \,=\, -1\,, \tag{2.2.40}$$

for each value of E. The saddle-point evaluation of the r_0 integral, Eq. (2.2.39) gives,

$$\begin{aligned}\hat{\sigma}_{\text{tot}}^{\text{inst}}(E) &\approx \frac{1}{E^2}\sqrt{\frac{2\pi}{-\partial_{r_0}^2 \log G}}\Bigg|_{r_0=r_0(E)} e^{r_0(E)+\log G(r_0(E),E)} \\ &= \frac{1}{E^2}\sqrt{\frac{2\pi}{W''}}\Bigg|_{r_0=r_0(E)} e^{r_0(E)-W(r_0(E),E)},\end{aligned} \tag{2.2.41}$$

where we have defined,

$$W(r_0, E) \,=\, -\log G_0(r_0, E)\,, \qquad W'(r_0, E) \,=\, -\partial_{r_0} \log G(r_0, E)\,. \tag{2.2.42}$$

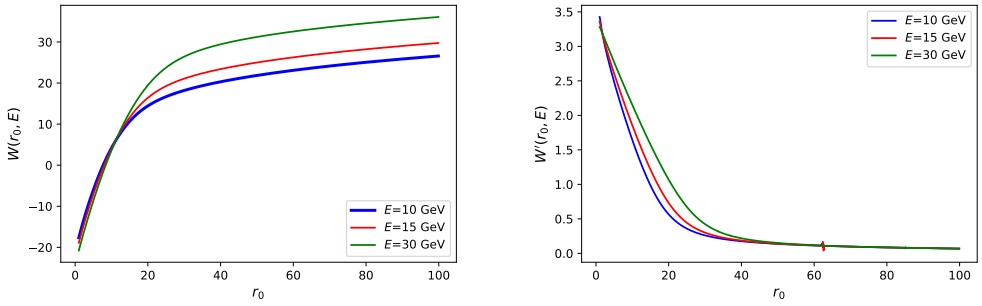

Figure 2.1: (left) $W(r_0, E)$ plotted for E=10, 15, 30 GeV and $0<r_0<100$. (right) $W'(r_0, E)$ plotted for E=10, 15, 30 GeV and $0<r_0<100$. NB one should ignore the small spike at $r_0 \sim 60$ as this is merely an artefact of the numerical accuracy of our differentiation and integration functions.

The numerical integration in Eq. (2.2.35) was carried out using the python package SciPy [37], which implements Gaussian quadrature, for E in the range in $10 < E < 2000$ GeV and for a wide range in r_0 to accommodate a sufficiently large interval around the expected values of the saddle-point $r_0(E)$ in Eq. (2.2.40). In Fig. 2.1 we plot the resulting functions $W(r_0, E)$ and $W'(r_0, E)$ for fixed values of $E = 10, 15, 30$ GeV in the range $0 < r_0 < 100$. The function $W(r_0, E)$ plays the role of the effective instanton-anti-instanton Euclidean action (this is because it arises from integrating the exponent of the classical action $e^{-\frac{4\pi}{\alpha_s}\mathcal{S}(z)}$ over the collective coordinates of non-negative modes of the $I\bar{I}$ configuration on the r.h.s. of Eq. (2.2.35)). The saddle-point value for r_0 is given by the equation $W'(r_0, E) = 1$ for each fixed value of E, as dictated by Eq. (2.2.40) above.

Having determined $W(r_0, E)$ and its derivatives as functions of r_0 and E we can now carry out the final integration over r_0 using the saddle-point approximation formula, Eq. (2.2.41), for the imaginary part of the forward elastic scattering amplitude and hence for the partonic instanton cross-section, $\hat{\sigma}_{\text{tot}}^{\text{inst}}(E)$. Our final results for the partonic instanton cross-section, Eq. (2.2.34), are displayed in Table 2.1.

Then the hadronic cross-sections are calculated from these partonic cross-sections using the NNPDF3.1luxQED NNLO dataset with $\alpha_s(M_Z) = 0.118$ [38, 39] and

$\sqrt{\hat{s}}$ [GeV]	50	100	150	200	300	400	500
$\langle n_g \rangle$	9.43	11.2	12.22	12.94	13.96	14.68	15.23
$\hat{\sigma}_{\rm tot}^{\rm inst}$ [pb]	207.33×10^{3}	1.29×10^{3}	53.1	5.21	165.73×10^{-3}	13.65×10^{-3}	1.89×10^{-3}

Table 2.1: The instanton cross-section presented for a range of partonic C.o.M. energies $\sqrt{\hat{s}} = E$ and the mean number of gluons at this energy calculated using Eq. (2.3.3).

$E_{\rm min}$ [GeV]	50	100	150	200	300	400	500
$\sigma_{p\bar{p}\to I}$ $\sqrt{s_{p\bar{p}}}$=1.96 TeV	2.62 μb	2.61 nb	29.6 pb	1.59 pb	6.94 fb	105 ab	3.06 ab
$\sigma_{pp\to I}$ $\sqrt{s_{pp}}$=14 TeV	58.19 μb	129.70 nb	2.769 nb	270.61 pb	3.04 pb	114.04 fb	8.293 fb
$\sigma_{pp\to I}$ $\sqrt{s_{pp}}$=30 TeV	211.0 μb	400.9 nb	9.51 nb	1.02 nb	13.3 pb	559.3 fb	46.3 fb
$\sigma_{pp\to I}$ $\sqrt{s_{pp}}$=100 TeV	771.0 μb	2.12 μb	48.3 nb	5.65 nb	88.3 pb	4.42 pb	395.0 fb

Table 2.2: Hadronic cross-sections for QCD instanton processes at a range of colliders with different C.o.M. energies $\sqrt{s_{pp}}$ evaluated using Eq. (2.2.43). The minimum allowed partonic energy is $E_{\rm min} = \sqrt{\hat{s}_{\rm min}}$.

displayed in Table 2.2. These are calculated using the usual formula

$$\sigma_{pp\to I}\left(\hat{s} > \hat{s}_{\rm min}\right) = \int_{\hat{s}_{min}}^{s_{pp}} {\rm d}x_1 {\rm d}x_2 \quad f\left(x_1, Q^2\right) f\left(x_2, Q^2\right) \hat{\sigma}\left(\hat{s} = x_1 x_2 s_{pp}\right) \qquad (2.2.43)$$

where s_{pp} is the centre-of-mass energy of the hadron collider, $\hat{\sigma}$ is the partonic instanton cross-section and $\hat{s}_{\rm min}$ is the minimum invariant mass squared of the produced system. NB here we are only considering the gluon initiated process, otherwise we require a sum over such integrals.

2.2.4 Instanton Recoil by a Jet

In this section we explain how to generalise the calculation of the instanton process presented above to the case where a jet is emitted from one of the initial state partons. This is of course an important process for collider studies as it allows one to recoil the instanton-generated multi-particle final state by a high-p_T jet.

When the jet is carrying momentum p produced from an initial parton p_1, the secondary gluon, q, entering the instanton vertex will necessarily have a virtuality

$q^2 = -Q^2 \neq 0$[1]. In the partonic centre of mass frame we have,

$$p_1 = (\sqrt{\hat{s}}/2, 0, p_L), \quad p_2 = (\sqrt{\hat{s}}/2, 0, -p_L), \text{ where } |p_L| = \sqrt{\hat{s}}/2,$$
$$p_1 = q + p,\ p = (|p_T|, p_T, 0), Q^2 = -q^2 = -(p_1 - p)^2 = \sqrt{\hat{s}}\, p_T. \tag{2.2.44}$$

Here we have assumed for simplicity that the jet momentum p is transverse, i.e. it does not have a longitudinal component.

The kinematic-invariant CoM energy for the parton-level process is, as before, $\sqrt{\hat{s}}$, where $\hat{s} = (p_1 + p_2)^2$. On the other hand, the invariant mass entering the instanton vertex $\sqrt{s'}$ is now different,

$$s' = (q + p_2)^2 = \hat{s} - 2Q^2 = \sqrt{\hat{s}}(\sqrt{\hat{s}} - 2p_T). \tag{2.2.45}$$

The virtuality Q of an incoming gluon leg, induced by a non-zero p_T, introduces a multiplicative form-factor $e^{-Q\rho}$ into the instanton vertex. This is a well-known result [34, 36, 40] that is a direct consequence of Fourier transforming the instanton field to momentum space to obtain $A^{\rm inst}_{LSZ}(q)$, where the momentum q has a large virtuality, Q^2. For the instanton cross-section one needs to compute $A^{\rm inst}_{LSZ}(q)\, A^{\rm inst}_{LSZ}(p_2)\, A^{\overline{\rm inst}}_{LSZ}(-q)\, A^{\overline{\rm inst}}_{LSZ}(-p_2)$, in analogy with Eq. (2.2.17), which gives the overall form-factor,

$$\exp\left(-Q(\rho + \bar{\rho})\right) = \exp\left(-\frac{Q}{E}\sqrt{y\,(x + 1/x + 2)}\right) \tag{2.2.46}$$

that needs to be included in the integral Eq. (2.2.23). On the right hand side of this equation we used our standard dimensionless variables x and y defined in Eq. (2.2.32)-(2.2.33).

The second modification of the integral in Eq. (2.2.23) is that the the energy variable E corresponds to the instanton vertex energy $E = \sqrt{s'}$ defined in Eq. (2.2.45), which is smaller than the overall invariant mass $\sqrt{\hat{s}}$ of the parton-level process.

[1] In the complementary scenario where a high-p_T jet is emitted from the instanton vertex in the *final state*, no virtualities arise, all momenta entering and leaving the instanton vertex are on-shell, and the formalism presented in the earlier section requires no modifications.

In summary, the instanton parton-level cross-section $\hat{\sigma}_{\rm tot}^{\rm inst}\left(\sqrt{\hat{s}}, p_T\right)$ is computed as follows:

1. For each pair of physical variables $\hat{s}$, p_T, introduce the auxiliary variables E and Q,

$$Q^2 = p_T\sqrt{\hat{s}}, \qquad E^2 = \hat{s} - 2Q^2. \tag{2.2.47}$$

2. Numerically compute the integral,

$$\tilde{G}(r_0, E, Q) = \frac{\kappa^2\pi^4}{2^{17}}\sqrt{\frac{\pi}{3}}\int_0^\infty r^2 \mathrm{d}r \int_0^\infty \frac{\mathrm{d}x}{x}\int_0^\infty \frac{\mathrm{d}y}{y}\left(\frac{4\pi}{\alpha_s}\right)^{21/2}\left(\frac{1}{1-\mathcal{S}(z)}\right)^{7/2} \mathcal{K}_{\rm ferm}(z)\exp\left(-\frac{4\pi}{\alpha_s}\mathcal{S}(z) - \frac{\alpha_s}{4\pi}\frac{x+1/x}{4}y\log y - \frac{Q}{E}\sqrt{y\left(x+\frac{1}{x}+2\right)}\right) \tag{2.2.48}$$

and use it to evaluate the expression for the cross-section,

$$I(E,Q) = \frac{1}{E^2}\mathrm{Im}\int_{-\infty}^{+\infty}\mathrm{dr_0}\,\mathrm{e^{r_0}}\,\tilde{\mathrm{G}}(\mathrm{r_0},\mathrm{E},\mathrm{Q}), \tag{2.2.49}$$

in the saddle-point approximation, as before.

3. The cross-section in physical variables is then obtained via,

$$\hat{\sigma}_{\rm tot}^{\rm inst}(\sqrt{\hat{s}}, p_T) = I(E,Q)\Big|_{Q^2=p_T\sqrt{\hat{s}},\, E^2=\hat{s}-2p_T\sqrt{\hat{s}}} \tag{2.2.50}$$

Table 2.3 presents the results for the instanton cross-section at parton level for a range of partonic CoM energies, $\sqrt{\hat{s}}$, and for a fixed value of the recoiled jet transverse momentum $p_T = 150$ GeV. The resulting cross-sections are negligibly small. To complement these results we have also computed instanton cross-sections for the case where p_T is scaled with the energy. Table 2.4 presents the results at parton level where the recoiled jet transverse momentum is chosen as $p_T = \sqrt{\hat{s}}/3$.

From the results in Tables 2.3 and 2.4 we see that the cross-sections calculated for the processes where the instanton recoils against a jet with large momentum are too small to be observable at any present or envisioned high-energy collider. While increasing the transverse momentum for objects that are difficult to reconstruct

$\sqrt{\hat{s}}$ [GeV]	310	350	375	400	450	500
$\hat{\sigma}_{\text{tot}}^{\text{inst}}$ [pb]	3.42×10^{-23}	1.35×10^{-18}	1.06×10^{-17}	1.13×10^{-16}	9.23×10^{-16}	3.10×10^{-15}

Table 2.3: The instanton partonic cross-section recoiled against a hard jet with $p_T = 150$ GeV emitted from an initial state and calculated using Eq. (2.2.50). Results for the cross-section are shown for a range of partonic C.o.M. energies $\sqrt{\hat{s}}$.

$\sqrt{\hat{s}}$ [GeV]	100	150	200	300	400	500
$\hat{\sigma}_{\text{tot}}^{\text{inst}}$ [pb]	1.68×10^{-7}	1.20×10^{-9}	3.24×10^{-11}	1.84×10^{-13}	4.38×10^{-15}	2.38×10^{-16}

Table 2.4: The cross-section presented for a range of partonic C.o.M. energies $\sqrt{\hat{s}} = E$ where the recoiled p_T is scaled with the energy, $p_T = \sqrt{\hat{s}}/3$.

by recoiling them against a hard object is often a popular method to improve the sensitivity of the LHC to new physics, see e.g. [41–44], the instanton shields itself from such an option. The physical intuition for this suppression comes from the fact the the physical size corresponding to these large virtualities is much smaller than the scale of the instanton and so the instanton, in some sense, feels the effect of the gluon to a much lesser extent.

Consequently, the only way to obtain sensitivity to instantons is to disentangle their spherical radiation profile, made of fairly soft jets, from SM QCD backgrounds.

2.3 Phenomenology

2.3.1 Gluon Production

We now wish to perform a phenomenological study of instantons at the LHC. In order to do this we need to gain a better understanding of the gluons produced by the instanton. In our approach of computing the total partonic cross-section via the optical theorem in Eq. (2.2.34) and Eq. (2.2.35) we have already effectively summed over the number of gluons in the final state, n_g. This sum can be uncovered by using the series expansion, Eq. (2.2.30), of the exponent of the instanton–anti-instanton

action on the right hand side of Eq. (2.2.35),

$$G(r_0,E) = \frac{\kappa^2\pi^4}{2^{17}}\sqrt{\frac{\pi}{3}}\int_0^\infty r^2\mathrm{d}r\int_0^\infty\frac{\mathrm{d}x}{x}\int_0^\infty\frac{\mathrm{d}y}{y}\left(\frac{4\pi}{\alpha_s}\right)^{21/2}\left(\frac{1}{1-\mathcal{S}(z)}\right)^{7/2}\mathcal{K}_{\rm ferm}(z) \times\sum_{n_g=0}^{\infty}\frac{1}{n_g!}\left(U_{\rm int}\right)^{n_g}\exp\left(-\frac{4\pi}{\alpha_s}-\frac{\alpha_s}{4\pi}\frac{x+1/x}{4}y\log y\right). \tag{2.3.1}$$

The mean value of n_g (i.e. the value that gives the dominant contribution to the integral) is then easily found to be given by the expectation value of the interaction potential,

$$\langle n_g\rangle = \langle U_{\rm int}\rangle, \tag{2.3.2}$$

where the expectation value of $\langle U_{\rm int}\rangle$ is obtained by inserting $U_{\rm int} = \frac{4\pi}{\alpha_s(y;E)}\left(1-\mathcal{S}(z)\right)$ into the integrand on the right hand side of Eq. (2.2.34) and Eq. (2.2.35) and normalising by $1/(E^2\hat{\sigma}^{\rm inst}_{\rm tot})$.

In practice, we compute

$$\langle n_g\rangle = \frac{1}{G(r_0,E)}\frac{\kappa^2\pi^4}{2^{17}}\sqrt{\frac{\pi}{3}}\int_0^\infty r^2\mathrm{d}r\int_0^\infty\frac{\mathrm{d}x}{x}\int_0^\infty\frac{\mathrm{d}y}{y}\left(\frac{4\pi}{\alpha_s(y;E)}\right)^{21/2}\left(\frac{1}{1-\mathcal{S}(z)}\right)^{7/2} \mathcal{K}_{\rm ferm}(z)\frac{4\pi}{\alpha_s(y;E)}\left(1-\mathcal{S}(z)\right)\cdot\exp\left(-\frac{4\pi}{\alpha_s(y;E)}\mathcal{S}(z)-\frac{\alpha_s(y;E)}{4\pi}\frac{x+1/x}{4}y\log y\right). \tag{2.3.3}$$

On the right hand side we have integrated over the y, x, r variables. The variable r_0 is taken to be at its saddle-point value for each fixed value of the energy E.

To account for the possibility of the new shifted saddle-point we perform the following calculation:

$$\langle n_g\rangle = \frac{1}{\mathrm{Im}\int_{-\infty}^{+\infty}\mathrm{d}r_0\,e^{r_0}\,G(r_0,E)}\times \mathrm{Im}\int_{-\infty}^{+\infty}\mathrm{dr_0\,e^{r_0}}\frac{\kappa^2\pi^4}{2^{17}}\sqrt{\frac{\pi}{3}}\int_0^\infty\mathrm{r^2dr}\int_0^\infty\frac{\mathrm{dx}}{\mathrm{x}}\int_0^\infty\frac{\mathrm{dy}}{\mathrm{y}}\left(\frac{4\pi}{\alpha_\mathrm{s}(\mathrm{y;E})}\right)^{21/2}\left(\frac{1}{1-\mathcal{S}(\mathrm{z})}\right)^{7/2} \mathcal{K}_{\rm ferm}(z)\frac{4\pi}{\alpha_s(y;E)}\left(1-\mathcal{S}(z)\right)\cdot\exp\left(-\frac{4\pi}{\alpha_s(y;E)}\mathcal{S}(z)-\frac{\alpha_s(y;E)}{4\pi}\frac{x+1/x}{4}y\log y\right). \tag{2.3.4}$$

2.3.2 Instanton Signals at Hadron Colliders

Since the global event topology of instanton processes is spherically symmetric, and therefore distinctly different from perturbative-QCD events, event shape observables [45] can be a powerful way to identify these processes.

The transverse sphericity tensor is defined as

$$S^{\alpha\beta} = \frac{\sum_i p_i^\alpha p_i^\beta}{\sum_i \left|\mathbf{p}_i^2\right|}, \tag{2.3.5}$$

where α, β run over transverse spatial indices and i runs over the number of particles. Here p_i is the two-dimensional transverse component of momentum. The transverse sphericity observable is then defined as $S = \frac{2\lambda_2}{\lambda_1+\lambda_2}$ where $\lambda_2 < \lambda_1$ are the two eigenvalues of the transverse sphericity tensor. Transverse sphericity takes values between 0 and 1 with higher values denoting a higher degree of spherical symmetry. Therefore we would expect instanton processes to have a higher transverse sphericity than background processes which in general have some angular dependence.

Spherocity is defined as

$$S_0 = \frac{\pi^2}{4} \min_{\vec{n}} \left(\frac{\sum_i \left|\vec{p}_{\perp,i} \times \vec{n}\right|}{\sum_i \left|\vec{p}_{\perp,i}\right|} \right)^2, \tag{2.3.6}$$

where $\vec{n}$ is a unit vector with zero longitudinal component and $\vec{p}_i$ are the transverse momenta. Again, S_0 takes values between 0 and 1, with 1 representing a completely isotropic event and 0 being a pencil-like event. This variable is closely related to transverse thrust which is defined as

$$\tau = 1 - \max_{\vec{n}} \frac{\sum_i \left|\vec{p}_i \cdot \vec{n}\right|}{\sum_i \left|\vec{p}_i\right|}, \tag{2.3.7}$$

where $\vec{n}$ is a unit vector and $\vec{p}_i$ are the transverse momenta. Thrust is 0 for pencil-like events and 0.5 for spherically symmetric events. The vector $\vec{n}$ which maximises this expression is known as the thrust axis.

The final shape variable we consider is broadening. The thrust axis automatically divides the event into a left hemisphere, $\mathcal{L}$ and a right hemisphere, $\mathcal{R}$. Left and right

broadening are then defined as

$$\mathcal{B}_{\mathcal{L}} = \sum_{i \in \mathcal{L}} \frac{|\vec{p}_i \times \vec{n}|}{\sum_i |\vec{p}_i|}, \quad \mathcal{B}_{\mathcal{R}} = \sum_{i \in \mathcal{R}} \frac{|\vec{p}_i \times \vec{n}|}{\sum_i |\vec{p}_i|} \tag{2.3.8}$$

where $\vec{n}$ is the thrust axis and $\vec{p}_i$ are the transverse momenta. Total broadening $\mathcal{B}$ is then the sum of the left and right broadening, $\mathcal{B} = \mathcal{B}_{\mathcal{L}} + \mathcal{B}_{\mathcal{R}}$, and takes values between 0 and 0.5 with 0.5 being spherically symmetric.

To show the different shapes for these observables between various perturbative SM processes and instanton events at the LHC and the Tevatron, we generate the background events using Pythia 8 [46]. For the perturbative SM processes we consider the ones with largest cross-section and jet-rich final states, i.e. high and low-pT multi-jet events (QCD events simulated by Pythia), min-bias events, $t\bar{t}$ production and W+jets events. For the signal we use RAMBO [47] to populate the phase space of the instanton final state. Each event contains four $q\bar{q}$ pairs and a poisson-distributed number of gluons, with a mean in accordance to n_g in Table 2.1.

All processes are analysed using Fastjet [48]. For the LHC we reconstruct jets using the anti-k_T algorithm [49] with a cone-size of $R = 0.4$ and $p_T \geq 10$ GeV. At the Tevatron jets were analysed using the k_T algorithm [49] with a cone-size of $R = 0.7$ and were required to have $p_T \geq 5$ GeV. Leptons are required to have $p_T \geq 0.5$ GeV. It should be noted that the instanton processes are not showered or hadronised, but this should not significantly affect the analysis as the position and energy of the reconstructed jets are conserved to a good accuracy.

We show in Fig. 2.2 the distribution for the p_T of the leading jet, in Fig. 2.3 broadening, in Fig. 2.4 transverse sphericity and in Fig. 2.5 thrust for the LHC and the Tevatron. The differences in the histograms between the LHC and Tevatron originate in the different jet definitions and p_T thresholds. This leads to more spherical events and thus higher values for thrust and transverse sphericity at the Tevatron. For the backgrounds we include the processes that have the largest perturbatively calculable cross-sections. Most of these processes, in particular high-energy multijets and W+jets events, show a more pronounced pencil-like structure than the instanton

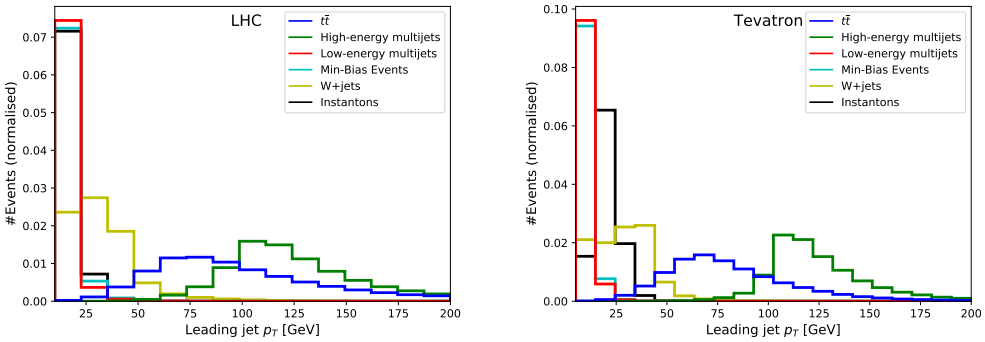

Figure 2.2: The distribution of the p_T of the leading jet for our background processes and instantons at the LHC (left) and Tevatron (right).

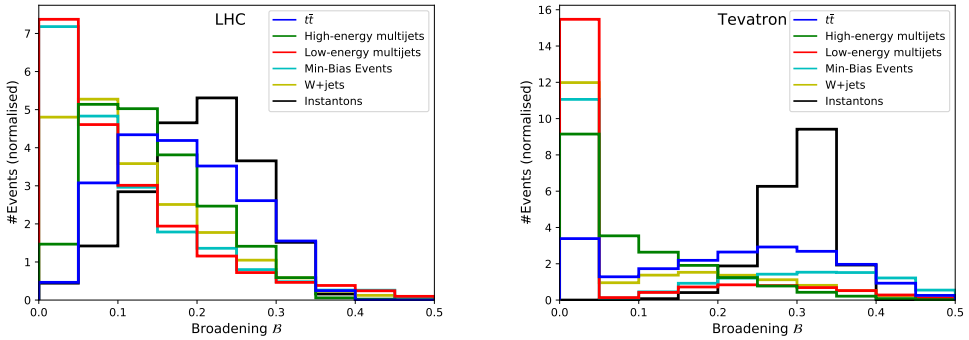

Figure 2.3: The distribution of the broadening of events for our background processes and instantons at the LHC (left) and Tevatron (right).

events. Overall, analysing events with event shape observables provides a powerful method to discriminate instanton events from large Standard Model backgrounds.

2.3.3 QCD Instanton Search at the LHC

Searches in high-luminosity LHC runs

As a result of the trigger cuts imposed, we find that the LHC has very little sensitivity to QCD instantons in current and future high-luminosity runs. QCD instanton events produce no isolated leptons or a large amount of missing transverse energy, and so appear only as multi-particle events consisting of soft jets.

Missing transverse energy higher-level triggers require at least $E_{T\text{miss}} \geq 70$ GeV

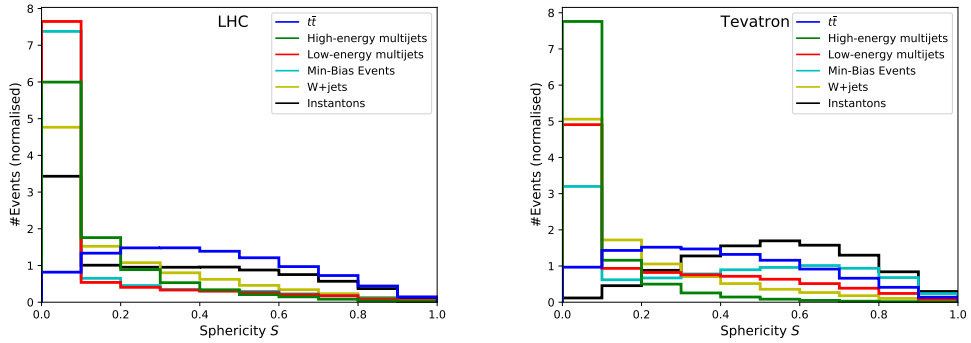

Figure 2.4: The distribution of the transverse sphericity of events for our background processes and instantons at the LHC (left) and Tevatron (right).

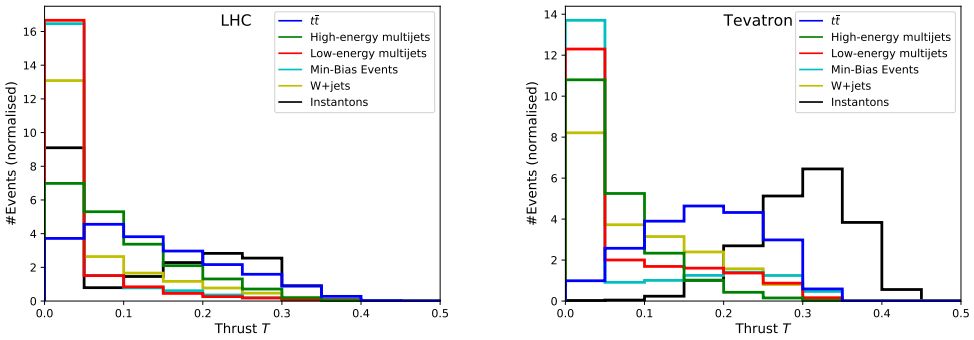

Figure 2.5: The distribution of the thrust of events for our background processes and instantons at the LHC (left) and Tevatron (right).

while single jet triggers are as high as $p_{T,j} \geq 360$ GeV [50]. In Sec. 2.2.4 we have shown that the emission of a hard jet from an initial state parton is not a viable strategy to produce an instanton. Further, the probability that one of the partons that originates in the instanton process has such a large momentum is very small as well. If one of the instanton-induced partons has a transverse momentum to pass the single-jet trigger requirements, the centre-of-mass energy of the instanton $\sqrt{\hat{s}}$ has to be at least of $\mathcal{O}(700)$ GeV. According to Table 2.2, this renders the hadronic instanton cross-section too small to be observable.

Thus, one would have to resort to multijet triggers, either with four jets of $p_{T,j} \geq 85$ GeV or six jets of $p_{T,j} \geq 45$ GeV. Both trigger requirements result in requiring instantons of fairly high partonic centre-of-mass energies of $\mathcal{O}(300)$ GeV. Generating

100000 signal events as described in Sec. 2.3 and reconstructing them with the anti-kT jet algorithm, we find that none of the events pass multijet triggers, which results in an upper limit on the instanton cross-section that passes such trigger cuts of $\sigma_{pp\to I}^{\text{trigger}} \lesssim 10$ fb. Disentangling instanton processes with less than 10 fb of cross-section from large QCD backgrounds during the event reconstruction step is a highly challenging task.

Due to increased pileup in future high-luminosity LHC runs and at future hadron colliders, e.g. the FCC-hh, trigger thresholds for jets will have to be increased, which will significantly reduce sensitivity to QCD instanton processes. Special trigger strategies would have to be developed for instantons to pass trigger requirements in such a jet-rich environment. One could speculate about the inclusion of event-shape observables directly in the trigger strategy and a highly optimised interplay between high-level and low-level triggers. As shown in Figs. 2.2, 2.3, 2.4 and 2.5, instanton events have a very different event topology compared to QCD-induced multi-jet or resonance-associated production processes. Incorporating such observables in the trigger setup and reconstruction strategies might retain some sensitivity to instanton processes in future runs at high-energy hadron colliders.

Search in low-luminosity LHC runs

Rather than focusing on high-luminosity runs, we propose to pursue a different search strategy. The biggest obstacles to the discovery of QCD instanton processes are the high trigger thresholds, which are a necessity to avoid triggering on pileup in high-luminosity runs. Low-luminosity LHC runs had minimalistic trigger requirements [51], i.e. min-bias triggers which required only a single charged track with an energy of 400 MeV. Remarkably, practically all QCD instanton events would pass min-bias triggers. ATLAS and CMS [52] both are in possession of un-prescaled min-bias datasets which are however often only used to determine the luminosity for low-pileup runs, rather than searching for new phenomena.

To assess whether these datasets can provide sensitivity to QCD instanton processes, we generate event samples as outlined in Sec. 2.3 with a hadronic centre-of-mass energy of $\sqrt{s} = 13$ TeV. For the event selection we require that each event should have at least six jets $n_j \geq 6$ with a minimum $p_{T,j} \geq 10$ GeV and that these jets form a thrust value of $\tau \geq 0.2$. This already confidently separates instanton signal events from QCD-induced background events. For an instanton with a minimum $\sqrt{\hat{s}} \geq 100$ GeV, which can be imposed through a requirement on the invariant mass of the final state jets, we find $\frac{s}{\sqrt{b}} = 50.1$ and for $\sqrt{\hat{s}} \geq 200$ GeV we have $\frac{s}{\sqrt{b}} = 7.1$. This shows a very good sensitivity for instanton processes in min-bias events, which can be further increased by lowering the $p_{T,j}$ requirements.

2.3.4 QCD Instanton Search at the Tevatron

We deduce from the observations in Sec. 2.3.3 that future runs at high-energy high-luminosity colliders are likely to become even less sensitive to QCD instanton processes. Consequently, looking in the other direction instead, e.g. at the Tevatron, might provide yet another way to search for QCD instantons. In the top row of Table 2.2 we show the hadronic cross-sections at Tevatron energies, depending on the partonic centre-of-mass energy of the instanton process.

We recast several jet-rich searches and measurements by CDF [53–55]. While a large fraction of instanton events would pass the trigger criteria, the event selection criteria applied in the analysis removed the predominant fraction of instanton events. Thus, the results provided in [53–55] did not allow one to set an experimental constraint on the instanton cross-section. However, if this data was reanalysed and event reconstruction strategies following Sec. 2.3.3 were applied, the Tevatron could set stringent limits on the hadronic instanton cross-section.

2.4 Conclusions

Instantons are the best motivated, yet unobserved, non-perturbative effects predicted by the Standard Model. Being able to study instantons in scattering processes would provide a new window to phenomenological exploration of the QCD vacuum and it would allow the tensioning of non-perturbative theoretical methods developed for gauge theories with data.

In our calculation we used the optical theorem to calculate the total instanton cross-section from the elastic scattering amplitude by carrying out an integral over the instanton collective coordinates, and taking into account the hard-hard initial state interactions calculated in [20]. The inclusion of these interactions is essential as it provides a cut-off for the integral over the instanton scale size ρ which otherwise diverges in the IR in any QCD-like theory when no explicit external scales (such as the vev of a scalar field, highly virtual momenta or high temperature) are present. This theoretical approach was first presented and applied recently in [12]. We improved on the results of [12] here by using a more robust integration method by directly computing integrals over all instanton–anti-instanton collective coordinates that correspond to positive modes of the quadratic fluctuation operators in the instanton–anti-instanton background. We then also calculated the mean number of gluons in the final state using a novel and more direct approach based on computing the expectation value of the instanton–anti-instanton interaction potential.

Most of the earlier studies of QCD instanton-induced processes, prior to [12], were specific to deep-inelastic scattering (DIS) [34, 36, 56]. In this case, it was the deep inelastic momentum scale Q that was essential for obtaining infrared safe instanton contributions in the DIS settings and at relatively low CoM energies. The H1 and ZEUS Collaborations have searched for QCD instantons at the HERA collider [57–59]. In the electroweak sector of the Standard Model, phenomenological consequences of similar non-perturbative processes were also studied in detail in the literature, including recent papers [60–62], and references therein.

In this work we have re-examined the phenomenology of QCD instanton contributions to high-energy scattering processes at hadron colliders. We showed that although the instanton cross-sections are very large in a hadron collider, surprisingly such colliders have little sensitivity to instantons due to the trigger criteria necessary to reduce the data rate. Although instantons produce many final state particles, the event is isotropic and the energy is divided between all particles resulting in few particles with large p_T, one of the principal trigger requirements in a hadron collider. The higher energy instantons which could potentially pass such triggers have a vanishingly small cross-section and would not be seen in sufficient numbers in the LHC to be distinguishable from the QCD background. However examination of data collected with a minimum bias trigger [51, 52] showed that it should be possible to either discover instantons or severely constrain their cross-section with such data, which was previously only used for luminosity calibration. We also examined data from the Tevatron and showed that certain triggers should have recorded many instanton events on tape but the selection criteria used in later analyses would render the analyses insensitive to instantons. With a new set of selection criteria this would also be another possible avenue for discovery.

Chapter 3

The Electroweak Instanton

Instantons arise not only in QCD but also in the electroweak sector of the Standard Model. In particle collisions at sufficiently high energies, electroweak instanton-dominated processes are characterized by high-multiplicity final states (as in QCD) which are rare in normal SM backgrounds and which would lead to them being easy to separate from background in a detector environment. They have so far eluded detection as calculations in [29, 63–65] predict the instanton cross-section to be exponentially suppressed at energies below the sphaleron mass scale[2],

$$E_{\rm np} = \frac{\pi m_W}{\alpha_W} \simeq 7.4\,\text{TeV}. \tag{3.0.1}$$

It is only when partonic CoM energies become of the order of the sphaleron scale that one could expect electroweak instanton cross sections to become observable in a collider [29, 56, 63–65].

Instantons in QCD were recently investigated in [2,12] (this progress was summarised in the previous chapter) where it was shown that, at least in principle, QCD instantons are observable at the LHC. This is largely due to the fact that instantons

[2]The instanton is the field which tunnels between degenerate vacua while the sphaleron is the solution which goes over the barrier. The sphaleron mass is the height of the barrier that separates the adjacent topologically non-trivial vacua [66]. Its Standard Model value is $M_{\rm sph} = f(m_H^2/m_W^2)\pi m_W/\alpha_W \simeq 9$ TeV. In this chapter we will use the simpler, parametrically similar to $M_{\rm sph}$ scale, $E_{\rm np}$, defined in Eq. (3.0.1), which plays the role of the intrinsic non-perturbative scale of the weak sector of the Standard Model.

produce a spherically symmetric final state and hence it is possible to discriminate from background using shape variables. This signal would be even more pronounced in the case of electroweak instantons due to the many final state leptons, coming from both the initial instanton process and the subsequent decay of gauge and Higgs bosons. The suppression of the instanton cross section is given by $e^{-2S_I} = e^{-\frac{4\pi}{\alpha}}$ and it is due to the fact that $\alpha_s \gg \alpha_w$ that QCD instantons are observable at the LHC while observation of electroweak instantons would require a collider such as the proposed FCC to reach sufficient CoM energies.

Importantly, the function in the exponent also contains terms coming from the instanton–anti-instanton interaction and the effects of quantum corrections in the instanton background. The maximum cross section for the instanton process is then determined by the saddle point of this exponent. The calculation in [2, 12] critically relied on the inclusion of quantum effects due to interactions of the hard initial-state gluons in the instanton background, which was instrumental in cutting off contributions of QCD instantons of large size and thus resolving the infrared problem associated with them. It should be noted that electroweak instantons do not suffer from the infrared problem of large-size instantons in the same way as QCD instantons did, as the vev of the Higgs provides a cutoff on the instanton size. Nevertheless, the effect of the radiative exchanges between the highly energetic initial state partons, should lead in both cases to the suppression of instanton rates in the asymptotic high-energy regime[1].

In this chapter we will take into account a resummed quantum correction arising from the exchange of weak gauge bosons in the initial state. We will show that this term leads to an exponential suppression of the cross section for the electroweak instanton at high energies, while the Higgs contributions suppress it in the low-energy

[1]Most earlier studies of QCD instanton-induced processes were specific to deep-inelastic scattering (DIS) [36, 56]. In this case, it was the deep inelastic momentum scale Q that was essential for obtaining infrared safe instanton contributions in DIS settings and at relatively low CoM energies. The H1 and ZEUS Collaborations have searched for QCD instantons at the HERA collider [57–59]. However the work in the previous chapter allowed the computation of instanton cross sections in non-DIS settings.

range. Due to these effects, the saddle point value of the exponent is not greatly reduced compared to its maximum (negative) value and so the cross section remains suppressed and unobservable at all energies.

3.1 The Instanton in the Electroweak Sector of the Standard Model

We note that $\Pi_3\left(SU(2)\times U(1)\right) = \Pi_3\left(SU(2)\right)\times\Pi_3\left(U(1)\right) = \Pi_3\left(SU(2)\right)$ since $U(1)$ is simply connected and so its homotopy group is trivial. Hence all of the instanton theory developed in the previous two chapters is unaffected by the presence of the hypercharge gauge group. Thus the instanton in the electroweak theory is not greatly different from that of QCD. However we must now find the solution for the scalar equations of motion. The equations of motion (in Euclidean space) are given by

$$D_\mu D_\mu H = 0 \tag{3.1.1}$$

with the boundary condition that $|H| \to v/\sqrt{2}$ as $x^2 \to \infty$, i.e. that the Higgs doublet at infinity goes to the usual vacuum. Note that we have neglected the Higgs potential in the above equations of motion but this would give a subleading effect in any case [11]. It can be shown that the solution to this equation is given by[1]

$$H = \frac{v}{\sqrt{2}}\frac{\sigma^+_\mu x_\mu}{\sqrt{x^2+\rho^2}}\begin{pmatrix}1\\0\end{pmatrix}. \tag{3.1.2}$$

With this solution the Higgs field then contributes to the action as

$$S \supset \int \mathrm{d}^4x\,\left(D_\mu H\right)^\dagger\left(D_\mu H\right) = \pi^2 v^2\rho^2. \tag{3.1.3}$$

We see that this provides a natural cutoff for the integration over the instanton size and indeed numerical estimates for the instanton cross section in the electroweak

[1] The proof of the solution uses the equalities $i\eta_{a\mu\nu}\sigma^a = \sigma^+_{\mu\nu}$ and $\sigma^+_{\mu\nu}\sigma^+_\rho = \delta_{\nu\rho}\sigma^+_\mu - \delta_{\mu\rho}\sigma^+_\nu - \epsilon_{\mu\nu\rho\alpha}\sigma^+_\alpha$ where $\sigma^+_{\mu\nu} = \frac{1}{2}\left(\sigma^+_\mu\sigma^-_\nu - \sigma^+_\nu\sigma^-_\mu\right)$.

theory were studied as early as 1991 [17, 40] since it was not plagued by the infrared problems of QCD.

The other thing to consider are the fermion zero modes of the electroweak theory. The previous considerations of fermions still largely apply but as the $SU(2)$ gauge group couples only to left-handed particles, the electroweak instanton couples only to left-handed particles and we only obtain one left-handed anti-fermionic zero mode for each light doublet (and not an additional right-handed fermionic zero mode as we had in QCD).

In QCD the fermionic zero modes provided the violation of the axial symmetry but in the electroweak sector, they provide for the anomalous violation of baryon and lepton number which are preserved at the level of the classical Lagrangian.

3.2 Observation of the Electroweak Instanton

We will now attempt to compute the cross section for the electroweak instanton following similar methods as in the previous chapter. However, as a first approximation we will ignore all pre-exponential factors and treat only those terms appearing in the exponent. We will consider the instanton-dominated electroweak process with two quarks in the initial state,

$$q + q \to 7\bar{q} + 3\bar{l} + n_w W + n_Z Z + n_H H. \tag{3.2.1}$$

The number of gauge and Higgs bosons in the final state is not fixed and may grow large. However the number of final-state fermions is fixed at leading order by both the number of fermionic zero modes in the instanton background as well as by the anomalous violation of baryon and lepton number. It should be noted that at the energies considered in this paper all fermions are light and so we obtain one anti-fermion zero mode from each left handed doublet (with 3 for each quark due to color) giving the above result. Note that two of the final-state anti-fermion zero modes are inverted to become initial state fermions.

The total cross-section, σ_I, for instanton-generated $2 \to$ *anything* processes is most easily obtained from the imaginary part of the forward elastic $2 \to 2$ amplitude computed in the background of the instanton–anti-instanton ($I\bar{I}$) configuration,

$$\sigma_I = \frac{1}{E^2}\mathrm{Im}\mathcal{A}_4^{\mathrm{I\bar{I}}}(\mathrm{p}_1, \mathrm{p}_2, -\mathrm{p}_1, -\mathrm{p}_2), \tag{3.2.2}$$

where $E = \sqrt{s} = \sqrt{(p_1 + p_2)^2}$ is the CoM energy of the two incoming particles. The amplitude itself is given by an integral over the instanton and anti-instanton parameters of a characteristic semi-classical exponential suppression factor, $e^{-\frac{4\pi}{\alpha_w}\mathcal{F}}$, that will be defined below[1] (c.f. Eq. (3.2.4)), so that,

$$\sigma_I \sim \mathrm{Im}\int \mathrm{d}\rho\,\mathrm{d}\bar{\rho}\,\mathrm{d}^4\mathrm{R}\,\mathrm{d}^3\mathrm{u}\;\mathrm{e}^{-\frac{4\pi}{\alpha_\mathrm{w}}\mathcal{F}}. \tag{3.2.3}$$

The integration variables in Eq. (3.2.3) are the instanton and anti-instanton sizes, ρ and $\bar{\rho}$, the separation vector between the I and $\bar{I}$ positions, $R_\mu = (R_0, \vec{R})$, and the unit 4-vector, u_μ, that characterizes the relative orientation between I and $\bar{I}$ in the $SU(2)$ space. At present we are primarily interested in the exponent in Eq. (3.2.3) and thus we have ignored for now all non-exponential terms in the integrand. The function in the exponent reads,

$$-\frac{4\pi}{\alpha_w}\mathcal{F} = -S_{I\bar{I}} + ER_0 - \frac{\alpha_w}{16\pi}(\rho^2 + \bar{\rho}^2)E^2\,\log\left(E^2/m_W^2\right), \tag{3.2.4}$$

where the first factor is the Euclidean action of the instanton–anti-instanton configuration, the second term, ER_0, comes from the initial and final particles in the forward elastic scattering amplitude [40,67] and the third term is the quantum effect due to resummed hard radiative corrections in the instanton and anti-instanton background [19].

At large instanton–anti-instanton separation, $R/\rho \gg 1$, (anti-)instantons of small sizes, $\rho\, m_W \ll 1$, interact weakly and the $I\bar{I}$ action in the electroweak theory can be computed in the nearly dilute instanton gas limit, giving a well-known expression

[1] The normalization by $\frac{4\pi}{\alpha_w}$ of the function $\mathcal{F}$ in the exponent is chosen for convenience and to recall that at low energies the exponential suppression of the rate is in terms of twice the instanton action $S_I = \frac{2\pi}{\alpha_w}$.

(see e.g. [40, 67]),

$$S_{I\bar{I}} = \frac{4\pi}{\alpha_w}\left[1 - 2\frac{\rho^2\bar{\rho}^2}{R^4}\left(\frac{4(u\cdot R)^2}{R^2} - 1\right) + \frac{1}{4}\left((m_W\rho)^2 + (m_W\bar{\rho})^2\right)\right] + \dots . \quad (3.2.5)$$

The first term $\propto 1$ in brackets in Eq. (3.2.5) represents twice the classical instanton action, the second term $\propto (\rho/R)^4$ is the leading-order interaction potential between the instanton and the anti-instanton (it has the form of a dipole-dipole interaction in 4D), and the final term $\propto (m_W\rho)^2$ is the Higgs field contribution to the instanton–anti-instanton action[1].

It then follows that in the weak-coupling limit, $\frac{4\pi}{\alpha_w} \gg 1$, the integral in Eq. (3.2.3) is dominated by the saddle-point of $\mathcal{F}$ in Eq. (3.2.4). The saddle-point is given by,

$$u_\mu = R_\mu/R\,, \quad R_\mu = (R_{0*}, \vec{0}), \quad \rho = \bar{\rho} = \rho_*, \quad (3.2.6)$$

where

$$R_{0*} = \frac{6^{1/3}}{m_W}\frac{\varepsilon^{1/3}}{\left(1 + \frac{\varepsilon^2}{8}\log\left(\frac{\varepsilon\pi}{\alpha_w}\right)\right)^{2/3}}, \quad \rho_* = \frac{6^{1/6}}{2m_W}\frac{\varepsilon^{2/3}}{\left(1 + \frac{\varepsilon^2}{8}\log\left(\frac{\varepsilon\pi}{\alpha_w}\right)\right)^{5/6}}. \quad (3.2.7)$$

In the equations above we introduced the parameter ε as the ratio of the collision energy E to the sphaleron-induced non-perturbative scale $E_{\rm np}$,

$$\varepsilon = \frac{E}{\pi m_W/\alpha_w} = \frac{E}{E_{\rm np}}. \quad (3.2.8)$$

Now let us consider the saddle-point value of the function $\mathcal{F}$ in Eq. (3.2.4) that appears in the exponent of the semi-classical instanton rate, computed in the low-energy and the high-energy regimes. To this end we would like to rewrite the saddle-point solution, Eq. (3.2.7), in terms of the dimensionless variables $\chi = R_{0*}/\rho_*$ and $\hat{\rho} = \rho_* m_W$ representing the $I\bar{I}$ separation and the scale size. We find,

$$\chi = 6^{1/6}2\frac{\left(1 + \frac{\varepsilon^2}{8}\log\left(\frac{\varepsilon\pi}{\alpha_w}\right)\right)^{1/6}}{\varepsilon^{1/3}} \to \begin{cases} 2^{7/6}3^{1/6}\cdot\varepsilon^{-1/3}, & \varepsilon \to 0 \\ 2^{2/3}3^{1/6}\cdot\left(\log\left(\frac{\varepsilon\pi}{\alpha_w}\right)\right)^{1/6}, & \varepsilon \to \infty \end{cases} \quad (3.2.9)$$

[1] The dots in Eq. (3.2.5) stand for the omitted higher order terms in the large-separation and small instanton size expansion, $\frac{4\pi}{\alpha_w}\left(\mathcal{O}(\rho/R)^6 + \mathcal{O}((\rho/R)^2(m_W\rho)^2) + \mathcal{O}(m_W\rho)^4\right)$.

$$\hat{\rho} = \frac{6^{1/6}\varepsilon^{2/3}}{2\left(1+\frac{\varepsilon^2}{8}\log\left(\frac{\varepsilon\pi}{\alpha_w}\right)\right)^{5/6}} \to \begin{cases} 6^{1/6}2^{-1}\cdot\varepsilon^{2/3}, & \varepsilon\to 0 \\ 6^{1/6}2\sqrt{2}\cdot\varepsilon^{-1}\left(\log\left(\frac{\varepsilon\,\pi}{\alpha_w}\right)\right)^{-5/6}, & \varepsilon\to\infty \end{cases} \tag{3.2.10}$$

From Eq. (3.2.10) it follows that the variable $\hat{\rho}$ that characterizes the (anti-)instanton size is small (i.e. power-like suppressed with ε) in both the low-energy and the high-energy regimes. Thus it is justifiable to neglect the higher-order-in-$\hat{\rho}$ corrections to the expression, Eq. (3.2.4), for $\mathcal{F}$.

The inverse separation $1/\chi$ is small in the low-energy regime, $1/\chi \sim \varepsilon^{1/3} \to 0$, while in the opposite regime of asymptotically high energies, it is only logarithmically suppressed, $1/\chi \sim \log^{-1/6}(E/m_W)$. This implies that we need to take into account higher order corrections in powers of $1/\chi$ to the semiclassical exponent in Eq. (3.2.4). Hence we conclude from Eqs. (3.2.9)-(3.2.10) that we can continue working with small instantons, but in the high-energy limit we will also have to include higher-order-in-ρ/R corrections to the dipole-dipole interactions of instantons. This will be done in the following section.

For now, we can present the saddle-point value of the semiclassical exponent based on the leading-order expression. It is instructive to cancel the factor of $4\pi/\alpha_w$ on both sides of Eq. (3.2.4) and define the function $S(\chi)$ via,

$$S_{I\bar{I}} = \frac{4\pi}{\alpha_w}\left(S(\chi)+\frac{1}{2}\hat{\rho}^2\right), \tag{3.2.11}$$

where $S(\chi)$ corresponds to the pure gauge field part of the $I\bar{I}$ action, Eq. (3.2.5). In the maximally attractive relative orientation channel, $u_\mu = R_\mu/R$, we have,

$$S(\chi) = 1 - 6/\chi^4 + \dots . \tag{3.2.12}$$

Using the saddle-point equations, we find a surprisingly compact expression for the

holy-grail function $\mathcal{F}$ computed on the saddle-point[1],

$$\mathcal{F}_* = S(\chi) - \frac{1}{2}\chi S'(\chi). \tag{3.2.13}$$

At energies much below the sphaleron mass we reproduce the well-known low-energy expression [40, 67, 68],

$$\mathcal{F}_* = 1 - \frac{18}{\chi^4} + \mathcal{O}(1/\chi^6) = 1 - \frac{6^{1/3}3}{2^4}\varepsilon^{4/3} + \mathcal{O}(\varepsilon^2), \tag{3.2.14}$$

$$\sigma_I \sim e^{-\frac{4\pi}{\alpha_w}\left(1-\frac{6^{1/3}3}{2^4}\varepsilon^{4/3}\right)} \ll 1 \qquad \text{for } \varepsilon \ll 1. \tag{3.2.15}$$

To access the high-energy regime, we need to extend this analysis to finite separations.

3.2.1 Accounting for the higher-order terms in $I\bar{I}$ interactions

The action of the instanton–anti-instanton configuration is known in the electroweak theory to next-to-next-to-leading-order (NNLO) in the expansion in inverse separation, ρ/R, and the instanton scale size, $m_w\rho$, parameters. The expression generalising the leading-order formula, Eq. (3.2.5), was derived in [69]. In terms of the dimensionless variables,

$$\chi = R/\rho, \qquad \hat{\rho} = m_W\rho, \tag{3.2.16}$$

for the symmetric configuration, $\rho = \bar{\rho}$, in the maximally attractive $I\bar{I}$ interaction channel, the instanton–anti-instanton action reads,

$$\begin{aligned} S_{I\bar{I}} = \frac{4\pi}{\alpha_w}\Bigg[S(\chi) + \frac{1}{2}\hat{\rho}^2\left(1 + \frac{1}{\chi^2} - \frac{12}{\chi^4}\log\chi\right) \\ + \frac{1}{2}\hat{\rho}^4\left(\left(\frac{3}{2} - \frac{1}{2}\frac{m_H^2}{m_W^2}\right)\log\chi + \left(\frac{3}{2} - \frac{m_H^2}{m_W^2}\right)\log\hat{\rho} - \frac{m_H^2}{m_W^2}\log\left(\frac{m_H}{m_W}\right)\right)\Bigg]. \end{aligned} \tag{3.2.17}$$

As before, $S(\chi)$ appearing on the right hand side of Eq. (3.2.17), denotes the terms in the normalized $I\bar{I}$ action that arise solely from the gauge field components of the

[1] We note that $\mathcal{F}_*$ in Eq. (3.2.13) depends only on the χ variable, while the dependence on $\hat{\rho}$ has cancelled out.

instanton–anti-instanton configuration. To the order $\mathcal{O}(\chi^{-8}\log\chi)$ it reads,

$$S(\chi) = 1 - \frac{6}{\chi^4} + \frac{24}{\chi^6} + \frac{72}{\chi^8}\log\chi. \tag{3.2.18}$$

The remaining terms in the square brackets in Eq. (3.2.17) account for the Higgs field components and their interactions with the gauge fields, including the mass effects. The overall expression Eq. (3.2.17) gives the $I\bar{I}$ action up to the order $\hat{\rho}^4$, $\hat{\rho}^2\chi^{-4}$ and χ^{-8}. The corresponding instanton holy-grail function $\mathcal{F}$, Eq. (3.2.4), then takes the form,

$$\begin{aligned}\mathcal{F} = &-\frac{1}{4}\varepsilon\hat{\rho}\chi + S(\chi) + \frac{1}{2}\hat{\rho}^2\left(1 + \frac{\varepsilon^2}{8}\log\left(\frac{\varepsilon\pi}{\alpha_w}\right) + \frac{1}{\chi^2} - \frac{12}{\chi^4}\log\chi\right)\\ &+\frac{1}{2}\hat{\rho}^4\left(\left(\frac{3}{2} - \frac{1}{2}\frac{m_H^2}{m_W^2}\right)\log\chi - \left(\frac{3}{2} - \frac{m_H^2}{m_W^2}\right)\log\hat{\rho} - \frac{m_H^2}{m_W^2}\log\left(\frac{m_H}{m_W}\right)\right).\end{aligned} \tag{3.2.19}$$

The saddle-point solution, $\hat{\rho}(\varepsilon)$, $\chi(\varepsilon)$, is determined by solving the equations,

$$\partial_\chi\mathcal{F}(\chi,\hat{\rho};\varepsilon) = 0 \qquad \partial_{\hat{\rho}}\mathcal{F}(\chi,\hat{\rho};\varepsilon) = 0, \tag{3.2.20}$$

which is then used to compute the value of $\mathcal{F}$ on the saddle-point, $\mathcal{F}_*(\varepsilon)$, that dominates the instanton cross-section integral, Eq. (3.2.3), in the steepest-descent, or semi-classical approximation.

The low-energy limit

At energies much below the sphaleron scale, $\varepsilon \ll 1$, we can neglect the $\frac{\varepsilon^2}{8}\log\left(\frac{\varepsilon\pi}{\alpha_w}\right)$ term on the first line in Eq. (3.2.19) relative to 1, and from this determine the value of $\mathcal{F}_*(\varepsilon)$ at the corresponding saddle-point solution:

$$\mathcal{F}_* = 1 - \frac{6^{1/3}3}{2^4}\varepsilon^{4/3} + \frac{3}{32}\varepsilon^2 + \frac{1}{64}\frac{3^{2/3}}{2^{1/3}}\left(\frac{m_H^2}{m_W^2} - \frac{4}{3}\right)\varepsilon^{8/3}\log(1/\varepsilon) + \mathcal{O}(\varepsilon^{8/3}). \tag{3.2.21}$$

The first three terms on the right hand side of Eq. (3.2.21) were computed in [40] and the NNLO term in the ε expansion $\sim \varepsilon^{8/3}\log(1/\varepsilon)$ was derived in [69].

Our main objective is to go beyond the known low-energy regime established by Eq. (3.2.21). To this end we will now consider the opposite extreme of the high-

energy limit, $\varepsilon \gg 1$, with the ultimate aim to be able to match the two regimes at intermediate values of ε where the energy is of the order of the sphaleron mass, showing that our expression in the high-energy limit correctly reproduces the known low-energy result, giving us confidence that, for the first time, we have valid results for the electroweak instanton cross section at all values of the energy.

The high-energy limit

As we already noted in the previous section, instantons remain small in the high-energy range; according to the second equation in Eq. (3.2.10) the dominant value of the instanton size is $\hat{\rho} \sim \varepsilon^{-1} \log^{-5/6}(\varepsilon\pi/\alpha_w) \to 0$ when $\varepsilon \to \infty$.

Thus we can neglect all $\sim \hat{\rho}^4$ terms and most of the $\sim \hat{\rho}^2$ terms in the expression for $\mathcal{F}$ on the right hand side of Eq. (3.2.19). The only $\sim \hat{\rho}^2$ term that we must retain in the $\varepsilon \to \infty$ limit is the term enhanced by ε^2, namely the $\frac{1}{2}\hat{\rho}^2 \frac{\varepsilon^2}{8} \log \frac{\varepsilon\pi}{\alpha_w}$ contribution arising from the resummed hard quantum corrections in the $I\bar{I}$ background. With this we have,

$$\mathcal{F} = -\frac{1}{4}\varepsilon\hat{\rho}\chi + S(\chi) + \frac{1}{2}\hat{\rho}^2 \left(\frac{\varepsilon^2}{8} \log\left(\frac{\varepsilon\pi}{\alpha_w}\right) + 1 \right). \tag{3.2.22}$$

In practice, to facilitate the comparison between the high-energy and the low-energy limits, we have also retained the order-1 term in addition to the order-ε^2 term in the brackets on the right hand side of Eq. (3.2.22).

Our earlier analysis of the saddle-point solution for the $I\bar{I}$ separation variable χ in the second equation in Eq. (3.2.9), indicates that $1/\chi$ is only logarithmically suppressed in the high-energy limit, and hence we cannot continue using the large separation approximation to the gauge-field instanton–anti-instanton action, $S(\chi)$, in the form in Eq. (3.2.18). We need the expression for $S(\chi)$ valid at all finite separations.

This is where the gradient flow approach, a.k.a. the valley method, of Balitsky and Yung [18, 31] for constructing instanton–anti-instanton configurations at arbitrary values of instanton and anti-instanton collective coordinates in gauge theory becomes

indispensable and solves the problem. This method is explained in more detail in Appendix A. Using the conformal invariance of classical Yang-Mills theory, in [18] Yung found an exact solution of the valley equation for the instanton–anti-instanton gauge field configuration, $A_\mu^{I\bar{I}}$. The action on this configuration was computed in [17, 32, 33] and gives,

$$S_{I\bar{I}}^{\text{gauge}}(z) = \frac{16\pi^2}{g^2}\left(3\frac{6z^2-14}{(z-1/z)^2} - 17 - 3\log(z)\left(\frac{(z-5/z)(z+1/z)^2}{(z-1/z)^3} - 1\right)\right) \tag{3.2.23}$$

where the variable z is the conformal ratio of the (anti-)instanton collective coordinates,

$$z = \frac{R^2+\rho^2+\bar{\rho}^2+\sqrt{(R^2+\rho^2+\bar{\rho}^2)^2-4\rho^2\bar{\rho}^2}}{2\rho\bar{\rho}}, \tag{3.2.24}$$

which plays the role of the single negative mode of the instanton–anti-instanton valley configuration along which the instantons attract each other.

The expression for $S(\chi)$ that we need to use on the right hand side of Eq. (3.2.22) follows from the above,

$$S(\chi) = 3\frac{6z^2-14}{(z-1/z)^2} - 17 - 3\log(z)\left(\frac{(z-5/z)(z+1/z)^2}{(z-1/z)^3} - 1\right)\Bigg|_{z=z(\chi)}, \tag{3.2.25}$$

$$z(\chi) = \frac{1}{2}\left(\chi^2 + \chi\sqrt{\chi^2+4} + 2\right). \tag{3.2.26}$$

$\mathcal{S}(\chi)$ is plotted in Fig. 3.1.

The saddle-point equations, Eq. (3.2.20), for $\mathcal{F}$ given in Eq. (3.2.22) read,

$$\frac{1}{4}\varepsilon\hat{\rho} = S'(\chi), \quad \frac{1}{4}\varepsilon\chi = \hat{\rho}\left(\frac{\varepsilon^2}{8}\log\left(\frac{\varepsilon\pi}{\alpha_w}\right)+1\right). \tag{3.2.27}$$

Their solutions are given by:

$$\frac{\chi}{2\left(\log\left(\frac{\varepsilon\pi}{\alpha_w}\right)+8\varepsilon^{-2}\right)} = S'(\chi), \tag{3.2.28}$$

$$\hat{\rho} = \varepsilon^{-1}4S'(\chi), \tag{3.2.29}$$

where Eq. (3.2.28) gives an equation for χ that can be solved numerically or graphically, as indicated in Fig. 3.2. The solution for $\hat{\rho}$ is then read off from the second

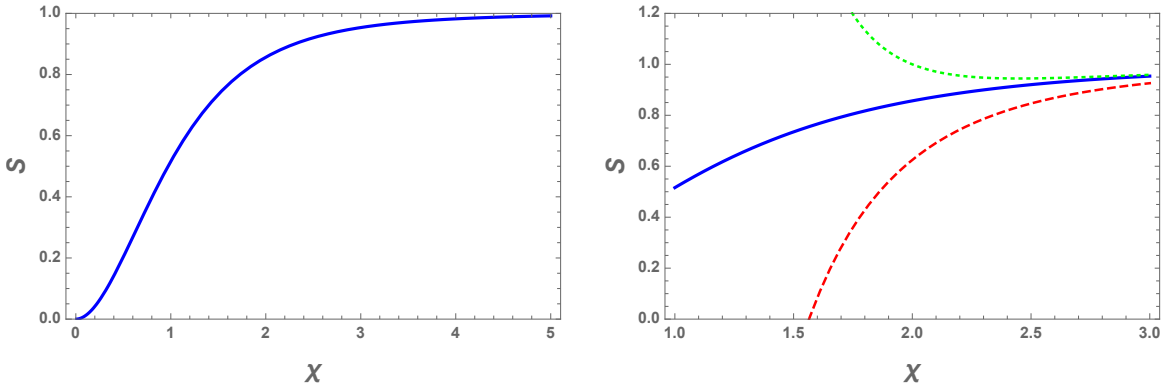

Figure 3.1: The action, Eq. (3.2.25), of the instanton–anti-instanton gauge configuration as a function of $\chi = R/\rho$ (solid line). $S(\chi)$ approaches one as $\chi \to \infty$ where the interaction potential vanishes, and $S \to 0$ as $\chi \to 0$ where the instanton and the anti-instanton annihilate into the perturbative vacuum. The plot on the right also shows the leading-order (dashed line) and the next-to-leading-order (dotted line) approximations in Eq. (3.2.18). The regime of interest to us for matching the high-energy and the low-energy regimes is $\chi \sim 2$, which is far away from the perturbative annihilation region.

equation, Eq. (3.2.29).

Eq. (3.2.28) is satisfied when the coefficient in front of χ,

$$C(\varepsilon) = \frac{1}{2\left(\log\left(\frac{\varepsilon\pi}{\alpha_w}\right) + \frac{8}{\varepsilon^2}\right)}, \tag{3.2.30}$$

matches the slope of $S(\chi)$. This coefficient is plotted on the left panel in Fig. 3.2 and has a maximum at $\varepsilon = 4$,

$$\max_\varepsilon C(\varepsilon) = \frac{1}{2\log\left(\frac{4\pi}{\alpha_w}\right) + 1} \simeq 0.078, \quad \text{at } \varepsilon = 4. \tag{3.2.31}$$

The $I\bar{I}$ separation, χ, is minimal, $\chi_{\min} = 2.06$, at the critical value of $\varepsilon = 4$ and grows at both higher, $\varepsilon > 4$, and lower, $\varepsilon < 4$, energies.

The holy-grail function, Eq. (3.2.22), computed on the solutions $\chi(\varepsilon)$, $\hat{\rho}(\varepsilon)$ at the saddle-point, Eqs. (3.2.28)-(3.2.29), takes the form,

$$\mathcal{F}_* = S(\chi) - \frac{1}{2}\chi S'(\chi), \tag{3.2.32}$$

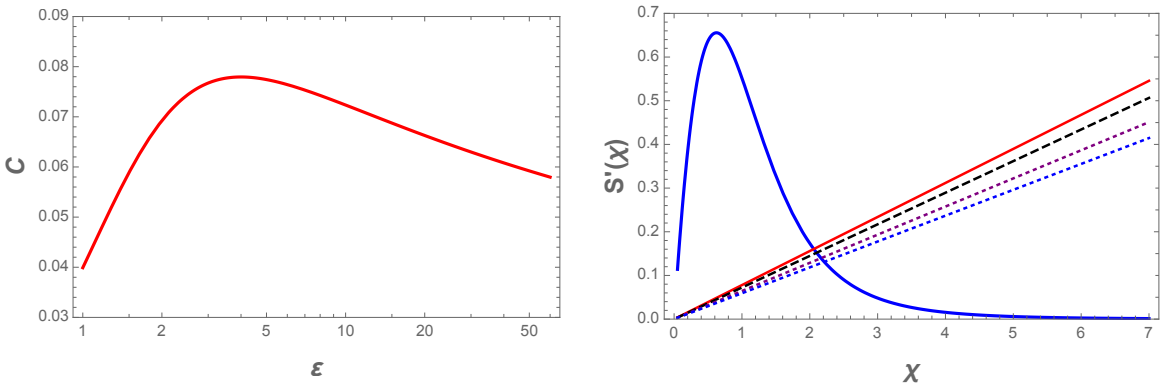

Figure 3.2: The plot on the left depicts the function $C(\varepsilon)$ in Eq. (3.2.30) with a local maximum at $\varepsilon = 4$. The plot on the right shows the derivative of the action, $S'(\chi)$, (solid blue line) and the linear function $C(\varepsilon)\chi$ for various values of the energy ε. The steepest possible slope of $C(\varepsilon)\chi$ is at $\varepsilon = 4$ (solid red line), with higher energies represented by $\varepsilon = 10$ (dashed black), $\varepsilon = 25$ (dotted purple) and $\varepsilon = 50$ (dotted blue line). The saddle-point values of χ are given by the intersection points of the $S'(\chi)$ curve with the lines $C(\varepsilon)\chi$ for each value of ε.

where we made use of the saddle-point equations, Eq. (3.2.27), in arriving at the compact expression above. Note that $\mathcal{F}_*$ is given by the same formula in terms of S as in the low-energy limit in Eq. (3.2.13).

Table 3.1 presents a selection of the saddle-point values, $\chi(\varepsilon)$, $\hat{\rho}(\varepsilon)$, along with the corresponding values for the normalized $I\bar{I}$ action, $S(\chi)$, and the holy grail function, $\mathcal{F}_*$, in the high-energy range, starting with $\varepsilon = 30$ and going down in energy past the turning point $\varepsilon = 4$, where $\mathcal{F}_*$ is minimal, down to a minimum energy of $\varepsilon = 0.5$.

The instanton suppression factor, $\mathcal{F}_*(\varepsilon)$, is plotted in Fig. 3.3 over the entire energy range. It can be seen from the data in Table 3.1 and from Fig. 3.3 that instanton–anti-instanton separations are never below $\chi_{\rm min} \simeq 2.06$, thus staying clear from the perturbative region. It should be noted from the data in Table 3.1 that our instantons remain small over the whole range of energies considered, justifying the use of our approximations, and the $I\bar{I}$ action is large, $S \geq 0.867$. The instanton suppression factor is significant with the minimal value of the holy-grail function, $\mathcal{F} \simeq 0.70$,

ε	χ	$\hat{\rho}$	$S(\chi)$	F_*
30	2.178	0.018	0.884	0.735
20	2.150	0.028	0.880	0.727
10	2.101	0.061	0.873	0.713
7.0	2.078	0.089	0.870	0.707
5.0	2.063	0.128	0.867	0.702
4.0	2.059	0.160	0.867	0.701
3.0	2.068	0.212	0.868	0.704
2.0	2.125	0.294	0.877	0.720
0.5	3.090	0.345	0.958	0.891

Table 3.1: Saddle-point solution for the instanton separation, $\chi = R/\rho$, and the instanton size, $\hat{\rho}$, along with the values for the $I\bar{I}$ action, $S(\chi)$, and the instanton suppression function, $\mathcal{F}_*$, in the range from $0.5 \leq \varepsilon = E/(\pi m_W/\alpha_w) \leq 30$. The saddle-point was obtained using the simplified analytic expression for $\mathcal{F}$ in Eq. (3.2.22). Instantons are exponentially suppressed at all energies with the minimal value of $\mathcal{F}_*$ at the critical energy $\varepsilon = 4$.

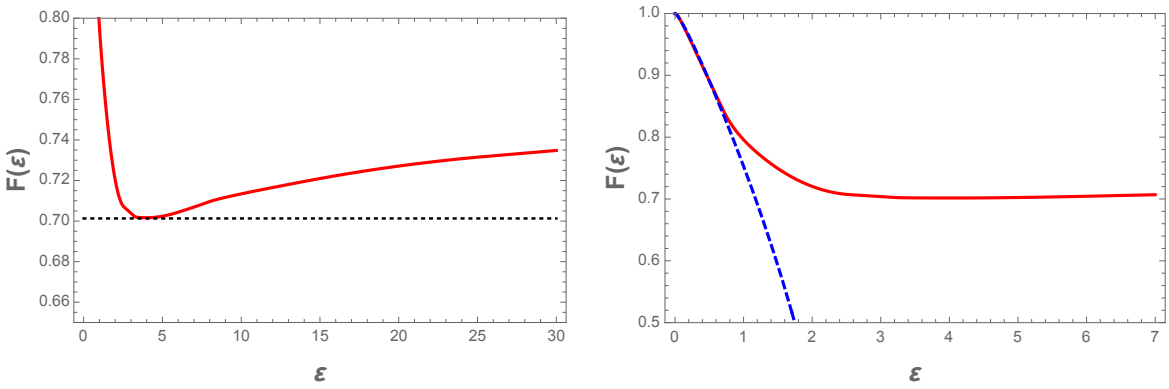

Figure 3.3: The instanton suppression holy grail function, $\mathcal{F}$, Eq. (3.2.32), (shown in red) plotted over a broad energy range, $0 \leq \varepsilon = \frac{E}{\pi m_W/\alpha_w} \leq 30$. The horizontal dotted line indicates the minimal value of $\mathcal{F} \simeq 0.70$ that occurs at $\varepsilon = 4$. The matching between the high-energy and the low-energy regimes is smooth as shown in the plot on the right. The known analytic expression, Eq. (3.2.21), for $\mathcal{F}(\varepsilon)$ (dashed blue line) shows a good match with our result for $\varepsilon < 1$.

loosing only 30% of the original 't Hooft instanton suppression. At energies lower and higher than the critical energy, $\varepsilon = \frac{E}{\pi m_W/\alpha_w} = 4$, the suppression of the instanton rate increases further. Electroweak instantons remain exponentially suppressed by at least $e^{-\frac{4\pi}{\alpha_w}0.70}$ and are unobservable in high-energy two-particle collisions for any value of the energy.

It should be noted in Fig. 3.3 that we correctly reproduce the already known low-energy result as promised earlier in this section. We have matched our high-energy results to the known low-energy results, giving us confidence that we have results which are valid at all energies.

In Table 3.2, we present the saddle-point values of $\hat{\rho}, \chi$ and $\mathcal{F}$ which come from a numerical solution of the full saddle-point equations coming from Eq. (3.2.19), taking into account all known terms, i.e. not neglecting the higher order $\hat{\rho}$ terms as we did above. It can be seen from this data that the inclusion of these higher order terms does not significantly affect our conclusions; the holy-grail function, $\mathcal{F}$, still does not drop far below 0.7, leading to an exponential suppression of electroweak instanton processes, indicating that they should be unobservable at colliders.

ε	χ	$\hat{\rho}$	$S(\chi)$	F_*
30	2.143	0.018	0.879	0.735
20	2.187	0.029	0.885	0.727
10	2.102	0.061	0.873	0.713
7.0	2.076	0.090	0.869	0.706
5.0	2.065	0.130	0.867	0.700
4.0	2.056	0.165	0.866	0.697
3.0	2.065	0.225	0.867	0.696
2.0	2.100	0.352	0.873	0.699
0.5	2.632	0.394	0.931	0.861

Table 3.2: Numerical solutions of the saddle point equations coming from Eq. (3.2.19) in the same energy range as in Table 1. Instantons remain exponentially suppressed at all energies with the minimal value of $\mathcal{F}_*$ at the critical energy $\varepsilon \simeq 3$.

3.3 More on hard quantum corrections

In this section we will give a brief overview of quantum corrections arising from interactions between gauge bosons [19] and between fermions in the initial state. In our calculation in the preceding section these quantum effects have been accounted for by the $\frac{\alpha_w}{16\pi}(\rho^2+\bar{\rho}^2)E^2\log\left(E^2/m_W^2\right)$ term in the holy grail function.

3.3.1 Quantum corrections from vector bosons

We first consider the instanton-generated $2\to n$ process in a pure gauge theory. The classical result and the leading order correction in instanton perturbation theory to this amplitude are shown in Fig. 3.4. We are concentrating here on quantum corrections due to initial state particles; other interactions involving initial-final and final-final state interactions are already accounted for in the optical theorem approach.

In order to capture the high-energy behavior of the perturbative expansion around the instanton, we need the expression for the gauge-field propagator in the instanton background in the high-energy limit. The required result was derived by Mueller in [20]. Starting from the full expression for the propagator from [70], upon continuation to Minkowski space and taking the on-shell limit, $p_1^2=0=p_2^2$, along with the high-energy limit, $2p_1.p_2=s\gg 1/\rho^2$, where ρ is the instanton size, the result of [20] is,

$$G_{\mu\nu}^{ab}\left(p_1,p_2\right)\to-\frac{g^2\rho^2 s}{64\pi^2}\log\left(s\right)A_\mu^a\left(p_1\right)A_\nu^b\left(p_2\right), \tag{3.3.1}$$

where $A_\mu^a\left(p_1\right)$ and $A_\nu^b\left(p_2\right)$ are the instanton solutions for the gauge fields in momentum space. The key point of this expression is that in the high-energy limit the instanton vector propagator is proportional to the product of the classical instanton fields – this fact will be relevant for the resumation of these effects. The coefficient in front of the instanton fields involves the large quantity $\rho^2 s\log s$ which compensates for the smallness of the perturbative coupling g^2.

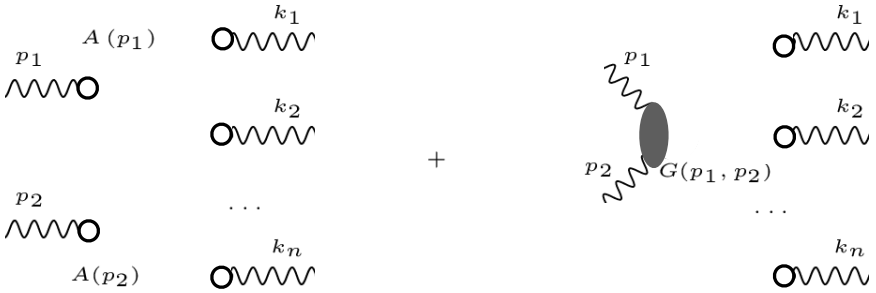

Figure 3.4: The classical contribution and the leading-order correction to the $2 \to n$ gauge-boson amplitude in the instanton background. Each tadpole represents an insertion of the instanton gauge field into the path integral, and the shaded blob corresponds to the vector-boson propagator $G^{ab}_{\mu\nu}\,(p_1, p_2)$ in the instanton background.

The two initial-state vector bosons are represented in the instanton perturbation theory as the product of two instanton field configurations, $A^a_\mu\,(p_1)\,A^b_\nu\,(p_2)$, shown as the two tadpoles on the left in the first diagram in Fig. 3.4. The first quantum correction to this initial state comes from the propagator, $G^{ab}_{\mu\nu}\,(p_1, p_2)$, as shown in the second diagram in Figure 3.4. The combined result of these two diagrams is the insertion of the factor,

$$\left(1 - \frac{g^2\rho^2 s}{64\pi^2}\log s\right) A^a_\mu\,(p_1)\,A^b_\nu\,(p_2)\,, \tag{3.3.2}$$

into the path integral to represent the 2-particle initial state in the corresponding $(2+n)$-point correlator.

In [19] Mueller computed the higher-order corrections to this result by summing over all loop-level perturbative diagrams to order N involving the two initial-state vector bosons in the instanton background. The result is,

$$\sum_{r=1}^{N} \frac{1}{r!}\left(-\frac{g^2\rho^2 s}{64\pi^2}\log\,(s)\right)^r A^a_\mu\,(p_1)\,A^b_\nu\,(p_2)\,. \tag{3.3.3}$$

This equation is justified in the limit $\rho^2 s \to \infty$ with $g^2 \to 0$ such that any power of $g^2\rho^2 s$ is counted as of order 1.

In the limit $N \to \infty$ we obtain the exponential factor,

$$\exp\left[-\frac{\alpha_w}{16\pi}\rho^2 E^2 \log\left(E^2/m_W^2\right)\right]. \tag{3.3.4}$$

The contribution of the Mueller term above to the cross-section is then,

$$\exp\left[-\frac{\alpha_w}{8\pi}\rho^2 E^2 \log\left(E^2/m_W^2\right)\right] = \exp\left[-\frac{4\pi}{\alpha_w}\frac{\hat{\rho}^2\varepsilon^2}{16}\log(\varepsilon\pi/\alpha_w)\right], \tag{3.3.5}$$

in agreement with the third term on the right hand side of Eq. (3.2.22) that we used in the previous section for the holy grail function $\mathcal{F}$.

Can one formally justify taking the $N \to \infty$ limit in Eq. (3.3.3)? To be able to do this, we have to demonstrate that the sum in Eq. (3.3.3) correctly approximates the instanton perturbation theory for values of N greater than the critical value, $N_{\rm crit} \sim \frac{\alpha_w}{16\pi}\rho^2 s$. This critical value is given by the argument of the exponent, and for values of r much above this $N_{\rm crit}$ each term in the sum in Eq. (3.3.3) is parametrically smaller than the exponent, Eq. (3.3.4), so it can be legitimately dropped. The expression in Eq. (3.3.3) was derived in [19] by retaining only the most dominant terms in the high-energy limit $s\rho^2 \gg 1$. The $N^{\rm th}$ term in Eq. (3.3.3) follows from the $(N-1)$-loop level diagrams shown in Fig. 9 in [19]. To justify the approximation where all sub-leading terms are not retained, it is required that $\rho^2 s/N^2 \gg 1$. Hence we can trust the sum in Eq. (3.3.3) only up to $N < \sqrt{\rho^2 s}$. This implies the exponentiation is valid provided [19],

$$\frac{\alpha_w}{16\pi}\rho^2 s < N < \sqrt{\rho^2 s}. \tag{3.3.6}$$

Mueller discusses this limit in the low-energy regime where the function in the exponent in Eq. (3.3.4) is sub-leading relative to the other terms in the holy grail function (specifically, it goes as $\varepsilon^{8/3}$ relative to the leading contributions, $\varepsilon^{4/3}$, where $\varepsilon \ll 1$). We want to consider instead the high-energy regime, $\varepsilon \gtrsim 1$, where the Mueller quantum effect, Eq. (3.3.4), plays the dominant role in cutting off the instanton size. This implies that the magnitude of the Mueller term is comparable to the other terms in the exponent (e.g. the constant term in the instanton–anti-instanton action) so $\frac{\alpha_w}{16\pi}\rho^2 s \sim \frac{2\pi}{\alpha_w} C$ where C is of the order of $1 - \mathcal{F}_*$, roughly 0.3

around the critical energy (and less than that otherwise). This gives the characteristic value of $\rho^2 s \sim \frac{32\pi^2}{\alpha_w^2} C$ where the Mueller exponent becomes important. Plugging this into the inequality, Eq. (3.3.6), we find,

$$\frac{2\pi}{\alpha_w} C < N < \frac{4\sqrt{2}\pi}{\alpha_w}\sqrt{C}. \tag{3.3.7}$$

Since we expect $C < 1$, this 'window of opportunity' for N is certainly not empty. So, while there is no rigorous proof of exponentiation, we are comfortably optimistic that the Mueller correction does exponentiate and Eq. (3.3.4) holds[1].

We should point out, however, that we cannot a priori exclude higher-order perturbative corrections to the Mueller term in the exponent of Eq. (3.3.4) that would be of the form,

$$\alpha_w(\alpha_w \rho^2 E^2)^2 \sim \frac{1}{\alpha_w}(\hat{\rho}\varepsilon)^4. \tag{3.3.8}$$

Such a term is subdominant relative to the Mueller term, $\sim \alpha_w \rho^2 E^2$, in the limit $\alpha_w \to 0$, $\rho^2 E^2 \to \infty$ with $\alpha_w \rho^2 E^2$ held fixed, and as such can potentially be generated in the instanton perturbation theory. Accounting for this correction, the exponent in Eq. (3.3.5) would be modified as follows,

$$\exp\left[-\frac{4\pi}{\alpha_w}\left(\frac{\hat{\rho}^2\varepsilon^2}{16} + A\hat{\rho}^4\varepsilon^4\right)\log(\varepsilon\pi/\alpha_w)\right], \tag{3.3.9}$$

where A is a constant. Parametrically, the saddle-point solution for $\hat{\rho}$ in the high-energy regime goes as $\hat{\rho} \sim 1/\varepsilon$, according to Eq. (3.2.29), and both terms are of the same order. This implies that the higher-order corrections to the Mueller term in the exponent (if present) could modify our conclusions. However, for a positive constant A, the instanton rate would become only more suppressed. On the other hand, for a negative A, one can always reach a sufficiently high energy, $\varepsilon_\star$, where the instanton size, ρ, is no longer cut-off either by the Mueller term or by the Higgs vev, and the IR problem of large instantons is re-introduced with the integral over ρ now

[1]There are of course many known examples of resummed perturbation theory that give rise to decaying exponentials. These include Sudakov form-factors [71] and further examples are provided by resummed leading-loop corrections to tree-level $1 \to n$ perturbative amplitudes near mass thresholds [72] contributing to another incarnation of a perturbative holy grail function.

exponentially divergent. We find such a UV/IR mixing[1] in the electroweak theory to be highly unlikely, and will assume on physical grounds that no exponentially growing corrections to the Mueller term are present.

Up to now we have only considered the initial-state corrections arising from interactions between gauge bosons, but as we will show in the next sub-section, the same result, Eq. (3.3.4), applies equally well to fermions in the initial state, which is our main case of interest for the process given in Eq. (3.2.1). The reason is that the initial state fermions will radiate gauge bosons.

3.3.2 Quantum corrections from initial fermions

We will now consider the instanton-generated process with fermions in the initial state. For simplicity consider the 2 fermions into n vector bosons process in a theory with 1 fermion flavor (generalization to the full process of Eq. (3.2.1) in the Standard Model is trivial as the differences involve only the final state),

$$q + q \to nW. \tag{3.3.10}$$

At the leading order in instanton perturbation theory, the two quarks q are represented by insertions of the instanton fermion zero modes, $\psi^{(0)}$, and the n final-state vector bosons, W, are represented by insertions of n instanton gauge-field configurations, A_μ, into the corresponding correlator. This leading-order classical contribution to the process in Eq. (3.3.10) is represented by the first diagram in Fig. 3.5.

The fermion zero modes, $\psi^{(0)}(x)$, are the non-trivial (and normalizable) solutions of the Dirac equation in the instanton background, $A_\mu(x)$,

$$\gamma^\mu(\partial_\mu - igA_\mu)\psi^{(0)}(x) = 0. \tag{3.3.11}$$

This implies that we can represent the LSZ-reduced fermion zero mode in terms of the fermion-vector boson vertex, as indicated in Fig. 3.6.

[1] This refers to the fact that at all energies below $\varepsilon_\star$ instanton cross-sections are IR safe, while at energies above $\varepsilon_\star$, contributions of large instantons become exponentially divergent.

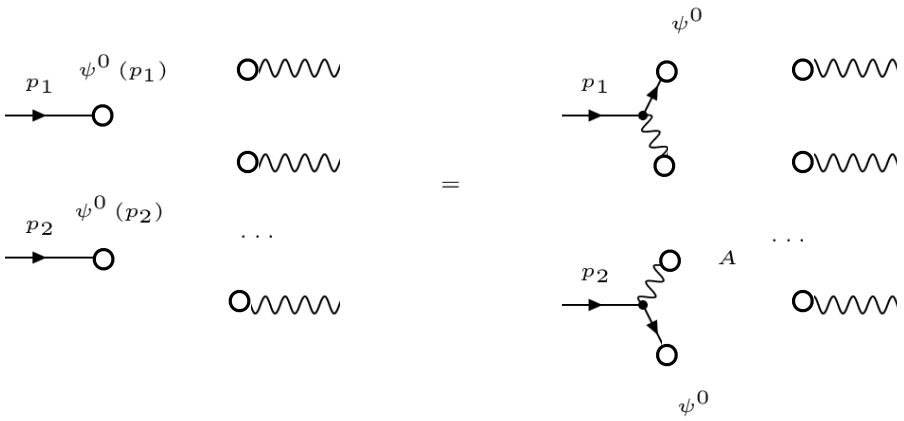

Figure 3.5: The leading-order diagram for the instanton process, Eq. (3.3.10) and its equivalent representation using the Dirac equation, Eq. (3.3.11).

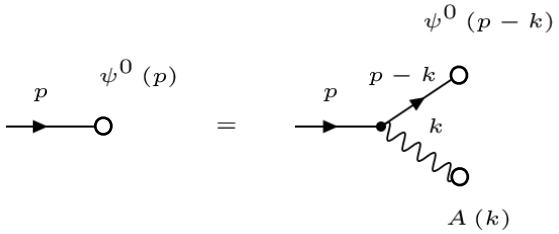

Figure 3.6: Pictorial representation of the Dirac equation, Eq. (3.3.11).

Using this we have the equivalent representation of the leading-order contribution to the process in Eq. (3.3.10) shown as the diagram on the right in Fig. 3.5. At the next-to-leading order in the instanton perturbation theory we simply connect the two gauge fields in this diagram by the propagator in the instanton background. This correction is represented by the second diagram in Fig. 3.7.

Using the known high-energy limit of the instanton vector propagator, we can write down the combined contribution of the two diagrams in Fig. 3.7 as,

$$\left(1-\frac{g^2\rho^2 s}{64\pi^2}\log s\right)\psi^{(0)}(p_1)\psi^{(0)}(p_2), \tag{3.3.12}$$

in a complete analogy with the corresponding expression for the initial-state gauge fields in Eq. (3.3.2). Now the problem has been reduced to keeping the dominant effects in the $\rho^2 s \to \infty$ limit in the instanton perturbation theory in the gauge sector. The outcome of this procedure is, as in the previous sub-section, the exponential

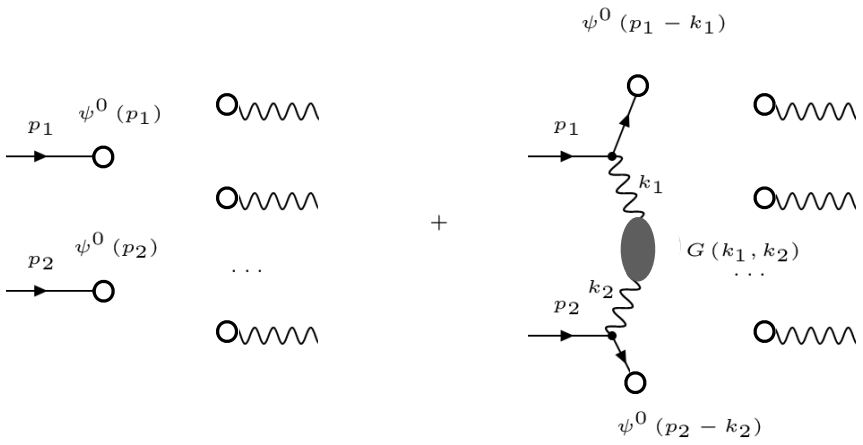

Figure 3.7: The leading and the next-to-leading order contributions to the instanton process with fermions in the initial state.

factor in Eq. (3.3.4),

$$\exp\left[-\frac{\alpha_w}{16\pi}\rho^2 E^2 \log\left(E^2/m_W^2\right)\right]\psi^{(0)}(p_1)\psi^{(0)}(p_2), \tag{3.3.13}$$

which reproduces the instanton contribution to the final term of the holy grail function, $\mathcal{F}$, that we used in Eq. (3.2.4).

3.4 Conclusions

In this chapter we have presented an updated calculation for the electroweak instanton cross section, combining the optical theorem formalism with the inclusion of quantum corrections arising from the initial state interactions, which result in the dominant effect in the high energy limit. A notable feature of our approach is that we were able to justify it in the high energy limit, where the energy is much greater than the sphaleron mass and where many earlier instanton-based estimates had failed. This was based in part on an assumption that there are no additional exponentially growing (and unphysical, as explained at the end of section 3.3.1) contributions generated at higher orders in instanton perturbation theory.

By interpolating between the high-energy and the low-energy results we have shown that electroweak instanton-dominated $2 \to n$ processes remain exponentially sup-

pressed at all energies and would not be observable, even in principle, at any collider. We did not provide a full calculation of the cross section involving all pre-exponential factors (which is possible, e.g. following the methods of [2]) as, given the magnitude of the exponential suppression, the cross section would still not reach an observable level.

It is interesting to compare our results to those of [73, 74]. The authors numerically computed rates for the electroweak transitions across the sphaleron barrier starting with processes containing a large number of particles $\sim N/\alpha_w \gg 1$ in the initial state, before taking the limit $N \to 0$ and assuming that it is smooth. The authors of [73, 74] also obtained that the cross section was exponentially suppressed at all energies. Their numerical results do not agree precisely with ours, but this should not be expected given the different starting points, methodologies and approximations. Nevertheless we consider the two approaches to be complimentary and they both lead to the same conclusions.

In our calculation, the electroweak instantons did not acquire a very substantial compensation of the original 't Hooft suppression factor, $e^{-4\pi/\alpha_w}$, that would correspond to $\mathcal{F} = 1$. Our results in Tables 3.1 and 3.2 (see also Fig. 3.3) for the instanton holy grail function, $\mathcal{F}$, show that the the 't Hooft suppression in the exponent is reduced by not more than $\sim 30\%$ over the entire energy range. This justifies neglecting contributions from the multi-instanton configurations that were considered in the 'premature unitarization' approach in [75–77] and were argued to suppress the instanton result if the function $\mathcal{F}$ was reduced by $\gtrsim 50\%$ in the original instanton calculation.

Chapter 4

A Classically Scale Invariant Extension of the Standard Model

We now shift away from considering tunnelling in the context of the Standard Model and consider tunnelling phenomena in the context of new physics. After the discovery of the Higgs boson in 2012 by the ATLAS and CMS experiments [78, 79], the Standard Model was complete and potentially valid all the way up to the Planck scale. However it is known that there are problems with the Standard Model and it cannot be a complete description of reality. One of these problems is the so-called hierarchy problem, the fact that the Higgs mass is unstable against quantum corrections; there is also the issue that we require dark matter in order to explain the observed density of the universe and new physics is also needed to explain the baryon asymmetry of the universe. The model proposed in this chapter goes some way to addressing each of these concerns and would also have experimentally observable consequences.

4.1 Classical Scale Invariance

In the Standard Model, the Higgs vev is introduced at tree level, but in the 1970s Coleman and Weinberg showed that it was possible for the tree level potential to

have its minimum at the origin and still develop a minimum away from the origin at loop level [80]. This idea was known as dimensional transmutation as we trade the dimensionful parameter of the Higgs quadratic term for the dimensionless parameter of the scalar coupling. As this also removes the dimension-2 operator in the standard model, it removes the source of corrections which depend quadratically on the UV cutoff and hence solves the Hierarchy problem [81, 82].

However due to the relationship induced between couplings in the dimensional transmutation it has been known since the 90s that the Standard Model Higgs is too heavy to come from a Coleman-Weinberg theory. To avoid this constraint one can apply the Coleman-Weinberg mechanism in a hidden sector [82–86] coupled to the Standard Model, for example via a Higgs portal interaction. This is the mechanism which will be investigated later in this chapter.

Firstly we must define the idea of the effective potential. Here we follow Quiros [1]. We start off with the partition function, although we now introduce a source term:

$$Z\left[j\right] = \int \mathcal{D}\phi\, e^{iS[\phi]+i\int d^4x\,\phi(x)j(x)}. \tag{4.1.1}$$

From this we then define the generating functional, W, and the effective action, Γ:

$$Z\left[j\right] = e^{iW[j]} \tag{4.1.2}$$

$$\Gamma\left[\bar{\phi}\right] = W\left[j\right] - \int \mathrm{d}^4x\,\bar{\phi}\left(x\right) j(x) \tag{4.1.3}$$

where

$$\bar{\phi}(x) = \frac{\delta W\left[j\right]}{\delta j(x)}. \tag{4.1.4}$$

We then Taylor expand the effective action to obtain

$$\Gamma\left[\bar{\phi}\right] = \sum_{n=0}^{\infty} \frac{1}{n!} \int \mathrm{d}^4x_1 \ldots \mathrm{d}^4x_n\, \bar{\phi}(x_1) \ldots \bar{\phi}(x_n) \Gamma^{(n)}\left(x_1, \ldots, x_n\right) \tag{4.1.5}$$

$$\Gamma\left[\bar{\phi}\right] = \sum_{n=0}^{\infty} \int \prod_{i=1}^{n} \left[\frac{\mathrm{d}^4p_i}{\left(2\pi\right)^4} \tilde{\phi}\left(-p_i\right)\right] \left(2\pi\right)^4 \delta^{(4)}\left(p_1 + \cdots + p_n\right) \Gamma^{(n)}\left(p_1, \ldots p_n\right) \tag{4.1.6}$$

where $\Gamma^{(n)}$ are the one-particle irreducible Green's functions and in going from the

first line to the second we have Fourier transformed $\Gamma^{(n)}$ and $\bar{\phi}$, i.e.

$$\Gamma^{(n)}(x) = \int \prod_{i=1}^{n} \left[\frac{\mathrm{d}^4 p_i}{(2\pi)^4} e^{ip_i x_i} \right] \delta^{(4)}(p_1 + \cdots + p_n)\, \Gamma^{(n)}(p) \tag{4.1.7}$$

$$\tilde{\phi}(p) = \int \mathrm{d}^4 x\, e^{-ip.x} \bar{\phi}(x). \tag{4.1.8}$$

If the theory under consideration is translationally invariant then $\bar{\phi}(x) = \phi_c$ where ϕ_c is some constant value. We then define the effective potential, $V_{eff}(\phi_c)$, as

$$\Gamma[\phi_c] = -\int \mathrm{d}^4 x\, V_{\text{eff}}(\phi_c). \tag{4.1.9}$$

We also have that $\tilde{\phi}_c(p) = (2\pi)^4 \phi_c \delta^{(4)}(p)$, substituting this into Eq. (4.1.6) yields:

$$\Gamma[\phi_c] = \sum_{n=0}^{\infty} \frac{1}{n!} \phi_c^n (2\pi)^4 \delta^{(4)}(0)\, \Gamma^{(n)}(p_i = 0) = \sum_{n=0}^{\infty} \frac{1}{n!} \phi_c^n \Gamma^{(n)}(p_i = 0) \int \mathrm{d}^4 x. \tag{4.1.10}$$

Hence we see that

$$V_{\text{eff}}(\phi_c) = -\sum_{n=0}^{\infty} \frac{1}{n!} \phi_c^n \Gamma^{(n)}(p_i = 0). \tag{4.1.11}$$

Having now defined the effective potential we follow [1,80] to illustrate the key ideas of classical scale invariance. We consider the theory of a single massless scalar:

$$\mathcal{L} = \frac{1}{2} \left(\partial_\mu \phi \right)^2 - \frac{\lambda}{4!} \phi^4. \tag{4.1.12}$$

We see from Eq. (4.1.11) that the effective potential is given by the sum of all Feynman diagrams where external legs have zero momentum. We perform the expansion in loops and sum over the diagrams shown in Fig. 4.1 to obtain the one-loop contribution:

$$V^1_{\text{eff}}(\phi_c) = i \sum_{n=1}^{\infty} \int \frac{\mathrm{d}^4 p}{(2\pi)^4} \frac{1}{2n} \left(\frac{\lambda \phi_c^2}{2p^2} \right)^n \tag{4.1.13}$$

where $V^1_{eff}(\phi_c)$ is the one loop contribution. We recognise this as the Taylor expansion for a logarithm and get

$$V^1_{\text{eff}}(\phi_c) = -\frac{i}{2} \int \frac{\mathrm{d}^4 p}{(2\pi)^4} \log \left(1 - \frac{\lambda \phi_c^2}{2p^2} \right). \tag{4.1.14}$$

We Wick rotate and discard a field-independent term (we discard $\log p^2$ as this would

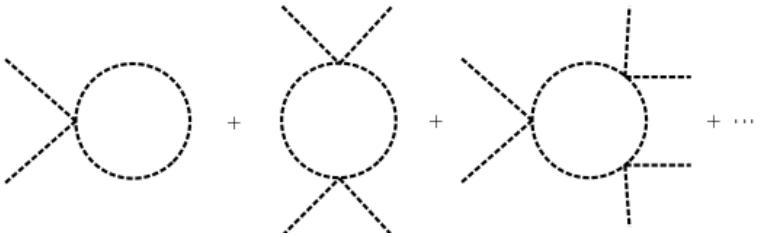

Figure 4.1: The infinite series of diagrams contributing to the one-loop effective potential arising from a scalar running in the loop.

only correspond to an overall shift of the potential) to obtain

$$V_{\text{eff}}^{1}\left(\phi_c\right)=\frac{1}{2}\int\frac{\mathrm{d}^4p}{\left(2\pi\right)^4}\log\left(p^2+m^2\left(\phi_c\right)\right) \tag{4.1.15}$$

where we have defined

$$m^2\left(\phi\right)=\frac{1}{2}\lambda\phi_c^2=\frac{d^2V_0}{d\phi_c^2}. \tag{4.1.16}$$

Note this equation is trivially modified to work in the case of a theory with intrinsic masses ($m^2\left(\phi\right)=\mu^2+\frac{1}{2}\lambda\phi_c^2$).

Clearly this integral diverges so we will work in dimensional regularisation and consider:

$$\begin{aligned}\frac{dV_{\text{eff}}^{1}}{dm^2}&=\frac{\mu^{2\epsilon}}{2}\int\frac{\mathrm{d}^{4-2\epsilon}p}{\left(2\pi\right)^{4-2\epsilon}}\frac{1}{p^2+m^2\left(\phi_c\right)}\\&=\frac{\mu^{2\epsilon}}{2\left(2\pi\right)^{4-2\epsilon}}\pi^{2-\epsilon}\left(m^2\left(\phi_c\right)\right)^{1-\epsilon}\Gamma\left(-1+\epsilon\right)\end{aligned} \tag{4.1.17}$$

where we have expanded to first order in ϵ and μ is the renormalisation scale. We then obtain after integration:

$$\begin{aligned}V_{\text{eff}}^{1}\left(\phi_c\right)&=\frac{\mu^{2\epsilon}}{2\left(2\pi\right)^{4-2\epsilon}}\pi^{2-\epsilon}\left(m^2\left(\phi_c\right)\right)^{2-\epsilon}\frac{\Gamma\left(-1+\epsilon\right)}{2-\epsilon}\\&=\frac{m^4\left(\phi_c\right)}{64\pi^2}\left(-\left(-\frac{1}{\epsilon}-\gamma_E+\log\left(4\pi\right)\right)+\log\left(\frac{m^2\left(\phi_c\right)}{\mu^2}\right)-\frac{3}{2}\right).\end{aligned} \tag{4.1.18}$$

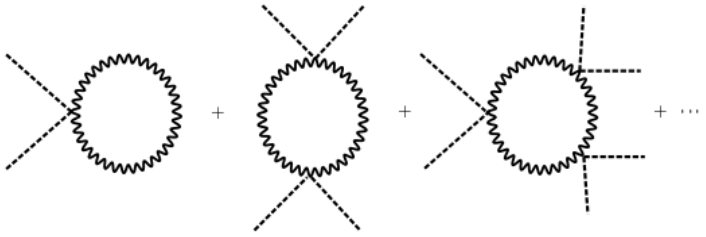

Figure 4.2: The infinite series of diagrams contributing to the one-loop effective potential arising from a boson running in the loop.

After substituting in the explicit form of $m(\phi_c)$, Eq. (4.1.16), and introducing the usual counterterms we have

$$V_{\text{eff}}(\phi_c) = \frac{1}{2}\delta m^2\phi_c^2 + \frac{\lambda+\delta\lambda}{4!}\phi_c^4 + \frac{\lambda^2\phi_c^4}{256\pi^2}\left(-\left(-\frac{1}{\epsilon}-\gamma_E+\log(4\pi)\right)+\log\left(\frac{m^2(\phi_c)}{\mu^2}\right)-\frac{3}{2}\right). \tag{4.1.19}$$

We shall work in the $\overline{MS}$ scheme and so we have

$$\delta m^2 = 0 \tag{4.1.20}$$

$$\delta\lambda = \frac{3\lambda^2}{32\pi^2}\left(-\frac{1}{\epsilon}-\gamma_E+\log(4\pi)\right) \tag{4.1.21}$$

$$V_{\text{eff}}(\phi_c) = \frac{\lambda}{4!}\phi_c^4 + \frac{\lambda^2\phi_c^4}{256\pi^2}\left(\log\left(\frac{m^2(\phi_c)}{\mu^2}\right)-\frac{3}{2}\right). \tag{4.1.22}$$

We now turn to massless scalar electrodynamics, following [80]. We have

$$\mathcal{L} = -\frac{1}{4}F_{\mu\nu}F^{\mu\nu}+\frac{1}{2}\left(\partial_\mu\phi_1 - eA_\mu\phi_2\right)^2+\frac{1}{2}\left(\partial_\mu\phi_2+eA_\mu\phi_1\right)^2-\frac{\lambda}{4!}\left(\phi_1^2+\phi_2^2\right)^2. \tag{4.1.23}$$

Due to the symmetry between ϕ_1, ϕ_2, the effective potential can only depend on $\phi_1^2+\phi_2^2$ so we shall compute the effective potential with all external legs being ϕ_1 and then utilise this knowledge. The case of ϕ_1, ϕ_2 running in the loop has already been covered. If we now consider the case of the gauge boson running in the loop we must resum the diagrams appearing in Fig. 4.2. The propagators are precisely the same as in the scalar case except the numerator now contains a factor (in the Landau gauge) of $\Delta^{\mu\nu} = g^{\mu\nu} - \frac{p^\mu p^\nu}{p^2}$ and the vertices will contain a factor of the metric which

will simply act to contract the numerators of adjacent propagators. Note that since we are working in the Landau gauge we do not need to consider terms arising from ghosts. Given the fact that $\Delta^{\mu\nu}\Delta_{\nu}^{\rho} = \Delta^{\mu\rho}$ we obtain

$$V_{eff}^{1,\text{boson}} = \Delta_{\mu}^{\mu} V_{eff}^{1,\text{scalar}} = 3V_{eff}^{1,\text{scalar}} \tag{4.1.24}$$

with the appropriate substitution of couplings. Here we have skipped over some subtleties regarding the evaluation of a trace in d dimensions; strictly speaking we have used the $\overline{DR}$ scheme where traces are considered in four dimensions whilst the integral is performed in d dimensions. Note that this result intuitively makes sense as a massive boson has 3 degrees of freedom compared to the single degree of freedom of a real scalar.

Hence we obtain for the full one loop effective potential:

$$\begin{aligned} V_{eff}(\phi_c) = \frac{\lambda}{4!}\phi_c^4 + \frac{\lambda^2\phi_c^4}{256\pi^2}\left(\log\left(\frac{m^2(\phi_c)}{\mu^2}\right) - \frac{3}{2}\right) \\ + \frac{\lambda^2\phi_c^4}{2304\pi^2}\left(\log\left(\frac{m^2(\phi_c)}{\mu^2}\right) - \frac{3}{2}\right) + \frac{3e^2\phi_c^4}{64\pi^2}\left(\log\left(\frac{m^2(\phi_c)}{\mu^2}\right) - \frac{3}{2}\right) \end{aligned} \tag{4.1.25}$$

where the first term is the tree level potential, the second term is the contribution from ϕ_1 running in the loop, the second term from ϕ_2 running in the loop (equivalent to the first term with $\lambda \to \lambda/3$ due to the change in the vertex factor) and the final term the contribution from the gauge boson running in the loop (coming from the first term with $\lambda \to 2e^2$ and an additional factor 3. If we now take λ to be order e^4 then we can drop the λ^2 terms and in addition since the renormalisation scale is arbitrary we shall take it to be the vev of the scalar field, $\langle\phi\rangle$). Hence

$$V_{eff}(\phi_c) = \frac{\lambda}{4!}\phi_c^4 + \frac{3e^2\phi_c^4}{64\pi^2}\left(\log\left(\frac{m^2(\phi_c)}{\langle\phi\rangle^2}\right) - \frac{3}{2}\right). \tag{4.1.26}$$

By definition we have that $V'_{eff}(\langle\phi\rangle) = 0$ where V' denotes the first derivative of the potential wrt ϕ_c so

$$\frac{\lambda}{6}\phi_c^3 - \frac{3e^4}{16\pi^2}\phi_c^3 = \left(\frac{\lambda}{6} - \frac{3e^4}{16\pi^2}\right)\phi_c^3 = 0. \tag{4.1.27}$$

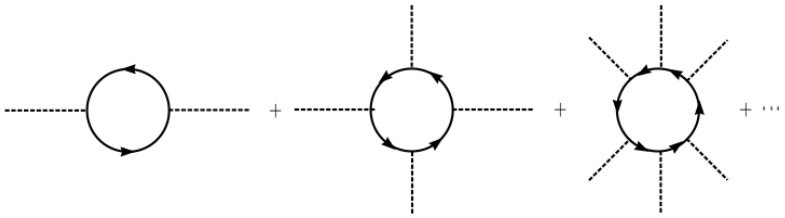

Figure 4.3: The infinite series of diagrams contributing to the one-loop effective potential arising from a fermion running in the loop.

Assuming $\phi_c \neq 0$ this then leads us to conclude that, at the renormalisation scale,

$$\lambda = \frac{9e^4}{8\pi^2}. \tag{4.1.28}$$

This is Coleman and Weinberg's phenomenon of dimensional transmutation, we can trade two dimensionless parameters, λ and e, (and then the vev would be the scale at which Eq. (4.1.28) holds) for a dimensionless parameter and a dimensionful parameter, $\langle\phi\rangle$ and e.g. e (and then λ is determined by Eq. (4.1.28)). This shows how a vev may develop in a scaleless theory. Note that some of our constants and coefficients differ from those in [80] due to a different choice of renormalisation scheme.

To conclude this section we shall anticipate the need to compute the effective potential in a theory with fermions and compute the series of diagrams in Fig. 4.3.

Firstly we note that the contribution from diagrams with an odd number of external legs vanishes as

$$Tr\left(\gamma^\mu \dots \gamma^\rho\right) = 0 \tag{4.1.29}$$

for any odd number of gamma matrices. For the remaining diagrams i.e. those in Fig. 4.3, the potential is given by

$$V_{eff}^{1,\text{fermion}}\left(\phi_c\right) = i\sum_{n=1}^{\infty}\frac{-1}{2n}Tr\left[\left(\frac{\not{p}m_f\left(\phi_c\right)}{p^2}\right)^{2n}\right] \tag{4.1.30}$$

where m_f contains the coupling and a factor of ϕ_c and we have an overall minus sign due to the fermion loop. Note that this method can only be applied to fermions without an intrinsic mass term, else in the following steps the numerator would not

simplify. Hence

$$V_{eff}^{\text{fermion}}(\phi_c) = -i\sum_{n=1}^{\infty}\frac{1}{2n}Tr\left(\frac{\not{p}m_f(\phi_c)}{p^2}\right)^{2n}$$
$$= -i\sum_{n=1}^{\infty}\frac{1}{2n}Tr\left(\frac{m_f^2(\phi_c)}{p^2}\right)^{n}Tr(\mathbb{1}) \tag{4.1.31}$$

after using the fact that $\not{p}\not{p} = p^2$. Note that the trace runs over spinor indices and so just gives a factor four for Dirac fermions. We now Wick rotate and again recognise the Taylor series of the logarithm to get

$$-2\int\frac{\mathrm{d}^4p}{(2\pi)^4}\log\left(p^2+m_f^2(\phi_c)\right) = -\frac{m^4(\phi_c)}{16\pi^2}\left(\log\left(\frac{m^2(\phi_c)}{\mu^2}\right)-\frac{3}{2}\right) \tag{4.1.32}$$

after again renormalising in the $\overline{DR}$ scheme (that is we have already subtracted the appropriate counterterms in Eq. (4.1.32)).

4.2 Introduction to Thermal Field Theory

Later in this chapter we will be interested in studying this model in the early universe, in particular how the theory might undergo a transition from a false minimum to a true minimum. In order to do this we must understand the effective potential in the early universe where the effects of finite temperature become important. So in this section we will develop the basics of QFT at finite temperature following [1]. At finite temperature the density operator is given by

$$\rho = e^{-\Phi}e^{-\beta H} \tag{4.2.1}$$

where H is the usual Hamiltonian of the system, $\Phi = \log\left(Tr\left(e^{-\beta H}\right)\right)$ and β is the inverse temperature. This is altered in the presence of a chemical potential but such considerations are unnecessary for our purposes. One can then define the grand canonical average of an operator to be

$$\langle O\rangle = Tr(O\rho) \tag{4.2.2}$$

and the thermal Green's function to be

$$G^C(x_1,\ldots,x_n) = \langle T_C \phi(x_1)\ldots\phi(x_n)\rangle \tag{4.2.3}$$

where time must be analytically continued into the complex plane, C denotes some path in the complex plane and T_C ordering along this path. In order to perform the ordering we parametrise the path as $t = z(\tau)$ for some function z and a real parameter τ. Then we can define the thermal heaviside and delta functions by

$$\theta_C(t) = \theta(\tau) \tag{4.2.4}$$

$$\delta_C(t) = \left(\frac{\partial z}{\partial \tau}\right)^{-1} \delta(\tau). \tag{4.2.5}$$

We then define products of fields by

$$T_C\phi(x)\,\phi(y) = \theta_C\left(x^0 - y^0\right)\phi(x)\,\phi(y) + \theta_C\left(y^0 - x^0\right)\phi(y)\,\phi(x). \tag{4.2.6}$$

We can also define the usual partition function

$$Z^\beta[j] = \langle T_C e^{i\int_C \mathrm{d}^4x\, j(x)\phi(x)}\rangle \tag{4.2.7}$$

where the integral is performed along the contour C. This also has the usual representation as the sum of Green's functions. The effective action is then defined in the same way as at zero temperature in the preceding section, Eq. (4.1.2) to Eq. (4.1.11). We now seek to compute propagators:

$$G^C(x-y) = \theta_C\left(x^0 - y^0\right)G_+(x-y) + \theta_C\left(y^0 - x^0\right)G_-(x-y) \tag{4.2.8}$$

where

$$G_+(x-y) = \langle\phi(x)\,\phi(y)\rangle \tag{4.2.9}$$

$$G_-(x-y) = G_+(y-x). \tag{4.2.10}$$

If we now consider G_+ in the Heisenberg representation:

$$\langle\phi(\mathbf{x},t)\,\phi(\mathbf{y},t)\rangle = e^{-\Phi}Tr\left(\phi(\mathbf{x},t)\,\phi(\mathbf{y},t)\,e^{-\beta H}\right)$$

$$
\begin{aligned}
&= e^{-\Phi} Tr\left(\phi\left(\mathbf{x},t\right) e^{-\beta H} e^{\beta H} \phi\left(\mathbf{y},t\right) e^{-\beta H}\right) \\
&= e^{-\Phi} Tr\left(\phi\left(\mathbf{x},t\right) e^{-\beta H} e^{i(-i\beta H)} \phi\left(\mathbf{y},t\right) e^{-i(-i\beta H)}\right) \\
&= e^{-\Phi} Tr\left(\phi\left(\mathbf{x},t\right) e^{-\beta H} \phi\left(\mathbf{y},t-i\beta\right)\right) \\
&= e^{-\Phi} Tr\left(\phi\left(\mathbf{y},t-i\beta\right) \phi\left(\mathbf{x},t\right) e^{-\beta H}\right) \\
&= \left\langle \phi\left(\mathbf{y},t-i\beta\right) \phi\left(\mathbf{x},t\right)\right\rangle
\end{aligned} \tag{4.2.11}
$$

where we have used the usual formula for the time evolution of fields as well as cyclicity of the trace. This is known as the Kubo-Martin-Schwinger (KMS) relation and is usually expressed as

$$
G_{+}\left(t-i\beta,\mathbf{x}\right) = G_{-}\left(t,\mathbf{x}\right). \tag{4.2.12}
$$

After Wick rotation to work with imaginary time this implies periodicity in Euclidean time with period β. After using the usual commutators for the scalar field we see that the fields themselves must also be periodic. If we now consider performing a Fourier expansion of a scalar field, ϕ, in Euclidean time we have (neglecting the overall normalisation):

$$
\phi\left(\tau,\mathbf{x}\right) \propto \sum_{n} e^{-i\omega_n \tau} \phi\left(\omega_n,\mathbf{x}\right). \tag{4.2.13}
$$

Note that the periodicity means that we have a Fourier series rather than a Fourier transform. Furthermore, the periodicity now implies

$$
\phi\left(\tau+\beta,\mathbf{x}\right) = \phi\left(\tau,\mathbf{x}\right) \implies \omega_n = \frac{2n\pi}{\beta}. \tag{4.2.14}
$$

These are known as the Matsubara modes.

There is a lot of rich theory in considering QFT at finite temperature; one can proceed, as at zero temperature, by Fourier expanding fields, imposing commutation relations and then (where it diverges from the zero temperature case) computing thermal averages. We shall ignore this theory for the sake of brevity as it will not be useful in the rest of this section. We shall simply seek to compute the propagator.

As usual it satisifies the equation (after Wick rotation):

$$\left(-\frac{\partial^2}{\partial\tau^2}-\nabla^2+m^2\right)G\left(x-y\right)=\delta\left(\tau_x-\tau_y\right)\delta^{(3)}\left(\mathbf{x}-\mathbf{y}\right) \tag{4.2.15}$$

which after Fourier transformation becomes

$$\left(\omega_n^2+\mathbf{k}^2+m^2\right)G\left(\omega_n,\mathbf{k}\right)=1 \tag{4.2.16}$$

which finally yields

$$G\left(\omega_n,\mathbf{k}\right)=\frac{1}{\omega_n^2+\mathbf{k}^2+m^2}. \tag{4.2.17}$$

Having now dealt with scalars we turn to fermions. Eq. (4.2.11) follows in exactly the same way but as we now impose anti-commutators this implies that the fermion fields are anti-periodic, i.e.

$$\psi\left(\mathbf{x},0\right)=-\psi\left(\mathbf{x},\beta\right). \tag{4.2.18}$$

The fermion fields can be expanded in exactly the same way as Eq. (4.2.13) although now the anti-periodicity, Eq. (4.2.18), gives

$$\omega_n=\frac{\left(2n+1\right)\pi}{\beta}. \tag{4.2.19}$$

The Fermionic propagator satisifes (in Euclidean space)

$$\left(-\gamma^1\partial_1-\gamma^2\partial_2-\gamma^3\partial_3-\gamma^4\partial_4-m\right)S\left(x,y\right)=\delta^{(3)}\left(\mathbf{x}-\mathbf{y}\right). \tag{4.2.20}$$

This equation becomes (after Fourier transforming):

$$\left(i\gamma.\mathbf{p}+i\omega_n\gamma^4-m\right)S\left(p\right)=1. \tag{4.2.21}$$

Finally we obtain

$$S\left(p\right)=\frac{-i\left(\gamma.\mathbf{p}+\omega_n\gamma_4\right)-m}{\omega_n^2+\mathbf{p}^2+m^2}. \tag{4.2.22}$$

Having now derived the propagators we give a brief summary of the Feynman rules (in momentum space) at finite temperature. The modifications are relatively straightforward, the propagators are given above (but must be appropriately continued back

to Minkowski space), the vertex rules are unchanged, loops come with a factor of $1/\beta$ and in addition to integrating over loop momenta, one must also sum over the Matsubara modes.

Having covered the basics of thermal field theory we will now compute the effective potential again, but now at finite temperature. For the case of a scalar running in the loop, Fig. 4.1, the modifications above give

$$V(\phi_c) = \frac{1}{2\beta}\sum_{n=-\infty}^{\infty}\sum_{k=1}^{\infty}\int\frac{\mathrm{d}^3p}{(2\pi)^3}\left(\frac{\lambda\phi_c^2/2}{\omega_n^2+\mathbf{p}^2}\right)^k \tag{4.2.23}$$

$$= \frac{1}{2\beta}\sum_{n=-\infty}^{\infty}\int\frac{\mathrm{d}^3p}{(2\pi)^3}\log\left(\omega_n^2+\mathbf{p}^2+m^2(\phi_c)\right) \tag{4.2.24}$$

where $m(\phi_c)$ is defined in the same way as at zero temperature, Eq. (4.1.16). Before computing the integral, it is convenient to first compute the sum over Matsubara modes:

$$\sum_{n=-\infty}^{\infty}\log\left(\omega_n^2+x^2\right) \tag{4.2.25}$$

where $x^2 = \mathbf{p}^2 + m^2(\phi_c)$. To do this we shall use the identity

$$\sum_{n=1}^{\infty}\frac{y}{y^2+n^2} = -\frac{1}{2y}+\frac{\pi}{2}+\pi\frac{e^{-2\pi y}}{1-e^{-2\pi y}} \tag{4.2.26}$$

and compute

$$\begin{aligned}
\frac{\partial}{\partial x}\sum_{n=-\infty}^{\infty}\log\left(\omega_n^2+x^2\right) &= \sum_{n=-\infty}^{\infty}\frac{2x}{\omega_n^2+x^2}\\
&= \sum_{n=-\infty}^{\infty}\frac{2x}{\left(\frac{2n\pi}{\beta}\right)^2+x^2}\\
&= \frac{\beta}{\pi}\sum_{n=-\infty}^{\infty}\frac{\frac{x\beta}{2\pi}}{n^2+\left(\frac{x\beta}{2\pi}\right)^2}\\
&= \frac{2\beta}{\pi}\sum_{n=1}^{\infty}\frac{\frac{x\beta}{2\pi}}{n^2+\left(\frac{x\beta}{2\pi}\right)^2}+\frac{2}{x}\\
&= \beta+\frac{2\beta e^{-x\beta}}{1-e^{-x\beta}}
\end{aligned} \tag{4.2.27}$$

where we have used the fact the sum is even in n, applied Eq. (4.2.26) and added

on the $n = 0$ term. Hence

$$\sum_{n=-\infty}^{\infty} \log\left(\omega_n^2 + x^2\right) = x\beta + 2\log\left(1 - e^{-x\beta}\right) \tag{4.2.28}$$

after discounting a (potentially infinite) constant which does not depend on x (and hence not on ϕ_c and we are only interested in the ϕ_c dependence). Therefore

$$V(\phi_c) = \frac{1}{2}\int \frac{\mathrm{d}^3 p}{(2\pi)^3}\left(x + \frac{2}{\beta}\log\left(1 - e^{-x\beta}\right)\right). \tag{4.2.29}$$

Before computing this integral we show that

$$x\int \frac{\mathrm{d}t}{2\pi i}\frac{1}{-t^2 + x^2 - i\epsilon} = \frac{1}{2} \tag{4.2.30}$$

which can be computed by closing the integration in the upper half plane and picking up the pole at $t = -\sqrt{x^2 - i\epsilon}$ with residue $1/2x$. This implies that

$$-\frac{i}{2}\int \frac{\mathrm{d}t}{2\pi}\log\left(-t^2 + x^2 - i\epsilon\right) = \frac{x}{2} \tag{4.2.31}$$

and therefore

$$\begin{aligned}\frac{1}{2}\int \frac{\mathrm{d}^3 p}{(2\pi)^3}x &= -\frac{i}{2}\int \frac{\mathrm{d}^4 p}{(2\pi)^4}\log\left(-p_0^2 + x^2 - i\epsilon\right) \\ &= \frac{1}{2}\int \frac{\mathrm{d}^4 p}{(2\pi)^4}\log\left(p^2 + m^2(\phi_c)\right)\end{aligned} \tag{4.2.32}$$

after Wick rotating. We see that this is equal to the zero-temperature contribution and hence (at the one-loop level) the finite temperature potential factorises into the zero-temperature part and and a finite temperature part. The finite temperature part is given by

$$\frac{1}{\beta}\int \frac{\mathrm{d}^3 p}{(2\pi)^3}\log\left(1 - e^{-x\beta}\right). \tag{4.2.33}$$

If we then perform the integral in spherical polar co-ordinates we obtain

$$\frac{1}{2\pi^2\beta}\int \mathrm{d}r\, r^2 \log\left(1 - e^{-\beta\sqrt{r^2 + m^2(\phi_c)}}\right). \tag{4.2.34}$$

Performing a change of variables $y = r\beta$ we have

$$\frac{1}{2\pi^2\beta^4}\int \mathrm{d}y\, y^2 \log\left(1 - e^{-\sqrt{y^2 + \beta^2 m^2(\phi_c)}}\right)$$

$$= \frac{1}{2\pi^2\beta^4} J_B\left(m^2\left(\phi_c\right)\beta^2\right) \tag{4.2.35}$$

where

$$J_B\left(m^2\left(\phi_c\right)\beta^2\right) = \int_0^\infty \mathrm{d}y\, y^2 \log\left(1 - e^{-\sqrt{y^2+\beta^2 m^2(\phi_c)}}\right) \tag{4.2.36}$$

is the bosonic thermal function. As in the zero-temperature case, the computation for gauge bosons is exactly the same with an additional factor of three.

If we now attempt to compute the fermionic contribution at finite temperature we start with

$$-\frac{2}{\beta}\sum_{n=-\infty}^{\infty}\int\frac{\mathrm{d}^3p}{(2\pi)^3}\log\left(\omega_n^2 + \mathbf{p}^2 + m^2\left(\phi_c\right)\right), \tag{4.2.37}$$

as is the case in the scalar theory we simply replace p^2 by $\omega_n^2 + \mathbf{p}^2$, although now $\omega_n = (2n+1)\,\pi/\beta$ and we cannot use the same summation identities as previously. As before we consider the derivative

$$\begin{aligned}\frac{\partial}{\partial x}\sum_{n=-\infty}^{\infty}\log\left(\omega_n^2 + x^2\right) &= \frac{\partial}{\partial x}\sum_{n=-\infty}^{\infty}\frac{2x}{\omega_n^2 + x^2}\\ &= \frac{2\beta}{\pi}\sum_{n=-\infty}^{\infty}\frac{\frac{x\beta}{\pi}}{(2n+1)^2 + \left(\frac{x\beta}{\pi}\right)^2}\\ &= \frac{4\beta}{\pi}\sum_{\text{odd } k>0}\frac{\frac{x\beta}{\pi}}{k^2 + \left(\frac{x\beta}{\pi}\right)^2}.\end{aligned} \tag{4.2.38}$$

Now we consider our previously used identity:

$$\begin{aligned}\sum_{\text{odd } n>0}\frac{y}{y^2+n^2} &= \sum_{n=1}^{\infty}\frac{y}{y^2+n^2} - \sum_{\text{even } n>0}\frac{y}{y^2+n^2}\\ &= \sum_{n=1}^{\infty}\frac{y}{y^2+n^2} - \sum_{n=1}^{\infty}\frac{y}{y^2+(2n)^2}\\ &= \sum_{n=1}^{\infty}\frac{y}{y^2+n^2} - \frac{1}{2}\sum_{n=1}^{\infty}\frac{\frac{y}{2}}{\left(\frac{y}{2}\right)^2+n^2}\\ &= -\frac{1}{2y} + \frac{\pi}{2} + \pi\frac{e^{-2\pi y}}{1-e^{-2\pi y}} - \frac{1}{2}\left(-\frac{1}{y} + \frac{\pi}{2} + \pi\frac{e^{-\pi y}}{1-e^{-\pi y}}\right)\\ &= \frac{\pi}{4} + \frac{\pi}{2}\frac{2e^{-2\pi y} - e^{-3\pi y} - e^{-\pi y}}{\left(1-e^{-\pi y}\right)\left(1-2^{-2\pi y}\right)}\\ &= \frac{\pi}{4} + \frac{\pi}{2}\frac{e^{-2\pi y} - e^{-3\pi y} + e^{-\pi y} - 1}{\left(1-e^{-\pi y}\right)\left(1-2^{-2\pi y}\right)\left(1+e^{\pi y}\right)}\end{aligned}$$

$$= \frac{\pi}{4} + \frac{\pi}{2}\frac{-\left(1-e^{-\pi y}\right)\left(1-2^{-2\pi y}\right)}{\left(1-e^{-\pi y}\right)\left(1-2^{-2\pi y}\right)(1+e^{\pi y})}$$
$$= \frac{\pi}{4} - \frac{\pi}{2}\frac{1}{1+e^{\pi y}}. \tag{4.2.39}$$

Hence

$$\frac{\partial}{\partial x}\sum_{n=-\infty}^{\infty}\log\left(\omega_n^2+x^2\right) = \frac{4\beta}{\pi}\left(\frac{\pi}{4} - \frac{\pi}{2}\frac{1}{1+e^{x\beta}}\right)$$
$$= \beta - \frac{2\beta}{1+e^{x\beta}} \tag{4.2.40}$$

and

$$\sum_{n=-\infty}^{\infty}\log\left(\omega_n^2+x^2\right) = x\beta + 2\log\left(1+e^{-x\beta}\right) \tag{4.2.41}$$

after again neglecting a (possibly infinite) constant. So the expression for the potential becomes

$$V(\phi_c) = -\frac{2}{\beta}\int\frac{\mathrm{d}^3p}{(2\pi)^3}\left(x\beta + 2\log\left(1+e^{-x\beta}\right)\right). \tag{4.2.42}$$

Again the first term becomes the zero-temperature contribution using the same proof as in the scalar case. The second term is the temperature dependent part and after shifting to spherical polar co-ordinates we have

$$-\frac{2}{\pi^2\beta}\int\mathrm{d}r\,r^2\log\left(1+e^{-\beta\sqrt{r^2+m^2(\phi_c)}}\right)$$
$$= -\frac{2}{\pi^2\beta^4}\int\mathrm{d}y\,y^2\log\left(1-e^{-\sqrt{y^2+\beta^2m^2(\phi_c)}}\right)$$
$$= -\frac{2}{\pi^2\beta^4}J_F\left(m^2(\phi_c)\,\beta^2\right) \tag{4.2.43}$$

after using the transformation $y = r\beta$ as before and we have defined the fermionic thermal function:

$$J_F\left(m^2(\phi_c)\,\beta^2\right) = \int_0^\infty\mathrm{d}y\,y^2\log\left(1+e^{-\sqrt{y^2+\beta^2m^2(\phi_c)}}\right). \tag{4.2.44}$$

4.3 Dark Matter theory

It has been known for many years that some matter additional to that observed in the Universe is needed to explain many observations. The first piece of evidence was seen in galactic rotation curves [87] and there have since been many other pieces of evidence, such as observations of galactic collisions [88] and data from the CMB experiment [89], which support the hypothesis of particle dark matter [90]. A popular model of dark matter is that the dark matter particle is charged under some new gauge group while being a singlet under the standard model gauge group and conversely all Standard Model particles are singlets under the dark gauge group. The number of particles in the dark sector (those charged under the new gauge group) varies heavily from model to model, some are very minimal including only one particle, while some contain multiple vectors, scalars and fermions. The dark sectors then 'communicate' with the Standard Model through either a Higgs portal or kinetic gauge mixing. See [43, 91–109] for examples.

In this section we will develop the necessary theory to calculate the relic density of dark matter in the model we wish to consider. In this section we shall follow [110]. We start by considering the rate of change of number of dark matter particles:

$$\frac{dN}{dt} = \frac{d}{dt}\left(n\left(t\right)a^{3}\left(t\right)\right) = \dot{n}\left(t\right)a^{3}\left(t\right) + 3n\left(t\right)a^{2}\left(t\right)\dot{a}\left(t\right) = \frac{1}{a^{3}\left(t\right)}\left(\dot{n}\left(t\right) + 3H\left(t\right)n\left(t\right)\right) \tag{4.3.1}$$

where we have defined the time dependent volume, $V\left(t\right) = a^{3}\left(t\right)$, n is the number density of dark matter with respect to the time-dependent volume, $H\left(t\right) = \frac{\dot{a}(t)}{a(t)}$ is the Hubble parameter and $a\left(t\right)$ is the scale factor appearing in the FLRW metric:

$$ds^{2} = dt^{2} - a^{2}\left(t\right)\left(dr^{2} + r^{2}d\theta^{2} + r^{2}\sin^{2}\theta\, d\phi^{2}\right). \tag{4.3.2}$$

Note that we have assumed a flat universe. The rate of change of numbers of dark matter must be related to the rate of production minus the rate of annihilation. In the absence of CP violation we can assume the matrix elements for these two processes to be the same. A careful derivation of the Boltzmann equation from first

principles leads to thermal averaging and the final result is:

$$\dot{n}(t) + 3H(t)\, n(t) = -\langle \sigma_{\chi\chi \to SM} v \rangle \left(n^2(t) - n_{eq}^2(t) \right) \tag{4.3.3}$$

where n_{eq} is the equilibrium number density of the dark matter. The thermally averaged cross section is defined as [111]

$$\langle \sigma_{ab\to cd} v \rangle = \frac{T}{8\pi^4 \bar{n}_a(T)\, \bar{n}_b(T)} \int \mathrm{d}s\, \sqrt{s} K_1\left(\frac{\sqrt{s}}{T}\right) p_{ab}^2(s)\, \sigma_{ab\to cd}(s) \tag{4.3.4}$$

where K_1 is the modified Bessel function of the first kind and we have defined

$$\bar{n}_a(T) = \frac{T}{2\pi^2} g_a m_a^2 K_2\left(\frac{m_a}{T}\right) \tag{4.3.5}$$

where g_a is the number of degrees of freedom of a and K_2 is the modified Bessel function of the second kind.

This formula is naturally generalised to the case of two dark matter particles. The full details can be found in [111].

4.4 Vacuum Decay

In this section we will derive the theory of phase transitions and how they produce gravitational waves. This was first covered by Callan and Coleman in [112, 113]. Following these papers we will consider a particle of unit mass in one dimension:

$$\mathcal{L} = \frac{1}{2}\dot{x}^2 - V(x). \tag{4.4.1}$$

If we consider a potential with two non-degenerate minima with a barrier between them and the particle initially residing in the minimum of greater potential then it is well known that the particle will tunnel from the false minimum (that of the higher potential) to the true minimum (that of the lower potential). The width for such a process, to leading order, is given by

$$\Gamma = A e^{-2\int_{x_0}^{\sigma} \mathrm{d}x \sqrt{2V}}. \tag{4.4.2}$$

where x_0 is the false minimum and σ is a point such that particle tunnels through the barrier and escapes with zero potential energy, i.e. $V(\sigma) = V(x_0) = 0$. We will not concern ourselves with the exponential prefactor and focus only on the term appearing in the exponent. This is easily extended to multiple dimensions by taking x and σ to be vectors and $\boldsymbol{\sigma}$ is the point which minimises this integral. That is, $\boldsymbol{\sigma}$ is the point such that:

$$\delta \int_{\mathbf{x}_0}^{\boldsymbol{\sigma}} \mathrm{d}s \, \sqrt{2V} = 0. \tag{4.4.3}$$

Following [112] we note that solutions to

$$\delta \int \mathrm{d}s \, \sqrt{2\,(E - V)} = 0 \tag{4.4.4}$$

are given by solutions to

$$\frac{d^2\mathbf{x}}{dt^2} = -\frac{\partial V}{\partial x} \tag{4.4.5}$$

$$\frac{1}{2}\left(\frac{d\mathbf{x}}{dt}\right)^2 + V = E. \tag{4.4.6}$$

We note that this can be mapped to our problem by taking $E = 0$ and $V \to -V$, and also fixing $\boldsymbol{\sigma}$ since this formulation of the problem requires fixed endpoints. We also note that (due to $V \to -V$) this problem is equivalent to a Wick rotation of Eq. (4.4.1) and so we will work with imaginary time τ. So we have

$$\frac{d^2\mathbf{x}}{d\tau^2} = \frac{\partial V}{\partial x} \tag{4.4.7}$$

$$\frac{1}{2}\left(\frac{d\mathbf{x}}{d\tau}\right)^2 - V = 0. \tag{4.4.8}$$

By Eq. (4.4.8), the particle can only come to rest at $\mathbf{x}_0$ asymptotically (as $V(x)$ gets closer to zero, the velocity of the particle becomes smaller). So we take

$$\lim_{\tau \to -\infty} \mathbf{x} = \mathbf{x}_0. \tag{4.4.9}$$

By time translation invariance we can say that the particle reaches $\boldsymbol{\sigma}$ at any time so we choose $\tau = 0$:

$$\mathbf{x}(0) = \boldsymbol{\sigma} \tag{4.4.10}$$

$$\left.\frac{d\mathbf{x}}{d\tau}\right|_{\tau=0} = \mathbf{0} \tag{4.4.11}$$

where the second line follows from the first by Eq. (4.4.8) and noting that $\boldsymbol{\sigma}$ is a zero of the potential. By Eq. (4.4.8) we have

$$2V = \frac{1}{2}\left(\frac{d\mathbf{x}}{d\tau}\right)^2 + V = \mathcal{L}_E \tag{4.4.12}$$

where $\mathcal{L}_E$ is the Euclidean Lagrangian. This also implies

$$\int_{\mathbf{x}_0}^{\boldsymbol{\sigma}} \mathrm{d}s\, \sqrt{2V} = \int_{-\infty}^{0} \mathrm{d}\tau\, \mathcal{L}_E. \tag{4.4.13}$$

By Eq. (4.4.11) this implies that variation wrt $\boldsymbol{\sigma}$ vanishes and so we can drop the requirement for $\boldsymbol{\sigma}$ to be fixed. By symmetry we see that the motion between $\tau = 0$ and $\tau = \infty$ is simply the reverse of the motion between $\tau = -\infty$ and $\tau = 0$. This motion is known as 'the bounce'. Hence the exponential factor is given by

$$-2\int_{\mathbf{x}_0}^{\boldsymbol{\sigma}} \mathrm{d}x\, \sqrt{2V} = -\int \mathrm{d}\tau\, \mathcal{L}_E = -S_E \tag{4.4.14}$$

where S_E is the Euclidean action for the bounce. We now move to QFT where the equation of motion is

$$\left(\frac{\partial^2}{\partial\tau^2} + \nabla^2\right)\phi = \frac{\partial V}{\partial\phi} \tag{4.4.15}$$

with boundary conditions

$$\lim_{\tau\to\pm\infty} \phi = \phi^- \tag{4.4.16}$$

$$\left.\frac{\partial\phi}{\partial\tau}\right|_{\tau=0} = 0 \tag{4.4.17}$$

where ϕ^- denotes the false vacuum. The exponential factor is still given by the (negative of the) Euclidean action

$$S_E = \int \mathrm{d}^4x \left(\frac{1}{2} \left(\frac{\partial \phi}{\partial \tau} \right)^2 + \frac{1}{2} \left(\nabla \phi \right)^2 + V\left(\phi \right) \right) \tag{4.4.18}$$

and in order for this to be finite we must also have

$$\lim_{|\mathbf{x}| \to \infty} \phi = \phi^+ \tag{4.4.19}$$

where ϕ^+ is the true vacuum. It was proven in [114] that the smallest action is given by the solution which is invariant under 4D spatial rotations, i.e. the solution is invariant under $O(4)$. So $\phi = \phi\left(\rho\right)$ where

$$\rho = \sqrt{\tau^2 + \mathbf{x}^2}. \tag{4.4.20}$$

Then the equation of motion becomes

$$\frac{d^2\phi}{d\rho^2} + \frac{3}{\rho} \frac{d\phi}{d\rho} = \frac{\partial V}{\partial \phi} \tag{4.4.21}$$

with boundary condition

$$\lim_{\rho \to \infty} \phi = \phi^+. \tag{4.4.22}$$

The Euclidean action is then given by

$$S_E = 2\pi^2 \int_0^\infty \mathrm{d}\rho\, \rho^3 \left(\frac{1}{2} \left(\frac{d\phi}{d\rho} \right)^2 + V(\phi) \right). \tag{4.4.23}$$

To finish our explanation of tunneling we note that at finite temperature it was shown in [115] that one should no longer look for the $O(4)$ invariant solution but the $O(3)$ invariant solution and the exponential factor is given by

$$-\frac{S_3}{T} = -\frac{4\pi}{T} \int_0^\infty \mathrm{d}\rho\, \rho^2 \left(\frac{1}{2} \left(\frac{d\phi}{d\rho} \right)^2 + V(\phi) \right) \tag{4.4.24}$$

where now ϕ must satisfy the equation

$$\frac{d^2\phi}{d\rho^2} + \frac{2}{\rho} \frac{d\phi}{d\rho} = \frac{\partial V}{\partial \phi}. \tag{4.4.25}$$

Note the change in coefficient of the second term.

Field	S	χ^1_L	χ^1_R	χ^2_L	χ^2_R
$U(1)_D$	1	$\frac{1}{2}$	$-\frac{1}{2}$	$-\frac{1}{2}$	$\frac{1}{2}$

Table 4.1: The charges of the dark sector particles under the new $U(1)_D$ symmetry. Note that this assignment of charges renders the theory anomaly-free.

4.5 A Phenomenological Analysis of Our Model

We introduce a classically scale-invariant model with a dark sector charged under a new $U(1)$ symmetry and coupled to the Standard Model through a Higgs portal coupling. Our model is similar to that considered in [116], although we extend their model by allowing our fermions to have different masses (as well as in later sections looking at the phase transition and associated gravitational waves). The model is given by

$$\mathcal{L} = \mathcal{L}_{\rm SM} + \mathcal{L}_{kin} + \mathcal{L}_Y - V_0\left(H, S\right) \tag{4.5.1}$$

where $\mathcal{L}_{SM}$ is the Standard Model Lagrangian without the Higgs potential, $\mathcal{L}_{kin}$ is the kinetic terms for the new fields[1]:

$$\mathcal{L}_{kin} = |D_\mu S|^2 - \frac{1}{4}F'_{\mu\nu}F'^{\mu\nu} + \overline{\chi}^a_L \not{D} \chi^a_L + \overline{\chi}^a_R \not{D}_\mu \chi^a_R. \tag{4.5.2}$$

All new particles, $S, \chi^{1,2}, A'_\mu$ are singlets under the standard model gauge group, $G_{\rm SM} = SU(3)_C \times SU(2)_L \times U(1)_Y$, and all SM particles are singlets under the new gauge group. The charges of the new particles are given in Table 4.1. $F'_{\mu\nu}$ is the field strength tensor associated with the gauge boson of the new $U\left(1\right)$ and there is implied summation over repeated indices.

$\mathcal{L}_Y$ is the Yukawa coupling of the dark sector:

$$\mathcal{L}_Y = -\left(y_{1,D}\overline{\chi}^1_L S \chi^1_R + y_{2,D}\overline{\chi}^2_L S \chi^2_R + h.c.\right). \tag{4.5.3}$$

[1]Note that the term $\epsilon F_{\mu\nu}F'^{\mu\nu}$, where $F_{\mu\nu}$ is the U(1)$_Y$ field strength tensor, is also allowed by gauge invariance but we neglect this term in light of strong collider constraints [117,118] and leave it for future work.

The tree-level potential for scalar fields of the new theory is given by:

$$V_0(H,\,S) = \lambda_H\left(H^\dagger H\right)^2 + \lambda_S\left(S^* S\right)^2 - \lambda_P\left(H^\dagger H\right)\left(S^* S\right). \tag{4.5.4}$$

Note that we require $\lambda_P > 0$ to create a true minimum away from the origin. Working in the unitary gauge where we can write

$$H = \frac{1}{\sqrt{2}}\begin{bmatrix}0\\ h\end{bmatrix} \quad S = \frac{s}{\sqrt{2}} \tag{4.5.5}$$

where h and s are real; then the classical scalar potential may be written as

$$V_0(h,\,s) = \frac{\lambda_H}{4}h^4 + \frac{\lambda_S}{4}s^4 - \frac{\lambda_P}{4}h^2 s^2. \tag{4.5.6}$$

Symmetry breaking in a classically scale invariant model was first considered in [80]. In models such as ours many authors consider λ_P to be small so that the back-reaction of the Standard Model on the dark sector is negligible and one can treat the dark sector in the original Coleman-Weinberg formalism (see e.g. [82, 86, 119]). However a more general formalism was later developed by Gildener and S. Weinberg in [120] to deal with theories of multiple scalars and it is this formalism we shall follow here in order to not be restricted in our choice of parameters.

We write our fields as

$$h = N_1\phi \quad s = N_2\phi \tag{4.5.7}$$

where $\vec{N}$ is a 2D unit vector. Then our tree-level potential becomes

$$V_0(h,\,s) = \phi^4\left(\frac{\lambda_H}{4}N_1^4 + \frac{\lambda_S}{4}N_2^4 - \frac{\lambda_P}{4}N_1^2 N_2^2\right). \tag{4.5.8}$$

To find the minimum we then require $\frac{\partial V_0}{\partial N_i} = 0$ and $V_0(\phi\mathbf{n}) = 0$ where $\mathbf{n}$ is the particular unit vector satisfying the above equations. This leads to the constraints:

$$\lambda_H n_1^2 - \frac{\lambda_P}{2}n_2^2 = 0 \tag{4.5.9}$$

$$\lambda_S n_2^2 - \frac{\lambda_P}{2}n_1^2 = 0 \tag{4.5.10}$$

$$\frac{\lambda_H}{4}n_1^4 + \frac{\lambda_S}{4}n_2^4 - \frac{\lambda_P}{4}n_1^2 n_2^2 = 0. \tag{4.5.11}$$

These equations are satisfied at some renormalisation scale $\mu = \Lambda_{GW}$. These can be solved to yield

$$n_1^2 = \frac{\lambda_P}{\lambda_P + 2\lambda_H} \tag{4.5.12}$$

$$n_2^2 = \frac{2\lambda_H}{\lambda_P + 2\lambda_H}. \tag{4.5.13}$$

We now expand the fields about their minima, writing $h = wn_1 + \tilde{h}$, $s = wn_2 + \tilde{s}$ where $w = \langle\varphi\rangle$ is a classically flat direction[1]. This leads to the mass matrix:

$$M^2 = w^2 \begin{bmatrix} 2\lambda_H n_1^2 & -\lambda_P n_1 n_2 \\ -\lambda_P n_1 n_2 & 2\lambda_s n_2^2 \end{bmatrix} \tag{4.5.14}$$

after using the relations in Eq. (4.5.9). By standard results of linear algebra, this matrix can be diagonalised by a rotation matrix of the form:

$$O = \begin{bmatrix} \cos\theta & -\sin\theta \\ \sin\theta & \cos\theta \end{bmatrix} \tag{4.5.15}$$

where

$$\tan(2\theta) = \frac{\lambda_P n_1 n_2}{\lambda_s n_2^2 - \lambda_H n_1^2}. \tag{4.5.16}$$

We can now write the mass eigenstates:

$$\begin{bmatrix} h_1 \\ h_2 \end{bmatrix} = O \begin{bmatrix} h \\ s \end{bmatrix} \tag{4.5.17}$$

where we identify h_1 with the SM higgs. The mass eigenvalues are given by

$$M^2_{h_1,h_2} = w^2 \left(\lambda_H n_1^2 + \lambda_s n_2^2 \pm \sqrt{\left(\lambda_H n_1^2 - \lambda_s n_2^2\right)^2 + \lambda_P^2 n_1^2 n_2^2} \right). \tag{4.5.18}$$

After using the relations in Eq. (4.5.12) to simplify this we obtain

$$M^2_{h_1} = \lambda_P w^2 \tag{4.5.19}$$

$$M^2_{h_2} = 0. \tag{4.5.20}$$

We recall that w is a classically flat direction that will be stabilised in Eq. (4.5.26)

[1]The value of w will be stabilised below by the inclusion of quantum effects.

and also note that Eq. (4.5.20) is true only at tree level (*cf.* Eq. (4.5.27) below). We shall take the tree level mass for h_1 but although h_2 is massless at tree level it receives sizeble corrections at the one-loop level which we shall calculate at the end of this section.

To find the new minimum of the theory we must calculate the infinite series of diagrams shown in Figs. 4.1,4.2,4.3 with external legs being either h or s and all possible scalars, fermions and bosons running in the loop. Calculating these diagrams (and counterterms in the $\overline{MS}$ scheme) leads to the 1-loop effective potential (see e.g. [1] for a review),

$$V_1(h,\, s) = \frac{1}{64\pi^2}\left(\sum_{\text{bosons}} n_i M_i^4(\phi)\left(\log\left(\frac{M_i^2(\phi)}{\Lambda_{GW}^2}\right) - \frac{3}{2}\right) - \sum_{\text{fermions}} n_i M_i^4(\phi)\left(\log\left(\frac{M_i^2(\phi)}{\Lambda_{GW}^2}\right) - \frac{3}{2}\right)\right). \tag{4.5.21}$$

Note that since h_2 is massless at tree level it does not contribute to the effective potential at one loop so our sum runs over h_1, W, Z, Z', t, χ_1, χ_2 with degrees of freedom $n_i = 1,\, 6,\, 3,\, 3,\, 12,\, 4,\, 4$ respectively. Note that all SM fermions contribute to the potential but, as is standard in the literature, we account only for the contribution of the top quark (with a factor of three due to colour) as this is the most significant. Since we are working in a theory with no intrinsic masses we can write for all particles, $M^2(\phi) = \frac{M^2\phi^2}{w^2}$, where M^2 is the observed mass matrix evaluated at $\phi = w$, so we may rewrite the above equation as

$$V_1(\phi) = A\phi^4 + B\phi^4 \log\left(\frac{\phi^2}{\Lambda_{GW}^2}\right) \tag{4.5.22}$$

where

$$A = \frac{1}{64\pi^2 w^4}\left(\sum_{\text{bosons}} n_i M_i^4\left(\log\left(\frac{M_i^2}{w^2}\right) - \frac{3}{2}\right) - \sum_{\text{fermions}} n_i M_i^4\left(\log\left(\frac{M_i^2}{w^2}\right) - \frac{3}{2}\right)\right) \tag{4.5.23}$$

$$B = \frac{1}{64\pi^2 w^4}\left(\sum_{\text{bosons}} n_i M_i^4 - \sum_{\text{fermions}} n_i M_i^4\right). \tag{4.5.24}$$

By definition $V'(w) = 0$ so we obtain the relationship:

$$\log\left(\frac{w}{\Lambda_{GW}}\right) = -\frac{1}{4} - \frac{A}{2B}. \tag{4.5.25}$$

which allows us to rewrite our potential as

$$V_1(\phi) = B\phi^4\left(\log\left(\frac{\phi^2}{w^2}\right) - \frac{1}{2}\right). \tag{4.5.26}$$

At the one loop level the mass of h_2 is given by[1]

$$M_{h_2}^2 = \left.\frac{\partial^2 V}{\partial \phi^2}\right|_{\phi=w} = 8Bw^2. \tag{4.5.27}$$

Finally we end this section with a summary of which parameters are free and which others are determined by the constraints previously listed. Firstly $v_h = 246$ GeV and $M_{h_1} = 125$ GeV are known from experiment. λ_h has a certain value within the Standard Model but it has not been experimentally measured so we shall regard this as undetermined. We have only one remaining degree of freedom in the scalar sector, once we have picked a value of e.g. w then λ_P is determined by Eq. (4.5.19) and once λ_P is determined then the remaining scalar couplings must take their values to satisfy Eq. (4.5.9) (with n_1 and n_2 already being determined by the vevs). For our purposes it shall be more convenient to take $\sin\theta$, the mixing angle as our free parameter and determine the scalar couplings and vevs from here.

We shall also take M_{h_2} as a free parameter and then M_{Z_D} is determined by Eq. (4.5.27), which in turn determines g_D as $M_{Z'} = g_D v_S$. Finally we have complete freedom in choosing the mass of our fermions, M_{χ_1}, M_{χ_2} and these in turn shall determine the yukawa couplings $y_{D,1}$, $y_{D,2}$. For later convenience we also define ΔM_χ as the mass splitting between the two fermions and without loss of generality we shall always take χ_1 to be the lighter of the two.

In summary, the free parameters of our model are $\sin\theta$, M_{h_2}, M_{χ_1} and M_{χ_2} .

[1] By examining previous relations one can show that h_2 and ϕ are the same field.

4.5.1 Relic density and Experimental Constraints

We can consider our model as a model of dark matter, with χ_1 and χ_2 serving as the dark matter candidates. To calculate the relic density we use MicrOMEGAs [121] with FeynRules [122] being used to generate the model file. At the same time we also use MicrOMEGAs to implement several experimental constraints on our model.

One of the primary constraints on dark sector models comes from direct detection experiments where dark sector particles can scatter off standard model nuclei. This happens in our model due to the mixing between the two scalars. This constraint can be implemented within MicrOMEGAs.

We also have constraints on the scalar sector of our model. There have been many searches at the LHC for additional light and heavy scalars. So far all such searches have produced null results and so these analyses constrain the valid parameter space of our model. We implement these constraints using the HiggsBounds and HiggsSignals codes [123, 124].

Below we plot the relic density as a function of some of our free parameters and also show some of the constraints coming from direct detection and collider searches. The relic density of the universe has been measured as $\Omega_{DM}h^2 = 0.1200 \pm 0.0020$ [125]. As can be seen in Fig. 4.4a, in order to obtain the correct relic density, we need the mass of our dark fermions to lie in the region around a resonance i.e. $M_{\chi_{1,2}} \approx M_{h_{1,2}}/2$, although it should be noted that the allowed region is not particularly narrow. This near-resonance regime is necessary in order for the dark matter to annihilate sufficiently quickly to not produce an overabundance. An alternative is to have the dark matter sufficiently heavy that the annihilation rate is enhanced by the phase space, as shown in Fig. 4.4b. Note that the smaller the value of $\sin\theta$ the narrower the resonance, or the larger the mass of the dark fermions should be as the annihilation rate is additionally suppressed. Here $\Delta M_\chi = |M_{\chi_1} - M_{\chi_2}|$ and we always choose χ_1 to be the lighter fermion.

Non-observation of dark matter at the LHC corresponds to an upper bound on

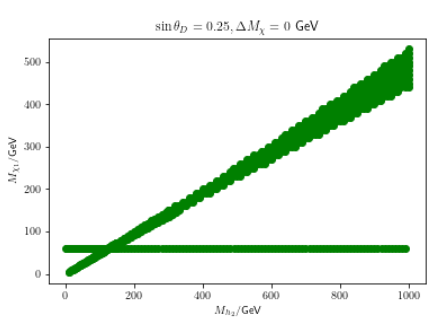

(a) The points which produce an acceptable relic abundance for $\sin\theta = 0.25$, $\Delta M_\chi = 0$ GeV.

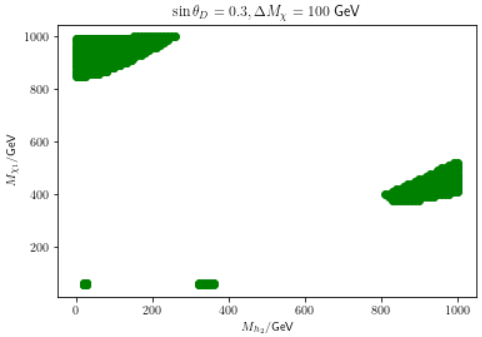

(b) The points which produce an acceptable relic abundance for $\sin\theta = 0.30$, $\Delta M_\chi = 100$ GeV.

Figure 4.4: Areas of our parameter space which do not produce an over-abundance of dark matter.

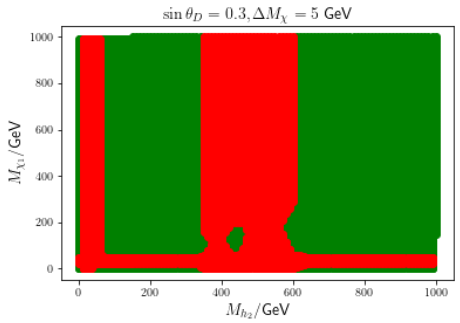

(a) Scatter plot of M_{h_2} against M_{χ_1} for $\sin\theta = 0.30, \Delta M_\chi = 5$ GeV with points allowed by constraints from the scalar sector in green and forbidden points in red.

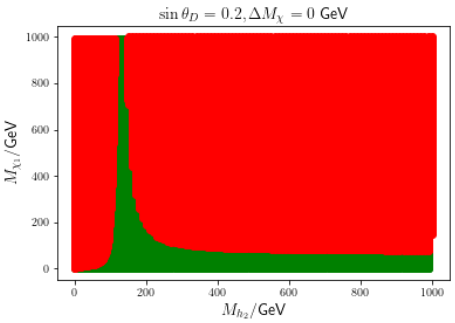

(b) Scatter plot of M_{h_2} against M_{χ_1} for $\sin\theta = 0.20, \Delta M_\chi = 0$ GeV with points allowed by constraints from the direct detection experiments in green and forbidden points in red.

Figure 4.5: Constraints from collider and direct detection experiments.

the value of $\sin\theta$. Experimental evidence requires $\sin\theta < 0.44$ independent of the mass of h_2 due to the observed Higgs signal rates at the LHC. There is also a mass-dependent constraint, which requires $\sin\theta \lesssim 0.32$ for $M_{h_2} \gtrsim 200$ GeV and $\sin\theta \lesssim 0.2$ for $M_{h_2} \gtrsim 400$ GeV, mostly coming from restrictions on the NLO corrections to the mass of the W boson (obviously other constraints exist but none as severe as those coming from the W boson mass in our considered parameter range) [126]. We also in general require $M_{h_2} > M_{h_1}/2$ to respect bounds coming from the decays of the SM Higgs to invisibles. We show an example plot of the allowed region of parameter space in Fig. 4.5a. The constraints are largely independent of the fermion mass splitting (although there is some effect).

There are also constraints on the masses of our dark fermions coming from direct detection experiments. Although the fermions do not interact directly with SM quarks/hadrons, they can still interact through the exchange of a mixed scalar, although such diagrams are suppressed by a factor of $\sin\theta$. Such interactions are proportional to $\frac{1}{M_{h_1}^2} - \frac{1}{M_{h_2}^2}$ [127] and so we require $M_{h_1} \approx M_{h_2}$ to avoid direct detection constraints. Alternatively we can suppress these diagrams by taking the yukawa coupling of the dark fermions to the scalars to be small i.e. our dark fermions will be light. As one would expect, these constraints become more relaxed for smaller values of $\sin\theta$. These constraints are shown in Fig. 4.5b and as for the scalar sector, the constraints are mostly independent of ΔM_χ.

4.5.2 Theoretical Constraints

We shall now examine constraints on the coupling constants coming from vacuum stability, perturbativity and unitarity. From Eq. (4.5.26), we see that the potential is bounded from below and hence the vacuum is stable if and only if $B \geq 0$. We note that by Eq. (4.5.27) any positive choice of M_{h_2} will determine the mass of the dark gauge boson in such a way that B is positive. We also require that the vacuum

be stable (bounded from below) at tree level which implies

$$\lambda_P^2 < 4\lambda_S\lambda_H\,, \quad \lambda_H > 0. \tag{4.5.28}$$

The requirement of perturbativity simply imples that we have $|g_i| <$ const. for all couplings g_i, i.e. $g_i = \lambda_P$, λ_H, $y_D \ldots$ [126]. We choose a constant of 2π in agreement with [101]. We derive and numerically solve the RG equations using SARAH [128], and list them in Appendix C.

Checking the resulting constraints involves evolving the various coupling constants up to high scales using numerical solutions to the RG equations. Rather than doing it for the entire parameter space we will check these constraints for a selection of bench mark points which we define in the next section. Also it is not necessary for these conditions to hold at arbitrarily high scales (perturbativity and vacuum stability are not absolute requirements in any case) as there may be new physics which arises at some higher scale which then contributes in such a way to e.g. stabilise the vacuum. Hence when we numerically check these constraints we only require them to hold up to Λ_{GW} (defined by Eq. (4.5.25)) and then give the higher scale at which they are violated, see Table 4.2.

We now consider constraints from perturbative unitarity for our theory. A partial wave expansion for a scattering amplitude gives

$$\mathcal{M}\left(s,\theta\right) = 16\pi \sum_{J=0}^{\infty} \left(2J+1\right) A_J\left(s\right) P_J\left(\cos\theta\right) \tag{4.5.29}$$

where P_J are the Legendre polynomials and A_J are the partial wave amplitudes. Unitarity then imposes the bound that $|ReA_0| < \frac{1}{2}$. We consider the tree level amplitudes for the processes: $Z'_L Z'_L \to Z'_L Z'_L$, $h_1 h_1 \to h_1 h_1$, $h_2 h_2 \to h_2 h_2$. We use FeynArts [129] and FeynCalc [130] to aid in the computation of the amplitudes. For the scalar process, the only relevant diagram at high energy is the four-point interaction (all others are suppressed by $\sim \frac{1}{s}$ due to internal propagators) and so

the demand for perturbative unitarity simply imposes

$$\frac{6}{16\pi}\left(\lambda_H \cos^4\theta_D - \lambda_P \sin^2\theta_D \cos^2\theta_D + \lambda_S \sin^4\theta_D\right) < \frac{1}{2} \tag{4.5.30}$$

$$\frac{6}{16\pi}\left(\lambda_H \sin^4\theta_D - \lambda_P \sin^2\theta_D \cos^2\theta_D + \lambda_S \cos^4\theta_D\right) < \frac{1}{2}. \tag{4.5.31}$$

For the vector boson scattering we obtain

$$\begin{aligned}\mathcal{M} = &-4\frac{g_D^2 v_s^2 \sin^2\theta_D}{M_{Z'}^4}\left(\frac{\left(s-2M_{Z'}^2\right)^2}{s-M_{h_1}^2} + \frac{\left(t-2M_{Z'}^2\right)^2}{t-M_{h_1}^2} + \frac{\left(u-2M_{Z'}^2\right)^2}{u-M_{h_1}^2}\right)\\ &- 4\frac{g_D^2 v_s^2}{M_{Z'}^4}\cos^2\theta_D\left(\frac{\left(s-2M_{Z'}^2\right)^2}{s-M_{h_2}^2} + \frac{\left(t-2M_{Z'}^2\right)^2}{t-M_{h_2}^2} + \frac{\left(u-2M_{Z'}^2\right)^2}{u-M_{h_2}^2}\right) \qquad (4.5.32)\\ \approx &-4\frac{\sin^2\theta_D}{M_{Z'}^2}\left(s+t+u+3M_{h_1}^2\right) - 4\frac{\cos^2\theta_D}{M_{Z'}^2}\left(s+t+u+3M_{h_2}^2\right) \qquad (4.5.33)\\ \approx &-4\sin^2\theta_D\left(4+3\frac{M_{h_1}^2}{M_{Z'}^2}\right) - 4\cos^2\theta_D\left(4+3\frac{M_{h_2}^2}{M_{Z'}^2}\right). \qquad (4.5.34)\end{aligned}$$

Hence we require

$$4\sin^2\theta_D\left(4+3\frac{M_{h_1}^2}{M_{Z'}^2}\right) + 4\cos^2\theta_D\left(4+3\frac{M_{h_2}^2}{M_{Z'}^2}\right) < 8\pi. \tag{4.5.35}$$

Eqs. (4.5.30), (4.5.31), (4.5.35) summarise the unitarity constraints that we require to hold for our model.

4.5.3 Phase transition and Gravitational Wave signal

To discuss the phase transition and gravitational waves we must first compute the one-loop effective potential at finite temperature. It is known that at one loop level, the potential factorises into the zero temperature potential (which we have already calculated) plus thermal corrections. The thermal corrections are given by

$$V_T = \frac{T^4}{2\pi^2}\left(\sum_{\text{bosons}} n_i J_B\left(\frac{M_i^2(\phi)}{T^2}\right) - \sum_{\text{fermions}} n_i J_F\left(\frac{M_i^2(\phi)}{T^2}\right)\right). \tag{4.5.36}$$

Finally to go beyond the simple one-loop expressions for the effective potential we were using until now, we now add the resummed contributions of the so-called 'daisy diagrams' (shown in Fig. 4.6) to improve the validity of perturbation theory. This

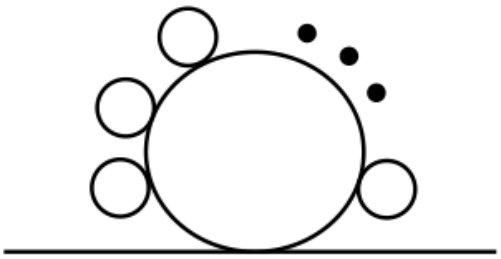

Figure 4.6: An example of a daisy diagram [1] with a scalar field appearing in the outside bubbles. This is then resummed to all orders (the outside series of bubbles) to obtain the thermal mass correction.

was first done for the Standard Model in [131, 132], and for our model we have

$$V_{\text{daisy}} = \frac{T}{12\pi} \sum_{\text{bosons}} n_i \left(M_i^3 \left(\phi \right) - \left(M_i^2 + \Pi_i \left(\phi, T \right) \right)^{\frac{3}{2}} \right) \tag{4.5.37}$$

where $\Pi_i \left(\phi, T \right)$ is the thermal mass correction. Note that, to leading order, fermions do not receive a thermal mass and so do not contribute to the daisy potential, Eq. (4.5.37), and also that it is only the longitudinal mode of the gauge bosons which receives a thermal mass, so the relevant degrees of freedom should be divided by three. The thermal masses are given by:

$$\Pi_{h/s} = \begin{bmatrix} T^2 \left(\frac{\lambda_H}{4} + \frac{\lambda_P}{24} + \frac{g'^2}{16} + \frac{3g_W^2}{16} + \frac{y_t^2}{4} \right) & 0 \\ 0 & T^2 \left(\frac{\lambda_S}{4} + \frac{\lambda_P}{24} + \frac{g_D^2}{4} + \frac{y_{\chi_1}^2}{12} + \frac{y_{\chi_2}^2}{12} \right) \end{bmatrix} \tag{4.5.38}$$

$$\Pi_{Z'} = \frac{g_D^2 T^2}{3} \tag{4.5.39}$$

$$\Pi_W = \frac{11}{6} g_W^2 T^2 \tag{4.5.40}$$

$$\Pi_Z = \frac{11}{6} \left(g_W^2 + g'^2 \right) T^2 \tag{4.5.41}$$

where the results for the W and Z bosons were taken from [131]. Hence the full one-loop effective potential is given by

$$V \left(\phi, T \right) = V_1 \left(\phi \right) + V_T \left(\phi, T \right) + V_{\text{daisy}} \left(\phi, T \right). \tag{4.5.42}$$

Note that to determine the mass of the scalars at finite temperature one must add

	$\sin\theta_D$	M_{h_2}	M_{χ_1}	M_{χ_2}	Ωh^2	Λ_{unit}	$\Lambda_{\text{pert.}}$	$\Lambda_{\text{stab.}}$
BP1	0.30	151 GeV	59.5 GeV	59.5 GeV	0.070	2.2×10^9 GeV	$> 10^{16}$ GeV	9.3×10^4 GeV
BP2	0.10	320 GeV	150 GeV	155 GeV	0.078	3.0×10^{15} GeV	$> 10^{19}$ GeV	3.2×10^5 GeV
BP3	0.40	121 GeV	591 GeV	592 GeV	0.118	6.3×10^8 GeV	$> 10^{10}$ GeV	8.9×10^4 GeV
BP4	0.20	331 GeV	61 GeV	161 GeV	0.077	1.8×10^6 GeV	$> 10^{12}$ GeV	2.0×10^5 GeV
BP5	0.30	120 GeV	901 GeV	1001 GeV	0.118	5.8×10^6 GeV	3.0×10^8 GeV	1.2×10^5 GeV

Table 4.2: Table showing our selection of benchmark points. The Λ show the scale at which we violate perturbative unitarity, perturbativity and vacuum stability respectively. All chosen points also obey the experimental constraints coming from collider searches and direct detection experiments. Note that due to numerical issues in the software we were unable to determine the exact scale at which perturbativity is violated for most of our benchmark points and so we indicate the maximum scale we were able to check.

Eqs. (4.5.14) and (4.5.38) before finding the eigenvalues. It is known that in order to generate matter-antimatter asymmetry via baryogenesis we must have a strongly first order electroweak phase transition. The order parameter for these transitions is given by the ratio ϕ_c/T_c, where the critical temperature, T_c, and the critical field strength, ϕ_c, are defined by

$$V(\phi_c, T_c) = 0 \tag{4.5.43}$$

$$\partial_\phi V(\phi_c, T_c) = 0, \tag{4.5.44}$$

i.e. ϕ_c is a local minimum of the potential that is degenerate with the minimum at the origin at T_c. To have a strongly first order phase transition we then require $\phi_c/T_c \gtrsim 1$. The numerical calculation of the order parameters and of various parameters associated with the gravitational wave signal becomes quite slow and so in this section rather than completing a full exploration of the phase space we choose several benchmark points consistent with the constraints from Sections 4.5.1, 4.5.2 and compute the order parameters and gravitational wave signal. Our benchmark points are listed in Table 4.2.

It is well known that a strongly first order phase transition will produce a gravitational wave signal. Here we calculate this signal and examine the possibility of

detection at both present detectors (LIGO, VIRGO etc.) and future detectors (LISA, DECIGO etc.).

A first order phase transition occurs when there is a potential barrier between a false minimum (usually at $\phi = 0$) and a true minimum. When this occurs the transition happens as bubbles of true vacuum nucleate in the false vacuum. A gravitational wave signal is produced by three different mechanisms, as reviewed in [133]: collisions between bubbles, sound waves in the plasma, and magnetohydrodynamic turbulence.

Before going on to calculate the signal we briefly outline some bubble nucleation theory necessary for our calculation. The vacuum at $\phi = 0$ only becomes metastable at temperatures $T < T_c$, however if the barrier is sufficiently high then the tunnelling rate may remain very small even for temperatures much below the critical temperature. Hence it is conventional to also define the *nucleation temperature* at which the probability of one bubble nucleating in one horizon volume is approximately one. The theory of such transitions and bubble nucleation was first addressed in [112,113] where it was shown that the decay rate was given by

$$\frac{\Gamma}{V} = Ae^{-S_4} \tag{4.5.45}$$

where the left-hand side is the decay rate per unit volume and on the right-hand side we have A which is a ratio of determinants of quadratic fluctuation operators around the bubble solution. S_4 is the action computed on the field profile, ϕ, satisfying the differential equation

$$\frac{d^2\phi}{d\rho^2} + \frac{3}{\rho}\frac{d\phi}{d\rho} = V'(\phi) \tag{4.5.46}$$

which is the Euler-Lagrange equation for a field in four dimensions with an $O(4)$ symmetry, $\phi(\mathbf{x}, t) = \phi(\rho)$, and the boundary conditions,

$$\lim_{\rho\to\infty} \phi(\rho) = 0\,, \quad \partial_\rho\phi(0) = 0. \tag{4.5.47}$$

The solution to this classical problem corresponds to the four-dimensional bubble or bounce configuration.

It was shown in [115] that when working in a theory at finite temperature this four-dimensional approach should be modified to the effectively three-dimensional set-up,

$$\frac{\Gamma}{V} = Ae^{-S_3/T} \tag{4.5.48}$$

and the field profile ϕ should satisfy

$$\frac{d^2\phi}{d\rho^2} + \frac{2}{\rho}\frac{d\phi}{d\rho} = V'(\phi) \tag{4.5.49}$$

with the same boundary conditions, Eq. (4.5.47). At finite temperature, due to the periodicity of the imaginary time-dimension $0 \leq \tau \leq 1/T$ in the Matsubara formalism, we essentially work in a three-dimensional theory[1]. Also note that on dimensional grounds it is convential to take the prefactor A to be $\mathcal{O}\left(T^4\right)$.

It was shown in [134] that the nucleation temperature, T_N, is given by solving the equation $S_3(T_N)/T_N \approx 140$. To describe the gravitational wave spectrum resulting from the first-order phase transition detailed above, it is conventional to define two more parameters, α and β, in addition to the nucleation temperature T_N, that characterise the phase transition:

$$\alpha = \frac{1}{\rho_{rad}(T_N)}\left(\Delta V(T_N) - T_N \frac{d\Delta V}{dT}\bigg|_{T=T_N}\right) \tag{4.5.50}$$

$$\frac{\beta}{H_*} = T_N \frac{d(S_3/T)}{dT}\bigg|_{T=T_N} \tag{4.5.51}$$

where H_* is the Hubble constant at the time of nucleation, ρ_{rad} is the radiation energy density[2] and $\Delta V(T) = V(0,T) - V(v(T),T)$ where $v(T)$ is the global minimum of the potential at temperature T. The gravitational wave energy density, Ω_{GW}, as a function of the frequency, f, is then given by the sum of the three production

[1] The D-dimensional action is given by $S_D = \int d\rho d\Omega_D \, \rho^{D-1}\left[\left(\frac{d\phi}{d\rho}\right)^2 + V(\phi)\right]$ where Ω_D is an integral over the surface of a D-dimensional sphere.

[2] $\rho_{rad}(T_N) = g_*\pi^2 T_N^4/30$ where g_*(=117.75 for our model) is the number of relativistic degrees in the plasma at T_N.

modes [133]

$$\Omega_{\rm Coll}\, h^2 = 1.67 \times 10^{-5} \left(\frac{H_*}{\beta}\right)^2 \left(\frac{\kappa\alpha}{1+\alpha}\right)^2 \left(\frac{100}{g_*}\right)^{\frac{1}{3}} \left(\frac{0.11 v_w^3}{0.42 + v_w^2}\right) S_{Coll}\,(f)$$
$$\Omega_{\rm SW}\, h^2 = 2.65 \times 10^{-6} \left(\frac{H_*}{\beta}\right) \left(\frac{\kappa_v\alpha}{1+\alpha}\right)^2 \left(\frac{100}{g_*}\right)^{\frac{1}{3}} v_w\, S_{SW}\,(f)$$
$$\Omega_{\rm MHD}\, h^2 = 3.35 \times 10^{-4} \left(\frac{H_*}{\beta}\right) \left(\frac{\kappa_{MHD}\alpha}{1+\alpha}\right)^{\frac{3}{2}} \left(\frac{100}{g_*}\right)^{\frac{1}{3}} v_w\, S_{MHD}\,(f) \qquad (4.5.52)$$

where $S\,(f)$ are known functions parametrising the dependence on frequency (i.e. determining the shape of the curve as a function of frequency), v_w is the velocity of the bubble walls and the κ-parameters denote the fraction of latent heat that is transformed into sources relevant to each production mode. The precise contribution of the different sources of gravitational waves and formulae for κ depend on the dynamics of the bubble walls, see [133] for more details. To determine which regime we lie in we must determine whether the bubble walls are relativistic and whether they 'runaway'($\gamma \to \infty$).

We do not expect runaway walls as our Z' bosons become massive during the transition and it is known that one should not expect runaway bubbles for a transition where gauge bosons gain a mass [135, 136]. A strongly first-order phase transition is expected to give highly relativistic bubble walls and so we take $v_w = 1$. The exact formulae for the $S(f)$ and κ (for our regime) are given in Appendix D. In this regime the contribution from collision of bubble walls is negligible so we do not include this in our calculations.

We calculate the bubble profile and the action on the profile using BubbleProfiler [137]. The nucleation temperatures and parameters α, β are shown in Table 4.3 for the benchmark points. The gravitational wave profiles are then plotted in Fig. 4.7 along with the sensitivities of current and planned gravitational wave detectors.

As can be seen from the figure, the gravitational waves produced by our model have too low a frequency to probed by aLIGO but would be probed by the next generation of space-based gravitational wave detectors such as LISA, DECIGO and BBO.

	T_c	ϕ_c	T_N	α	$\frac{\beta}{H_*}$
BP1	221 GeV	750 GeV	84.2 GeV	0.547	129
BP2	622 GeV	2313 GeV	115.2 GeV	5.70	63.5
BP3	129 GeV	586 GeV	30.8 GeV	10.1	85.4
BP4	449 GeV	1150 GeV	273.9 GeV	0.0698	290
BP5	152 GeV	802 GeV	<10 GeV	-	-

Table 4.3: Table showing the value of various parameters which are relevant to gravitational waves for our benchmark points. As can be seen from our values of ϕ_c, T_c, all of our benchmark points leads to a strongly first order phase transition. Note that for the fifth benchmark point the nucleation temperature is very low and our software encounters problems in this area. Hence we were unable to determine the exact nucleation temperature (it may be that the model does not nucleate in this region of parameter space) and so we do not determine the gravitational wave spectrum for this point.

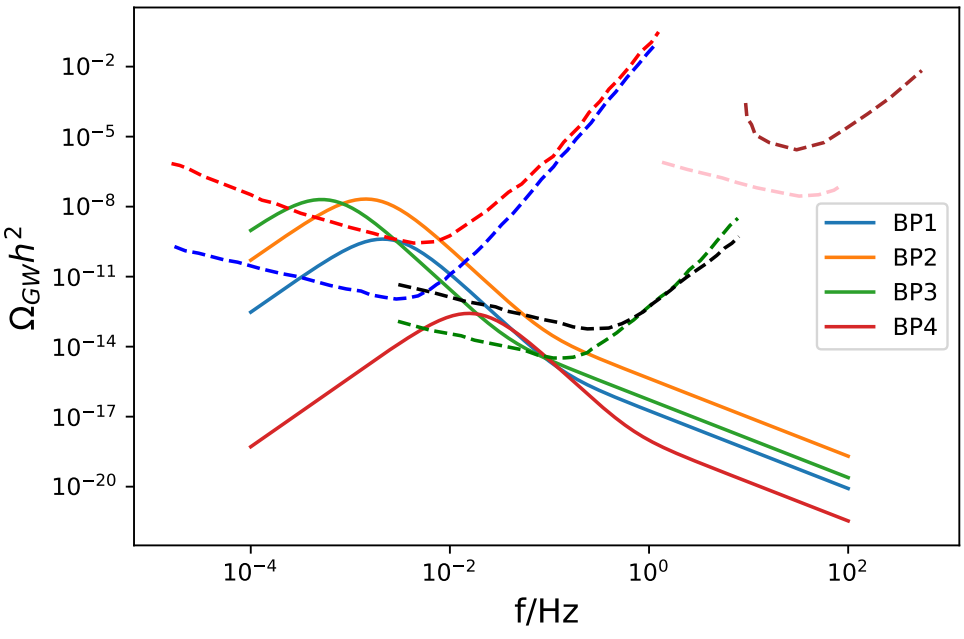

Figure 4.7: A plot showing the energy density of gravitational waves for the first four benchmark points. The dashed lines represent the sensitivities of current and future gravitational wave detectors: LISA (blue), eLISA (red), BBO (green), DECIGO (black), Einstein Telescope (pink) and aLIGO (brown).

4.6 Conclusion

We have shown in this chapter that a classically scale invariant model can evade all current theoretical and experimental constraints and still account for some or all of the observed dark matter abundance of the universe. Such a model is quite an attractive prospect as it is a relatively minimal model which can solve several problems of the Standard Model, primarily dark matter and the hierarchy problem, while also producing a gravitational wave signal which would be observable at the next generation of detectors.

In the context of a minimal model presented here, we have not addressed the question of matter-anti-matter asymmetry. One scenario considered in the literature in classically scale-invariant settings [103, 138] is to use a version of leptogenesis via sterile neutrino oscillations [139, 140], though this would require an extension of our minimal model.

On the other hand, it is reasonably straightforward to provide a realisation of cosmological inflation in the context of these types of models, following the approach of [141]. To achieve this we can extend the Higgs portal interactions of the theory, Eq. (4.5.4) to include an additional real-valued singlet field which is also non-minimally coupled to gravity. In the Einstein frame these interactions generate an exponentially flat potential for the canonically normalised singlet field. This, as explained in [141], provides a successful implementation of a slow-roll cosmological inflation, preserving the classical scale invariance of the model and without the need of perturbative unitarization below the Planck scale. In addition, the singlet can be used as a viable scalar-field Dark Matter component, in addition to fermionic Dark Matter discussed above.

Chapter 5

Conclusion

In conclusion there are many interesting consequences of tunnelling in Quantum Field Theory. One of the most striking is the instanton; the instanton arises naturally in any Yang-Mills theory and is therefore predicted by the Standard Model. After taking into account the effects coming from hard quantum corrections [20] we were able to numerically compute the instanton cross section [2], building on the work in [12].

In this work we also performed a phenomenological analysis and found that it should be feasible to discover the instanton in minimum-bias runs at the LHC. Further studies on the feasibility of detecting the instanton were carried out in [5–7].

However the story is very different when it comes to the electroweak instanton. The electroweak instanton is a very interesting process as it violates baryon and lepton number and is closely related to the sphaleron process which could be important for baryogenesis in the early universe. The electroweak instanton also has a completely different signature to the QCD instanton, whereas the QCD instanton looks much like other QCD processes, the electroweak instanton would produce many charged leptons, gauge bosons and Higgs bosons giving a very clean signal in the detector and requiring a very low number of events for discovery. It has been known since the early 1990's that the cross section of the electroweak instanton is exponentially suppressed at low energies [17, 40] but it was thought that there may be a chance it

would become unsuppressed at higher energies (although this scenario could not be studied as the instanton perturbation theory is no longer valid).

In this thesis it has been shown that the contribution coming from the vev of the Higgs boson suppresses the cross section at low energies (in contrast to the QCD instanton where there is no scalar and hence very large cross sections at low energies) and at higher energies the corrections coming from hard initial state interactions (Mueller's correction) suppresses the cross section, rendering the process exponentially suppressed at all energies and hence unobservable [3].

When the minima of the potential are not degenerate, tunnelling can have drastically different effects. This scenario is normally considered in the early universe, which is the approach considered in the previous section of this thesis. At high temperatures the electroweak symmetry of the Standard Model is unbroken, particles are massless and the Higgs boson does not develop a vev. At lower temperatures, thermal contributions to the potential change and a second minimum of the potential can develop away from the origin. If at this point there is still a barrier between the two minima then this is known as a first order phase transition and the nucleation of bubbles of true vacuum in the early universe can lead to the production of gravitational waves.

It has been known for a long time however that the Standard Model Higgs is too heavy to give a first order phase transition. Indeed the electroweak phase transition in the early universe is second order, also known as a smooth cross-over. However by augmenting the scalar sector of the standard model we can realise a first order phase transition in the early universe. In addition this also allows one to fix several shortcomings of the Standard Model at the same time; primarily by augmenting the model in a classically scale invariant way, the hierarchy problem is resolved and by adding fermions as well as a second scalar, it is possible to reproduce the correct relic density of the universe. In certain regions of parameter space, this model is compatible with all experimental and theoretical constraints and would also produce gravitational waves which could be detectable by future space-based detectors [4].

Appendix A

Instanton–anti-instanton valley configuration

The forward elastic scattering amplitude is obtained from the LSZ-reduced Green's function calculated using the the path integral in the instanton–anti-instanton background,

$$G\left(p_1,p_2,p_1,p_2\right)=\int DA_\mu[DqD\bar{q}]^{N_f}\prod_{i=1}^{4}A_{\mathrm{LSZ}}\left(p_i\right)e^{-S_E[A_\mu,q,\bar{q}]}. \tag{A.0.1}$$

The definition and the meaning of the instanton–anti-instanton field configuration is provided by the valley method of Balitsky and Yung [18,31] and the computation of the instanton cross-section using the optical theorem approach follows the approach developed in [17,32,33,40] and applied to QCD instantons at proton colliders in the recent paper [12].

Usually when performing a functional integral such as this, we would expand the action around the minimum, recalling that the linear term vanishes as instantons satisfy the equations of motion, and we would get the functional determinant of $\frac{\delta^2 S}{\delta A^2}$ but here we must be careful. If this operator possesses small or zero eigenvalues then the usual $(\det)^{-\frac{1}{2}}$ will become very large or singular as the Gaussian approximation fails. We must treat these zero/quasizero modes carefully. These modes arise when there is a symmetry or approximate symmetry of the system leaving the action

unchanged.

A typical example of a zero mode is the centre of the BPST instanton, the corresponding collective coordinate, x_0, does not affect the value of the instanton action and so translation is a symmetry. In general each symmetry of the system that is broken by the background field configuration (in our case the instanton) will have an associated collective coordinate, τ, with zero mode $\frac{\partial A^{\mathrm{cl}}}{\partial \tau}$, where $A^{\mathrm{cl}}(\tau)$ denotes the background field.

Quasi-zero modes can be understood in a similar fashion even though they do not correspond to an exact symmetry of the system. A typical example of a quasi-zero mode is the separation between the positions of the instanton and the anti-instanton in the instanton–anti-instanton configuration. At large separations the individual (anti-)instantons interact very weakly and the collective coordinate that corresponds to their separation becomes a nearly flat direction of the instanton–anti-instanton action. Once again we denote the background instanton–anti-instanton field configuration $A^{\mathrm{cl}}(\tau)$ and the quasi-zero mode is given by $\frac{\partial A^{\mathrm{cl}}}{\partial \tau}$. In general τ will now denote the set of all collective coordinates, for the zero and quasi-zero modes.

The background field configuration with a quasi-zero mode (i.e. a nearly flat direction in the action parameterised by the τ coordinate) can now be defined as a solution of the gradient flow equation, also known as the valley equation of Balitsky and Yung [18, 31],

$$\left.\frac{\delta S}{\delta A}\right|_{A=A^{\mathrm{cl}}(\tau)} \propto \epsilon^2(\tau)\,\frac{\partial A^{\mathrm{cl}}}{\partial \tau}. \tag{A.0.2}$$

If the background field is an exact classical solution, then the τ-collective-coordinate parameterises an exact zero mode and we have $\epsilon^2(\tau) = 0$ so the valley equation collapses to the Euler-Lagrange equation. However, in the case of a quasi-zero mode, τ is a pseudo-flat direction; the action is not at the exact minimum at any fixed value of τ. In this case Eq. (A.0.2) holds with a non-vanishing but small right hand side, so that $\epsilon^2(\tau) \ll 1$. The smallness of the parameter $\epsilon^2(\tau)$ characterises how flat the corresponding quasi-zero mode is.

To proceed with our calculation of the Green's function one uses the Fadeev-Popov procedure [18, 31]:

$$1 = \int \mathrm{d}\tau \left| \det \left(\frac{d}{d\tau} \left\langle A - A^{\mathrm{cl}}(\tau), \frac{\partial A^{\mathrm{cl}}}{\partial \tau} \right\rangle_w \right) \right| \delta \left(\left\langle A - A^{\mathrm{cl}}(\tau), \frac{\partial A^{\mathrm{cl}}}{\partial \tau} \right\rangle_w \right)$$
$$= \int \mathrm{d}\tau \det \left(\left\langle \frac{\partial A^{\mathrm{cl}}}{\partial \tau}, \frac{\partial A^{\mathrm{cl}}}{\partial \tau} \right\rangle_w \right) \delta \left(\left\langle A - A^{\mathrm{cl}}(\tau), \frac{\partial A^{\mathrm{cl}}}{\partial \tau} \right\rangle_w \right). \tag{A.0.3}$$

where $A^{\mathrm{cl}}(\tau)$ is the minimum of the action for fixed τ and $\langle A, B \rangle_w$ denotes the scalar product or an overlap of two field configurations,

$$\langle A, B \rangle_w = \int \mathrm{d}^4 x \, w(x) A(x) B(x). \tag{A.0.4}$$

Note that the definition of the overlap above uses a positive weight function $w(x)$ – the freedom to choose a convenient form of $w(x)$ is a well-known simplifying feature used in path integral expansions around instantons [11, 18, 142] and will be utilised in what follows. Taking into account the weight factor, the valley equation reads,

$$\left. \frac{\delta S}{\delta A} \right|_{A = A^{\mathrm{cl}}(\tau)} = \epsilon^2(\tau) \, w(x) \frac{\partial A^{\mathrm{cl}}}{\partial \tau}. \tag{A.0.5}$$

Inserting one of the factors of 1 in the form of Eq. (A.0.3) for each collective coordinate, and expanding the action $S(A)$ around the background field $A^{\mathrm{cl}}(\tau)$,

$$S(A) = S(A^{\mathrm{cl}}(\tau)) + \left\langle \frac{\delta S(A^{\mathrm{cl}}(\tau))}{\delta A}, (A - A^{\mathrm{cl}}(\tau)) \right\rangle_w$$
$$+ \frac{1}{2} \left\langle (A - A^{\mathrm{cl}}(\tau)), \Box(A^{\mathrm{cl}}(\tau))(A - A^{\mathrm{cl}}(\tau)) \right\rangle_w + \ldots \tag{A.0.6}$$

we get,

$$G = N \int \prod_i \mathrm{d}\tau_i \det \left(\left\langle \frac{\partial A_{\tau_i}}{\partial \tau}, \frac{\partial A_{\tau_j}}{\partial \tau} \right\rangle_w \right) \int DA \prod_i \delta \left(\left\langle A - A^{\mathrm{cl}}(\tau), \frac{\partial A^{\mathrm{cl}}(\tau)}{\partial \tau_i} \right\rangle_w \right)$$
$$\prod_{m=1}^{4} A_{\mathrm{LSZ}}(p_m) \, e^{-S\left(A^{\mathrm{cl}}(\tau)\right) - \frac{1}{2} \left\langle \left(A - A^{\mathrm{cl}}(\tau)\right), \Box(A^{\mathrm{cl}}(\tau)) \left(A - A^{\mathrm{cl}}(\tau)\right) \right\rangle_w}, \tag{A.0.7}$$

where $\Box\left(A^{\mathrm{cl}}(\tau)\right) = \left. \frac{\delta^2 S}{\delta A^2} \right|_{A = A^{\mathrm{cl}}}$. We note that the term linear in fluctuations in the expansion of the action (the second term on the right hand side of Eq. (A.0.6)) in fact does not contribute to the integral in Eq. (A.0.7). Indeed, the valley equation,

Eq. (A.0.5), requires that $\delta S/\delta A$ is proportional to $\partial A/\partial\tau$ when computed on our background configuration, $A^{\rm cl}(\tau)$, and then the delta-function in the integrand, Eq. (A.0.7), ensures that this linear term vanishes.

Now we can perform the functional integration [18],

$$G = N\int\prod_i \mathrm{d}\tau_i \det\left(\left\langle\frac{\partial A_{\tau_i}}{\partial\tau},\frac{\partial A_{\tau_j}}{\partial\tau}\right\rangle_w\right)\det{}^{-1/2}\left(\left\langle\frac{\partial A_\tau}{\partial\tau_i},\Box^{-1}\left(A_\tau\right)\frac{\partial A_\tau}{\partial\tau_j}\right\rangle\right)$$
$$\det{}^{-1/2}\left(\Box\left(A_\tau\right)\right)\prod_{m=1}^{4}A_{\rm LSZ}\left(p_m\right)e^{-S\left(A^{\rm cl}(\tau)\right)}. \qquad \text{(A.0.8)}$$

Since the $\frac{\partial A^{\rm cl}}{\partial\tau}$ play the role of zero and quasi-zero modes of the action, they are the eigenfunctions of $\Box(A^{\rm cl}(\tau))$ and so,

$$\Box\Big(A^{\rm cl}(\tau)\Big)\,\frac{\partial A^{\rm cl}}{\partial\tau_i} \;=\; \lambda_i\frac{\partial A^{\rm cl}}{\partial\tau_i}\,. \qquad \text{(A.0.9)}$$

This equation is valid at leading order in the small parameter ϵ^2 and follows from differentiating both sides of the valley equation with respect to τ and neglecting the $\epsilon^2(\tau)\,\partial^2 A^{\rm cl}/\partial\tau^2$ term.

This allows us to simplify the product of the three determinants in Eq. (A.0.8) into

$$\det{}^{1/2}\left(\left\langle\frac{\partial A^{\rm cl}}{\partial\tau_i},\frac{\partial A^{\rm cl}}{\partial\tau_j}\right\rangle\right)\left(\det{}^{(2p)}\left(\Box\left(A^{\rm cl}\left(\tau\right)\right)\right)\right)^{-1/2} \qquad \text{(A.0.10)}$$

where $\det^{(2p)}$ denotes the determinant with the $2p$ zero and quasi-zero modes $\{\lambda_i\}_{i=1}^{2p}$ removed (p modes for the instanton and p modes for the anti-instanton).

To leading order in the small-ϵ expansion we can also factorise the quadratic fluctuation determinant in the instanton–anti-instanton background $A^{\rm cl}(\tau) = A_{I\bar{I}}$ into a product of the instanton and the anti–instanton quadratic fluctuation determinants, $\det^{(2p)}\left(\Box\left(A_{I\bar{I}}\right)\right) \approx \det^{(p)}\left(\Box\left(A_I\right)\right)\det^{(p)}\left(\Box\left(A_{\bar{I}}\right)\right)$.

This gives us finally [18],

$$G = \int \mathrm{d}\mu_1\mathrm{d}\mu_2\prod_{m=1}^{4}A_{LSZ}\left(p_m\right)e^{-S\left(A^{\rm cl}(\tau)\right)} \qquad \text{(A.0.11)}$$

where

$$\mathrm{d}\mu_a = N \prod_{i=1}^{p} d\tau_{a,i} \det{}^{1/2} \left(\langle \frac{\partial A_a}{\partial \tau_{a,i}}, \frac{\partial A_a}{\partial \tau_{a,j}} \rangle \right) \left(\det{}^{(p)} \left(\Box \left(A_a \right) \right) \right)^{-1/2}, \tag{A.0.12}$$

are the instanton and anti-instanton collective coordinate integration measures.

Having established the form of the collective coordinate integrals for the instanton-anti-instanton case, what is left for us to determine is the instanton–anti-instanton configuration itself and in particular its action as a function of (anti-)instanton collective coordinates.

The instanton–anti-instanton valley trajectory $A_\mu^{I\bar{I}}$ was obtained in [18] by finding an exact solution of the valley equation, Eq. (A.0.5) for a particular choice of the weight function, $w(x)$, by exploiting the conformal invariance of the classical Yang-Mills action. The action on this configuration was computed in [32] and [17, 33] and it takes the form,

$$S_{I\bar{I}}(z) = \frac{16\pi^2}{g^2} \left(3 \frac{6z^2 - 14}{(z - 1/z)^2} - 17 - 3 \log(z) \left(\frac{(z - 5/z)(z + 1/z)^2}{(z - 1/z)^3} - 1 \right) \right) \tag{A.0.13}$$

where the variable z is the conformal ratio of the (anti-)instanton collective coordinates,

$$z = \frac{R^2 + \rho^2 + \bar{\rho}^2 + \sqrt{(R^2 + \rho^2 + \bar{\rho}^2)^2 - 4\rho^2\bar{\rho}^2}}{2\rho\bar{\rho}}. \tag{A.0.14}$$

z plays the role of the single negative quasi-zero mode of the instanton–anti-instanton valley configuration.

In the limit of large separation between the instanton centres, R/ρ, $R/\bar{\rho} \to \infty$, the conformal ratio $z \to R^2/\rho\bar{\rho} \to \infty$, and the instanton–anti-instanton action $S_{I\bar{I}}(z)$ becomes the sum of the individual instanton and anti-instanton actions,

$$\lim_{z\to\infty} S_{I\bar{I}}(z) = \frac{8\pi^2}{g^2} + \frac{8\pi^2}{g^2} + \mathcal{O}(1/z^2) = \frac{16\pi^2}{g^2}, \tag{A.0.15}$$

and

$$A_\mu^{I\bar{I}}(x) \longrightarrow A_\mu^I(x - x_0) + A_\mu^{\bar{I}}(x - x_0 - R). \tag{A.0.16}$$

In the opposite limit of a vanishing separation between the instanton centres,

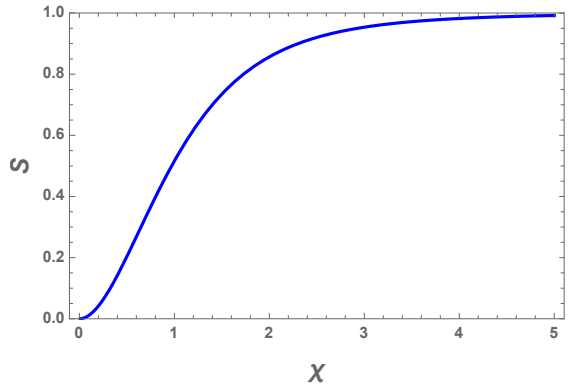

Figure A.1: The action, Eq. (2.2.19), of the instanton–anti-instanton configuration as a function of $\chi = R/\rho$ in units of $16\pi^2/g^2$. $S_{I\bar{I}}$ approaches the sum of the individual instanton actions at $\chi \to \infty$ where the instanton interaction vanishes, and $S_{I\bar{I}} \to 0$ at $\chi \to 0$ where the instanton and the anti-instanton mutually annihilate.

$R/\rho, R/\bar{\rho} \to 0$, the conformal ratio $z \to 1$ and the expression for the action $\mathcal{S}(z)$ goes to zero. This is in agreement with the expectation that in this limit the instanton and the anti-instanton annihilate to the perturbative vacuum, $A_\mu = 0$.

We can plot the action, $S_{I\bar{I}}$, as a function of the separation between the instanton centres, R, normalised by the instanton scale sizes. For simplicity, if we assume that the sizes are equal, $\rho = \bar{\rho}$, we can write down the action $S_{I\bar{I}}$ as a function of the vartiable $\chi = R/\rho$. It is plotted in Fig. A.1 in units of $16\pi^2/g^2$.

Appendix B

Integration over the relative orientations

To be able to integrate over relative orientations in the internal $SU(3)$ space, we need to know the form of the instanton–anti-instanton action for arbitrary values of their relative orientation matrix, Ω. However our exact valley configuration is only known for the maximally attractive channel, i.e. where the interaction potential, $U_{\rm int}(z,\Omega)$, is maximised over the relative orientations at each fixed value of z.

What is known however, is the form of the interaction potential, $U_{\rm int}(z,\Omega)$, in the limit of large separations. In this large-separations regime (i.e. $z \gg 1$) the instanton and the anti-instanton are known to have dipole-dipole interactions [143],

$$U_{\rm int}(z,\Omega) = \frac{1}{z^2}\left(2\,{\rm tr}O{\rm tr}O^\dagger - {\rm tr}(OO^\dagger)\right) + \mathcal{O}\left(\frac{1}{z^4}\log z\right), \qquad \text{(B.0.1)}$$

where O is the 2×2 matrix in the upper-left corner of the 3×3 matrix Ω describing the relative instanton–anti-instanton orientation.[2]

Lacking the precise solution of the instanton–anti-instanton valley for general orientations at *arbitrary* separations, we will simply assume that the full interaction

[2]The upper-left corner is selected by placing the instanton in the upper-left corner while allowing the anti-instanton to be anywhere in the $SU(3)$ internal space.

potential can always be written in the form (*c.f.* Eq. (2.2.28)),

$$U_{\rm int}(z,\Omega) = U_{\rm int}(z)\frac{1}{6}\left(2\,{\rm tr}O{\rm tr}O^\dagger - {\rm tr}(OO^\dagger)\right), \tag{B.0.2}$$

where $U_{\rm int}(z)$ is the maximally-attractive-orientation potential of Eqs. (2.2.19), (2.2.26). Clearly at large separations, to order $1/z^2$, this expression coincides with the known dipole-dipole interaction.

We can now represent the integral over the relative orientations as follows,

$$\int {\rm d}\Omega\, e^{-\frac{4\pi}{\alpha_s(\mu_r)}\mathcal{S}(z,\Omega)} = e^{-\frac{4\pi}{\alpha_s(\mu_r)}}\int {\rm d}\Omega e^{U_{\rm int}(z)\frac{1}{6}\left(2\,{\rm tr}O{\rm tr}O^\dagger - {\rm tr}(OO^\dagger)\right)}. \tag{B.0.3}$$

These types of integrals over $SU(3)$ matrices have been previously computed in the instanton literature, see Eq. (2.15) in [34]:

$$\int {\rm d}\Omega\, e^{\lambda\left(2{\rm tr}O{\rm tr}O^\dagger - {\rm tr}(OO^\dagger)\right)} = \frac{1}{9\sqrt{\pi}}(2\lambda)^{-7/2}e^{6\lambda}. \tag{B.0.4}$$

Substituting $\lambda = \frac{1}{6}U_{\rm int}(z)$ into the expression above, we now obtain the answer for our relative orientation integral in Eq. (B.0.3),

$$\int {\rm d}\Omega\, e^{-\frac{4\pi}{\alpha_s(\mu_r)}\mathcal{S}(z,\Omega)} = \frac{1}{9\sqrt{\pi}}\left(\frac{3}{U_{\rm int}(z)}\right)^{7/2} e^{-\frac{4\pi}{\alpha_s(\mu_r)}\mathcal{S}(z)} \tag{B.0.5}$$

which agrees with the expression, Eq. (2.2.31), quoted previously.

Appendix C

RG Equations

Below are the beta functions for the different coupling constants of the model in Chapter 4. These were used to evolve the constants to higher RG scales and check the scales at which perturbativity, unitarity and vacuum stablity are violated, see Table 4.2.

$$\beta^{(1)}_{g_D} = g_D^3 \tag{C.0.1}$$

$$\begin{aligned}\beta^{(1)}_{\lambda_H} = {} & \frac{27}{200}g'^4 + \frac{9}{20}g'^2 g_W^2 + \frac{9}{8}g_W^4 - \frac{9}{5}g'^2\lambda_H - 9g_W^2\lambda_H + 24\lambda_H^2 + \lambda_P^2 \\ & + 12\lambda_H \mathrm{Tr}\left(Y_d Y_d^\dagger\right) + 4\lambda_H \mathrm{Tr}\left(Y_e Y_e^\dagger\right) + 12\lambda_H \mathrm{Tr}\left(Y_u Y_u^\dagger\right) \\ & - 6\mathrm{Tr}\left(Y_d Y_d^\dagger Y_d Y_d^\dagger\right) - 2\mathrm{Tr}\left(Y_e Y_e^\dagger Y_e Y_e^\dagger\right) - 6\mathrm{Tr}\left(Y_u Y_u^\dagger Y_u Y_u^\dagger\right)\end{aligned} \tag{C.0.2}$$

$$\begin{aligned}\beta^{(1)}_{\lambda_P} = {} & \frac{1}{10}\lambda_P\left(-9g'^2 - 45g_W^2 - 60g_D^2 + 120\lambda_H - 40\lambda_P + 80\lambda_S\right. \\ & \left. + 20|y_{2,D}|^2 + 20|y_{1,D}|^2 + 60\mathrm{Tr}\left(Y_d Y_d^\dagger\right) + 20\mathrm{Tr}\left(Y_e Y_e^\dagger\right) + 60\mathrm{Tr}\left(Y_u Y_u^\dagger\right)\right)\end{aligned} \tag{C.0.3}$$

$$\beta^{(1)}_{\lambda_S} = 2\left(10\lambda_S^2 + 2\lambda_S|y_{2,D}|^2 + 2\lambda_S|y_{1,D}|^2 + 3g_D^4 - 6g_D^2\lambda_S - |y_{2,D}|^4 - |y_{1,D}|^4 + \lambda_P^2\right) \tag{C.0.4}$$

$$\beta^{(1)}_{y_{1,D}} = \frac{1}{2}y_{1,D}\left(2|y_{2,D}|^2 - 3g_D^2 + 4|y_{1,D}|^2\right) \tag{C.0.5}$$

$$\beta^{(1)}_{y_{2,D}} = \frac{1}{2}y_{2,D}\left(2|y_{1,D}|^2 - 3g_D^2 + 4|y_{2,D}|^2\right) \tag{C.0.6}$$

Appendix D

Gravitational wave formulae

The full gravitational wave formulae are given by Eq. 4.5.52 and were used in the calculation of the signals shown in Fig. 4.7 but the details of some components were omitted for brevity. The remaining parameters required for the calculation of the gravitational wave spectrum are given below. All formulae here are taken from [133]. Firstly we begin with the frequency dependence of the sound wave production.

$$S_{SW}(f) = \left(\frac{f}{f_{SW}}\right)^3 \left(\frac{7}{4+3\left(\frac{f}{f_{SW}}\right)^2}\right)^{\frac{7}{2}} \tag{D.0.1}$$

where

$$f_{SW} = 1.9 \times 10^{-2}\,\text{mHz}\left(\frac{1}{v_w}\right)\left(\frac{\beta}{H_*}\right)\left(\frac{T_*}{100\,\text{GeV}}\right)\left(\frac{g_*}{100}\right)^{\frac{1}{6}}. \tag{D.0.2}$$

The frequency dependence of the gravitational wave production by turbulence is given by

$$S_{turb}(f) = \frac{\left(\frac{f}{f_{turb}}\right)^3}{\left(1+\frac{f}{f_{turb}}\right)^{\frac{11}{3}}\left(1+\frac{8\pi f}{h_*}\right)} \tag{D.0.3}$$

where

$$f_{turb} = 2.7 \times 10^{-2}\,\text{mHz}\left(\frac{1}{v_w}\right)\left(\frac{\beta}{H_*}\right)\left(\frac{T_*}{100\,\text{GeV}}\right)\left(\frac{g_*}{100}\right)^{\frac{1}{6}} \tag{D.0.4}$$

$$h_* = 16.5 \times 10^{-3}\,\text{mHz}\left(\frac{T_*}{100\,\text{GeV}}\right)\left(\frac{g_*}{100}\right)^{\frac{1}{6}}. \tag{D.0.5}$$

The efficiencies of the two processes are given by

$$\kappa_v = \frac{\alpha}{0.73 + 0.083\sqrt{\alpha} + \alpha} \tag{D.0.6}$$

$$\kappa_{turb} = 0.05\kappa_v. \tag{D.0.7}$$

Bibliography

[1] M. Quiros, *Finite temperature field theory and phase transitions*, in *ICTP Summer School in High-Energy Physics and Cosmology*, pp. 187–259, 1, 1999, hep-ph/9901312.

[2] V. V. Khoze, D. L. Milne and M. Spannowsky, *Searching for QCD Instantons at Hadron Colliders*, *Phys. Rev. D* **103** (2021) 014017, [2010.02287].

[3] V. V. Khoze and D. L. Milne, *Suppression of Electroweak Instanton Processes in High-energy Collisions*, *Int. J. Mod. Phys. A* **36** (2021) 2150032, [2011.07167].

[4] V. V. Khoze and D. L. Milne, *Gravitational waves and dark matter from classical scale invariance*, 2212.04784.

[5] V. A. Khoze, V. V. Khoze, D. L. Milne and M. G. Ryskin, *Hunting for QCD instantons at the LHC in events with large rapidity gaps*, *Phys. Rev. D* **104** (2021) 054013, [2104.01861].

[6] V. A. Khoze, V. V. Khoze, D. L. Milne and M. G. Ryskin, *Central instanton production*, *Phys. Rev. D* **105** (2022) 036008, [2111.02159].

[7] M. Tasevsky, V. Khoze, D. Milne and M. Ryskin, *Searches for QCD instantons with forward proton tagging*, *Eur. Phys. J. C* **83** (2023) 35, [2208.14089].

[8] V. V. Khoze and D. L. Milne, *Optical effects of domain walls*, *Phys. Lett. B* **829** (2022) 137044, [2107.02640].

[9] M. E. Peskin and D. V. Schroeder, *An Introduction to quantum field theory.* Addison-Wesley, Reading, USA, 1995.

[10] A. I. Vainshtein, V. I. Zakharov, V. A. Novikov and M. A. Shifman, *ABC's of Instantons*, *Sov. Phys. Usp.* **25** (1982) 195.

[11] G. 't Hooft, *Computation of the Quantum Effects Due to a Four-Dimensional Pseudoparticle*, *Phys. Rev.* **D14** (1976) 3432–3450.

[12] V. V. Khoze, F. Krauss and M. Schott, *Large Effects from Small QCD Instantons: Making Soft Bombs at Hadron Colliders*, *JHEP* **04** (2020) 201, [1911.09726].

[13] C. G. Callan, Jr., R. F. Dashen and D. J. Gross, *The Structure of the Gauge Theory Vacuum*, *Phys. Lett.* **63B** (1976) 334–340.

[14] R. Jackiw and C. Rebbi, *Vacuum Periodicity in a Yang-Mills Quantum Theory*, *Phys. Rev. Lett.* **37** (1976) 172–175.

[15] A. A. Belavin, A. M. Polyakov, A. S. Schwartz and Yu. S. Tyupkin, *Pseudoparticle Solutions of the Yang-Mills Equations*, *Phys. Lett.* **B59** (1975) 85–87.

[16] G. 't Hooft, *Symmetry Breaking Through Bell-Jackiw Anomalies*, *Phys. Rev. Lett.* **37** (1976) 8–11.

[17] V. V. Khoze and A. Ringwald, *Nonperturbative contribution to total cross-sections in non-Abelian gauge theories*, *Phys. Lett.* **B259** (1991) 106–112.

[18] A. V. Yung, *Instanton Vacuum in Supersymmetric QCD*, *Nucl. Phys.* **B297** (1988) 47.

[19] A. H. Mueller, *Leading power corrections to the semiclassical approximation for gauge meson collisions in the one instanton sector*, *Nucl. Phys.* **B353** (1991) 44–58.

[20] A. H. Mueller, *First Quantum Corrections to Gluon-gluon Collisions in the One Instanton Sector*, *Nucl. Phys.* **B348** (1991) 310–326.

[21] S. Knapen, S. Pagan Griso, M. Papucci and D. J. Robinson, *Triggering Soft Bombs at the LHC*, *JHEP* **08** (2017) 076, [1612.00850].

[22] A. Bilal, *Lectures on Anomalies*, 0802.0634.

[23] J. A. Harvey, *TASI 2003 lectures on anomalies*, 9, 2005, hep-th/0509097.

[24] K. Fujikawa, *Path Integral Measure for Gauge Invariant Fermion Theories*, *Phys. Rev. Lett.* **42** (1979) 1195–1198.

[25] K. Fujikawa, *Path Integral for Gauge Theories with Fermions*, *Phys. Rev. D* **21** (1980) 2848.

[26] G. 't Hooft, *How Instantons Solve the U(1) Problem*, *Phys. Rept.* **142** (1986) 357–387.

[27] A. Hasenfratz and P. Hasenfratz, *The Scales of Euclidean and Hamiltonian Lattice QCD*, *Nucl. Phys.* **B193** (1981) 210.

[28] M. Luscher, *A Semiclassical Formula for the Topological Susceptibility in a Finite Space-time Volume*, *Nucl. Phys.* **B205** (1982) 483–503.

[29] A. Ringwald, *High-Energy Breakdown of Perturbation Theory in the Electroweak Instanton Sector*, *Nucl. Phys.* **B330** (1990) 1–18.

[30] P. B. Arnold and L. D. McLerran, *Sphalerons, Small Fluctuations and Baryon Number Violation in Electroweak Theory*, *Phys. Rev.* **D36** (1987) 581.

[31] I. I. Balitsky and A. V. Yung, *Collective - Coordinate Method for Quasizero Modes*, *Phys. Lett.* **168B** (1986) 113–119.

[32] V. V. Khoze and A. Ringwald, *Valley trajectories in gauge theories*, *CERN-TH-6082-91* (1991) .

[33] J. Verbaarschot, *Streamlines and conformal invariance in Yang-Mills theories*, *Nucl. Phys. B* **362** (1991) 33–53.

[34] I. I. Balitsky and V. M. Braun, *Instanton-induced contributions of fractional twist in the cross-section of hard gluon-gluon scattering in QCD*, *Phys. Rev.* **D47** (1993) 1879–1888.

[35] E. V. Shuryak and J. Verbaarschot, *On baryon number violation and nonperturbative weak processes at SSC energies*, *Phys. Rev. Lett.* **68** (1992) 2576–2579.

[36] A. Ringwald and F. Schrempp, *Instanton induced cross-sections in deep inelastic scattering*, *Phys. Lett.* **B438** (1998) 217–228, [hep-ph/9806528].

[37] P. Virtanen, R. Gommers, T. E. Oliphant, M. Haberland, T. Reddy, D. Cournapeau et al., *SciPy 1.0: Fundamental Algorithms for Scientific Computing in Python*, *Nature Methods* **17** (2020) 261–272.

[38] A. Buckley, J. Ferrando, S. Lloyd, K. Nordstrom, B. Page, M. Refenacht et al., *LHAPDF6: parton density access in the LHC precision era*, *Eur. Phys. J. C* **75** (2015) 132, [1412.7420].

[39] NNPDF collaboration, V. Bertone, S. Carrazza, N. P. Hartland and J. Rojo, *Illuminating the photon content of the proton within a global PDF analysis*, *SciPost Phys.* **5** (2018) 008, [1712.07053].

[40] V. V. Khoze and A. Ringwald, *Total cross-section for anomalous fermion number violation via dispersion relation*, *Nucl. Phys.* **B355** (1991) 351–368.

[41] G. D. Kribs, A. Martin, T. S. Roy and M. Spannowsky, *Discovering the Higgs Boson in New Physics Events using Jet Substructure*, *Phys. Rev. D* **81** (2010) 111501, [0912.4731].

[42] M. Schlaffer, M. Spannowsky, M. Takeuchi, A. Weiler and C. Wymant, *Boosted Higgs Shapes*, *Eur. Phys. J. C* **74** (2014) 3120, [1405.4295].

[43] P. Harris, V. V. Khoze, M. Spannowsky and C. Williams, *Constraining Dark Sectors at Colliders: Beyond the Effective Theory Approach*, *Phys. Rev. D* **91** (2015) 055009, [1411.0535].

[44] P. Harris, V. V. Khoze, M. Spannowsky and C. Williams, *Closing up on Dark Sectors at Colliders: from 14 to 100 TeV*, *Phys. Rev. D* **93** (2016) 054030, [1509.02904].

[45] A. Banfi, G. P. Salam and G. Zanderighi, *Resummed event shapes at hadron - hadron colliders*, *JHEP* **08** (2004) 062, [hep-ph/0407287].

[46] T. Sjöstrand, S. Ask, J. R. Christiansen, R. Corke, N. Desai, P. Ilten et al., *An introduction to PYTHIA 8.2*, *Comput. Phys. Commun.* **191** (2015) 159–177, [1410.3012].

[47] R. Kleiss, W. J. Stirling and S. D. Ellis, *A New Monte Carlo Treatment of Multiparticle Phase Space at High-energies*, *Comput. Phys. Commun.* **40** (1986) 359.

[48] M. Cacciari, G. P. Salam and G. Soyez, *FastJet User Manual*, *Eur. Phys. J. C* **72** (2012) 1896, [1111.6097].

[49] M. Cacciari, G. P. Salam and G. Soyez, *The anti-k_t jet clustering algorithm*, *JHEP* **04** (2008) 063, [0802.1189].

[50] ATLAS collaboration, M. Aaboud et al., *Performance of the ATLAS Trigger System in 2015*, *Eur. Phys. J. C* **77** (2017) 317, [1611.09661].

[51] ATLAS collaboration, *Luminosity determination for low-pileup datasets at $\sqrt{s} = 5$ and 13 TeV using the ATLAS detector at the LHC*, .

[52] CMS collaboration, *CMS luminosity measurement for the 2017 data-taking period at $\sqrt{s} = 13$ TeV*, .

[53] CDF collaboration, T. Aaltonen et al., *Search for resonant production of $t\bar{t}$ decaying to jets in $p\bar{p}$ collisions at $\sqrt{s} = 1.96$ TeV*, *Phys. Rev. D* **84** (2011) 072003, [1108.4755].

[54] CDF collaboration, T. Aaltonen et al., *Top-quark mass measurement using events with missing transverse energy and jets at CDF*, *Phys. Rev. Lett.* **107** (2011) 232002, [1109.1490].

[55] CDF collaboration, T. Aaltonen et al., *Measurements of the Top-quark Mass and the $t\bar{t}$ Cross Section in the Hadronic τ+ Jets Decay Channel at $\sqrt{s} = 1.96$ TeV*, *Phys. Rev. Lett.* **109** (2012) 192001, [1208.5720].

[56] A. Ringwald, *From QCD instantons at HERA to electroweak B + L violation at VLHC*, hep-ph/0302112.

[57] H1 collaboration, C. Adloff et al., *Search for QCD instanton induced processes in deep inelastic scattering at HERA*, *Eur. Phys. J.* **C25** (2002) 495–509, [hep-ex/0205078].

[58] ZEUS collaboration, S. Chekanov et al., *Search for QCD instanton induced events in deep inelastic ep scattering at HERA*, *Eur. Phys. J.* **C34** (2004) 255–265, [hep-ex/0312048].

[59] H1 collaboration, V. Andreev et al., *Search for QCD instanton-induced processes at HERA in the high- Q^2 domain*, *Eur. Phys. J.* **C76** (2016) 381, [1603.05567].

[60] A. Ringwald, K. Sakurai and B. R. Webber, *Limits on Electroweak Instanton-Induced Processes with Multiple Boson Production*, *JHEP* **11** (2018) 105, [1809.10833].

[61] A. Papaefstathiou, S. Platzer and K. Sakurai, *On the phenomenology of sphaleron-induced processes at the LHC and beyond*, 1910.04761.

[62] J. Ellis, K. Sakurai and M. Spannowsky, *Search for Sphalerons: IceCube vs. LHC*, *JHEP* **05** (2016) 085, [1603.06573].

[63] O. Espinosa, *High-Energy Behavior of Baryon and Lepton Number Violating Scattering Amplitudes and Breakdown of Unitarity in the Standard Model*, *Nucl. Phys.* **B343** (1990) 310–340.

[64] M. P. Mattis, *The Riddle of high-energy baryon number violation*, *Phys. Rept.* **214** (1992) 159–221.

[65] V. A. Rubakov and M. E. Shaposhnikov, *Electroweak baryon number nonconservation in the early universe and in high-energy collisions*, *Usp. Fiz. Nauk* **166** (1996) 493–537, [hep-ph/9603208].

[66] F. R. Klinkhamer and N. S. Manton, *A Saddle Point Solution in the Weinberg-Salam Theory*, *Phys. Rev.* **D30** (1984) 2212.

[67] V. I. Zakharov, *Classical corrections to instanton induced interactions*, *Nucl. Phys.* **B371** (1992) 637–658.

[68] S. Yu. Khlebnikov, V. A. Rubakov and P. G. Tinyakov, *Instanton induced cross-sections below the sphaleron*, *Nucl. Phys.* **B350** (1991) 441–473.

[69] I. Balitsky and A. Schafer, *Valley method versus instanton induced effective Lagrangian up to (E / E(sphaleron))**8/3*, *Nucl. Phys.* **B404** (1993) 639–683, [hep-ph/9304261].

[70] L. S. Brown, R. D. Carlitz, D. B. Creamer and C.-k. Lee, *Propagation Functions in Pseudoparticle Fields*, *Phys. Rev. D* **17** (1978) 1583.

[71] J. C. Collins, *Sudakov form-factors*, *Adv. Ser. Direct. High Energy Phys.* **5** (1989) 573–614, [hep-ph/0312336].

[72] M. V. Libanov, V. A. Rubakov, D. T. Son and S. V. Troitsky, *Exponentiation of multiparticle amplitudes in scalar theories*, *Phys. Rev.* **D50** (1994) 7553–7569, [hep-ph/9407381].

[73] F. L. Bezrukov, D. Levkov, C. Rebbi, V. A. Rubakov and P. Tinyakov, *Semiclassical study of baryon and lepton number violation in high-energy electroweak collisions*, *Phys. Rev.* **D68** (2003) 036005, [hep-ph/0304180].

[74] F. L. Bezrukov, D. Levkov, C. Rebbi, V. A. Rubakov and P. Tinyakov, *Suppression of baryon number violation in electroweak collisions: Numerical results*, *Phys. Lett.* **B574** (2003) 75–81, [hep-ph/0305300].

[75] V. I. Zakharov, *Unitarity constraints on multiparticle weak production*, *Nucl. Phys.* **B353** (1991) 683–688.

[76] M. Maggiore and M. A. Shifman, *Nonperturbative processes at high-energies in weakly coupled theories: Multi - instantons set an early limit*, *Nucl. Phys.* **B371** (1992) 177–190.

[77] G. Veneziano, *Bound on reliable one instanton cross-sections*, *Mod. Phys. Lett.* **A7** (1992) 1661–1666.

[78] ATLAS collaboration, G. Aad et al., *Observation of a new particle in the search for the Standard Model Higgs boson with the ATLAS detector at the LHC*, *Phys. Lett. B* **716** (2012) 1–29, [1207.7214].

[79] CMS collaboration, S. Chatrchyan et al., *Observation of a New Boson at a Mass of 125 GeV with the CMS Experiment at the LHC*, *Phys. Lett. B* **716** (2012) 30–61, [1207.7235].

[80] S. R. Coleman and E. J. Weinberg, *Radiative Corrections as the Origin of Spontaneous Symmetry Breaking*, *Phys. Rev. D* **7** (1973) 1888–1910.

[81] W. A. Bardeen, *On naturalness in the standard model*, in *Ontake Summer Institute on Particle Physics*, 8, 1995.

[82] R. Hempfling, *The Next-to-minimal Coleman-Weinberg model*, *Phys. Lett. B* **379** (1996) 153–158, [hep-ph/9604278].

[83] K. A. Meissner and H. Nicolai, *Conformal Symmetry and the Standard Model*, *Phys. Lett. B* **648** (2007) 312–317, [hep-th/0612165].

[84] W.-F. Chang, J. N. Ng and J. M. S. Wu, *Shadow Higgs from a scale-invariant hidden U(1)(s) model*, *Phys. Rev. D* **75** (2007) 115016, [hep-ph/0701254].

[85] R. Foot, A. Kobakhidze, K. L. McDonald and R. R. Volkas, *A Solution to the hierarchy problem from an almost decoupled hidden sector within a classically scale invariant theory*, *Phys. Rev. D* **77** (2008) 035006, [0709.2750].

[86] C. Englert, J. Jaeckel, V. V. Khoze and M. Spannowsky, *Emergence of the Electroweak Scale through the Higgs Portal*, *JHEP* **04** (2013) 060, [1301.4224].

[87] V. C. Rubin and W. K. Ford, Jr., *Rotation of the Andromeda Nebula from a Spectroscopic Survey of Emission Regions*, *Astrophys. J.* **159** (1970) 379–403.

[88] M. Markevitch, A. H. Gonzalez, D. Clowe, A. Vikhlinin, L. David, W. Forman et al., *Direct constraints on the dark matter self-interaction cross-section from the merging galaxy cluster 1E0657-56*, *Astrophys. J.* **606** (2004) 819–824, [astro-ph/0309303].

[89] Planck collaboration, P. A. R. Ade et al., *Planck 2015 results. XIII. Cosmological parameters*, *Astron. Astrophys.* **594** (2016) A13, [1502.01589].

[90] G. Bertone, D. Hooper and J. Silk, *Particle dark matter: Evidence, candidates and constraints*, *Phys. Rept.* **405** (2005) 279–390, [hep-ph/0404175].

[91] K. Cheung and T.-C. Yuan, *Hidden fermion as milli-charged dark matter in Stueckelberg Z- prime model*, *JHEP* **03** (2007) 120, [hep-ph/0701107].

[92] T. Hambye, *Hidden vector dark matter*, *JHEP* **01** (2009) 028, [0811.0172].

[93] M. Lindner, D. Schmidt and T. Schwetz, *Dark Matter and neutrino masses from global $U(1)_{B-L}$ symmetry breaking*, *Phys. Lett. B* **705** (2011) 324–330, [1105.4626].

[94] S. Baek, P. Ko, W.-I. Park and E. Senaha, *Higgs Portal Vector Dark Matter : Revisited*, *JHEP* **05** (2013) 036, [1212.2131].

[95] T. Hambye and A. Strumia, *Dynamical generation of the weak and Dark Matter scale*, *Phys. Rev. D* **88** (2013) 055022, [1306.2329].

[96] C. D. Carone and R. Ramos, *Classical scale-invariance, the electroweak scale and vector dark matter*, *Phys. Rev. D* **88** (2013) 055020, [1307.8428].

[97] V. V. Khoze, C. McCabe and G. Ro, *Higgs vacuum stability from the dark matter portal*, *JHEP* **08** (2014) 026, [1403.4953].

[98] V. V. Khoze and G. Ro, *Dark matter monopoles, vectors and photons*, *JHEP* **10** (2014) 061, [1406.2291].

[99] A. Alves, A. Berlin, S. Profumo and F. S. Queiroz, *Dirac-fermionic dark matter in U(1)$_X$ models*, *JHEP* **10** (2015) 076, [1506.06767].

[100] W. Rodejohann and C. E. Yaguna, *Scalar dark matter in the $B-L$ model*, *JCAP* **12** (2015) 032, [1509.04036].

[101] A. Karam and K. Tamvakis, *Dark matter and neutrino masses from a classically scale-invariant multi-Higgs portal*, *PoS* **CORFU2015** (2016) 073, [1603.08470].

[102] A. Karam and K. Tamvakis, *Dark Matter from a Classically Scale-Invariant $SU(3)_X$*, *Phys. Rev. D* **94** (2016) 055004, [1607.01001].

[103] V. V. Khoze and A. D. Plascencia, *Dark Matter and Leptogenesis Linked by Classical Scale Invariance*, *JHEP* **11** (2016) 025, [1605.06834].

[104] M. Bauer, S. Diefenbacher, T. Plehn, M. Russell and D. A. Camargo, *Dark Matter in Anomaly-Free Gauge Extensions*, *SciPost Phys.* **5** (2018) 036, [1805.01904].

[105] P. Foldenauer, *Light dark matter in a gauged $U(1)_{L_\mu - L_\tau}$ model*, *Phys. Rev. D* **99** (2019) 035007, [1808.03647].

[106] T. Nomura, H. Okada and S. Yun, *Vector dark matter from a gauged SU(2) symmetry*, *JHEP* **06** (2021) 122, [2012.11377].

[107] N. Baouche, A. Ahriche, G. Faisel and S. Nasri, *Phenomenology of the hidden SU(2) vector dark matter model*, *Phys. Rev. D* **104** (2021) 075022, [2105.14387].

[108] A. Tapadar, S. Ganguly and S. Roy, *Non-adiabatic evolution of dark sector in the presence of $U(1)_{L\mu - L\tau}$ gauge symmetry*, *JCAP* **05** (2022) 019, [2109.13609].

[109] A. Dasgupta, S. K. Kang and M. Park, *Neutrino mass and $(g-2)_\mu$ with dark $U(1)_D$ symmetry*, 2104.09205.

[110] M. Bauer and T. Plehn, *Yet Another Introduction to Dark Matter: The Particle Physics Approach*, vol. 959 of *Lecture Notes in Physics*. Springer, 2019, 10.1007/978-3-030-16234-4.

[111] G. Bélanger, F. Boudjema, A. Pukhov and A. Semenov, *micrOMEGAs4.1: two dark matter candidates*, *Comput. Phys. Commun.* **192** (2015) 322–329, [1407.6129].

[112] S. R. Coleman, *The Fate of the False Vacuum. 1. Semiclassical Theory*, *Phys. Rev. D* **15** (1977) 2929–2936.

[113] C. G. Callan, Jr. and S. R. Coleman, *The Fate of the False Vacuum. 2. First Quantum Corrections*, *Phys. Rev. D* **16** (1977) 1762–1768.

[114] S. R. Coleman, V. Glaser and A. Martin, *Action Minima Among Solutions to a Class of Euclidean Scalar Field Equations*, *Commun. Math. Phys.* **58** (1978) 211–221.

[115] A. D. Linde, *Decay of the False Vacuum at Finite Temperature*, *Nucl. Phys. B* **216** (1983) 421.

[116] Y. G. Kim, K. Y. Lee and S.-H. Nam, *Conformal invariance and singlet fermionic dark matter*, *Phys. Rev. D* **100** (2019) 075038, [1906.03390].

[117] A. Hook, E. Izaguirre and J. G. Wacker, *Model Independent Bounds on Kinetic Mixing*, *Adv. High Energy Phys.* **2011** (2011) 859762, [1006.0973].

[118] D. Curtin, R. Essig, S. Gori and J. Shelton, *Illuminating Dark Photons with High-Energy Colliders*, *JHEP* **02** (2015) 157, [1412.0018].

[119] S. Oda, N. Okada and D.-s. Takahashi, *Classically conformal U(1)' extended standard model and Higgs vacuum stability*, *Phys. Rev. D* **92** (2015) 015026, [1504.06291].

[120] E. Gildener and S. Weinberg, *Symmetry Breaking and Scalar Bosons*, *Phys. Rev. D* **13** (1976) 3333.

[121] G. Bélanger, F. Boudjema, A. Goudelis, A. Pukhov and B. Zaldivar, *micrOMEGAs5.0 : Freeze-in*, *Comput. Phys. Commun.* **231** (2018) 173–186, [1801.03509].

[122] A. Alloul, N. D. Christensen, C. Degrande, C. Duhr and B. Fuks, *FeynRules 2.0 - A complete toolbox for tree-level phenomenology*, *Comput. Phys. Commun.* **185** (2014) 2250–2300, [1310.1921].

[123] P. Bechtle, D. Dercks, S. Heinemeyer, T. Klingl, T. Stefaniak, G. Weiglein et al., *HiggsBounds-5: Testing Higgs Sectors in the LHC 13 TeV Era*, *Eur. Phys. J. C* **80** (2020) 1211, [2006.06007].

[124] P. Bechtle, S. Heinemeyer, T. Klingl, T. Stefaniak, G. Weiglein and J. Wittbrodt, *HiggsSignals-2: Probing new physics with precision Higgs measurements in the LHC 13 TeV era*, *Eur. Phys. J. C* **81** (2021) 145, [2012.09197].

[125] Particle Data Group collaboration, R. L. Workman and Others, *Review of Particle Physics*, *PTEP* **2022** (2022) 083C01.

[126] T. Robens and T. Stefaniak, *Status of the Higgs Singlet Extension of the Standard Model after LHC Run 1*, *Eur. Phys. J. C* **75** (2015) 104, [1501.02234].

[127] N. F. Bell, G. Busoni and I. W. Sanderson, *Self-consistent Dark Matter Simplified Models with an s-channel scalar mediator*, *JCAP* **03** (2017) 015, [1612.03475].

[128] F. Staub, *SARAH 4 : A tool for (not only SUSY) model builders*, *Comput. Phys. Commun.* **185** (2014) 1773–1790, [1309.7223].

[129] T. Hahn, *Generating Feynman diagrams and amplitudes with FeynArts 3*, *Comput. Phys. Commun.* **140** (2001) 418–431, [hep-ph/0012260].

[130] V. Shtabovenko, R. Mertig and F. Orellana, *FeynCalc 9.3: New features and improvements*, *Comput. Phys. Commun.* **256** (2020) 107478, [2001.04407].

[131] M. E. Carrington, *The Effective potential at finite temperature in the Standard Model*, *Phys. Rev. D* **45** (1992) 2933–2944.

[132] P. B. Arnold and O. Espinosa, *The Effective potential and first order phase transitions: Beyond leading-order*, *Phys. Rev. D* **47** (1993) 3546, [hep-ph/9212235].

[133] C. Caprini et al., *Science with the space-based interferometer eLISA. II: Gravitational waves from cosmological phase transitions*, *JCAP* **04** (2016) 001, [1512.06239].

[134] R. Apreda, M. Maggiore, A. Nicolis and A. Riotto, *Gravitational waves from electroweak phase transitions*, *Nucl. Phys. B* **631** (2002) 342–368, [gr-qc/0107033].

[135] D. Bodeker and G. D. Moore, *Electroweak Bubble Wall Speed Limit*, *JCAP* **05** (2017) 025, [1703.08215].

[136] D. Croon, V. Sanz and G. White, *Model Discrimination in Gravitational Wave spectra from Dark Phase Transitions*, *JHEP* **08** (2018) 203, [1806.02332].

[137] P. Athron, C. Balázs, M. Bardsley, A. Fowlie, D. Harries and G. White, *BubbleProfiler: finding the field profile and action for cosmological phase transitions*, *Comput. Phys. Commun.* **244** (2019) 448–468, [1901.03714].

[138] V. V. Khoze and G. Ro, *Leptogenesis and Neutrino Oscillations in the Classically Conformal Standard Model with the Higgs Portal*, *JHEP* **10** (2013) 075, [1307.3764].

[139] E. K. Akhmedov, V. A. Rubakov and A. Y. Smirnov, *Baryogenesis via neutrino oscillations*, *Phys. Rev. Lett.* **81** (1998) 1359–1362, [hep-ph/9803255].

[140] M. Drewes and B. Garbrecht, *Leptogenesis from a GeV Seesaw without Mass Degeneracy*, *JHEP* **03** (2013) 096, [1206.5537].

[141] V. V. Khoze, *Inflation and Dark Matter in the Higgs Portal of Classically Scale Invariant Standard Model*, *JHEP* **11** (2013) 215, [1308.6338].

[142] H. Levine and L. G. Yaffe, *Higher Order Instanton Effects*, *Phys. Rev. D* **19** (1979) 1225.

[143] C. G. Callan, Jr., R. F. Dashen and D. J. Gross, *Toward a Theory of the Strong Interactions*, *Phys. Rev.* **D17** (1978) 2717.